Saint-Petersburg State University

Liia A. Shakurova

Slip effects in gas mixtures with state-to-state kinetics and surface reactions

Speciality 1.1.9. Mechanics of fluids, gases and plasma

Dissertation is submitted for the degree
of Candidate of Physics and Mathematics

Translation from Russian

Supervisor:
Professor, Doctor of Science in Physics and Mathematics
Elena V. Kustova

Saint-Petersburg — 2024

Contents

pp.

Introduction

Overview of the current state-of-the art

Studies in modern aerospace science, high-speed aerodynamics, low-temperature plasma applications, environmental science require reliable models of fluid dynamics coupled to detailed kinetics of physical and chemical processes both in the gas phase and on the surface. The latter is particularly important for designing thermal protection systems of re-entry space vehicles.

At high altitudes, strongly nonequilibrium gas flows are commonly modeled using the Direct Monte–Carlo simulations (DSMC) [1—6] since traditional continuum approaches are not capable to describe strong deviations from equilibrium and rarefaction effects. On the other hand, advanced continuum approaches such as state-to-state (STS) models taking into account coupled vibrational-chemical kinetics, fluid dynamics and transport processes [7—9] may significantly extend the limits of validity of continuum modeling [10; 11].

State-to-state simulations of vibrational-chemical kinetics in non-equilibrium reacting flows represent one of the most advanced tools for modeling in the practical areas mentioned above. The approach is capable to capture fine non-equilibrium effects in a flow and evaluate their influence on fluid dynamics and mass and heat transfer; in the absence of experimental data, it can be used for verification of reduced fluid-dynamic models. The STS approach is now widely used for modeling spatially homogeneous [10; 12—14], one-dimensional (1-D) and quasi-one-dimensional problems such as shock heated flows [15—23], supersonic nozzle expansions [24; 25], stagnation-line flows [26—32] and some two-dimensional flows [33—38]. However, implementation of the STS approach for simulation of viscous reacting 2-D and 3-D flows is still limited by several factors. First, evaluation of state-specific transport coefficients is prohibitively computationally expensive [7; 9], especially for polyatomic gases [39; 40]. This limitation can be partially overcome by using simplified transport models [8; 41; 42] providing satisfactory agreement with the exact ones. Another issue of the approach is the absence of formal kinetic-theory methods for deriving boundary conditions (BCs) for the macroscopic flow variables including, in the STS approach, populations of all vibrational states.

As is known, the continuum model of the gas breaks down in the Knudsen layer adjacent to the surface of a solid body. However, in many cases, the use of the continuum approach can offer certain benefits when modeling non-equilibrium rarefied flows near solids. For an accurate description of such flows, it is crucial to capture rarefaction effects in the layer and the influence of heterogeneous reactions, which can be achieved through kinetic modeling. However, such modeling near solids demands high computational resources. The specific boundary conditions allow to overcome this issue of using expensive kinetic approaches. The conditions provide solutions at the external edge of the Knudsen layer that would match the solution of the Navier–Stokes equations in the bulk outer flow [43]. It is worth mentioning that these boundary conditions extend the applicability of the continuum approximation only to gas flows in the slip flow regime (Knudsen numbers within the approximate range of 0.001–0.25). Nevertheless, numerous applications exist where gas mixtures operate within such a regime, and the consideration of interaction with surface effects and heterogeneous processes is essential.

When accounting for complex physical effects caused by gas-surface interactions, kinetic approaches simply require specification of a scattering kernel. The commonly used models can be found in Refs. [44—49]. Discussion of applicability limits for the models can be found in works [47; 50—53]. The most widely used models are the Maxwell model [44], the Cercignani–Lampis (CL) one [47] and the Lord extension to the CL model [49; 54]. In the mentioned models knowledge of several accommodation coefficients is required. The latter could be determined through experimental measurements [55—57] or obtained via molecular dynamics simulations [58; 59]. Still, these scattering models are generally not adequate to reproduce the details of gas dynamics, as demonstrated by comparing the distributions obtained by them and by Molecular Dynamics (MD) trajectories [60; 61]. Unfortunately the applicability of molecular-dynamic calculations is limited by high computational costs. There are numerous extensions of these models, such as those discussed in [62; 63], but they still have certain limitations due to the difficulty of capturing interactions across a wide range of gases and surfaces.

Modeling heterogeneous reactions in DSMC is challenging due to the necessity of obtaining reaction probabilities, which are extracted from macroscopic, but not microscopic data. Advanced approaches successfully dealing with this problem can be found in [64—66]. For instance in [66], probabilities of adsorption and Eley–Rideal recombination are based on individual properties of each particular molecule

and frequencies of desorption whereas the Langmuir–Hinshelwood recombination probabilities are derived from macroscopic reaction rates.

As for continuum approaches, the physical effects of gas–solid interactions can be captured by the so-called slip conditions of macroscopic velocity and temperature (velocity slip and temperature jump). Deviations of these gas macroscopic parameters from those of the surface strongly depend on gas rarefaction, and with rising Knudsen number may cause a significant change in gas-dynamic parameters, which is commonly referred to as the «slip effect». The effect occurs due to the presence of gradients of macroscopic parameters near the wall, which leads to significant deviations of the velocity distribution function from the equilibrium distribution. Since these effects are obviously dependent on the scattering of particles by the solid wall, knowledge of the scattering kernel for modeling is required.

In the STS simulations, the temperature jump condition was taken into account using the assumption that the effects of the gaseous particle collisions inside the Knudsen layer can be neglected, because the layer width is comparable with the mean free path [67], and that the Fourier heat flux entering the Knudsen layer is equal to the heat flux in contact with the wall [68]. From the equality of these fluxes it is possible to calculate the temperature jump; the heat flux on the wall becomes proportional to the temperature jump itself as well as to the molecular and atomic number densities and thermal velocities [69]. Such a simplified description may provide rough estimates for the slip effect.

Heterogeneous reactions in the context of continuum techniques are commonly represented by boundary conditions for mass fluxes of gas mixture species. In the case of neglecting these processes, the mass fluxes are equal to zero. The surface of a solid body, where heterogeneous reactions are neglected, is commonly referred to as a non-catalytic surface. Otherwise, when the reactions are included in modeling, the surface is mentioned to be catalytic (or partially catalytic). At the macroscopic scale, coupled surface catalyticity and fluid dynamics are considered in [55; 70; 71] in the frame of one-temperature and multi-temperature approaches, and in the state-to-state approach — in [27; 28; 72]. However, in the STS simulations, a simple phenomenological model for the concentration jump was applied whereas both the temperature jump and velocity slip were commonly neglected. The only exception is the work [69] where the phenomenological approach for the temperature jump was implemented.

The boundary conditions for velocity, temperature and species populations, which in the state-to-state approximation include the populations of all vibrational states — velocity slip, temperature jump and wall mass fluxes expressions — are commonly referred to as slip boundary conditions. This terminology will also be applied throughout this work.

There are various techniques available to obtain slip boundary conditions capturing physical effects of gas-surface interactions. First, they can be modeled using slip coefficients, which are obtained from gas-surface simulations in the frame of kinetic or continuum modeling [73—76]; or found theoretically by numerical analysis of a flow in the Knudsen layer [77—79]. Secondly, the boundary conditions can be derived based on theoretical methods [80—84]. Additionally, the expressions can be obtained by numerical solution of the model Boltzmann equation in the Knudsen layer [85; 86]. Besides all the variety of the approaches, the slip conditions can be extracted from other simulations or experiments conducted near the solid wall.

In this study, the focus is on theoretical techniques. Such approaches include the half-flux method, initially proposed by Patterson [81] and developed by Shidlovskiy [87]; Grad's approach, based on the boundary condition for distribution function of reflected particles [80]; approach based on the kinetic boundary condition [88—90], developed in this work; and method, based on the analysis of the Knudsen layer adjacent to the boundary developed by Sone [91; 92].

Initially, in all the above mentioned theoretical methods a single-component gas with no internal degrees of freedom and specular-diffusive model has been considered (in some works only specular or diffusive scattering). The generalization for a multi-component gas mixture described in the frame of the one-temperature approach can be found in Refs. [43; 82; 93—95], for the multi-temperature case in Refs. [71; 96—98]. For the CL model, the temperature jump and velocity slip are obtained in Refs. [50; 95]. It is worth mentioning that in the majority of theoretical studies, the boundary conditions are derived for the model kinetic equation and not for the full Boltzmann equation; the exception are studies [71; 82; 96] based on the Chapman–Enskog formalism.

Including heterogeneous processes in strongly non-equilibrium fluid-dynamic problems is far more complicated, especially in the state-to-state approach. The first attempt to account for the chemical reactions in the slip equations was made by Scott [93]. On the basis of Maxwell kernel, he made an assumption that some part of diffusely reflected particles may recombine or dissociate on the surface and

used the recombination coefficient to describe such a model. Later, this approach was applied in works [71; 82; 96]. Surface recombination rate coefficients can be measured experimentally [55; 99—101] or calculated using molecular dynamics methods along with quasi-classical trajectory calculations [72; 102—104]; it is worth mentioning that in Refs. [72; 103], the recombination coefficients are vibrational state-specific. More rigorous kinetic theory to account for surface chemical reactions on crystal surfaces was developed in [83; 84] by taking into account physisorbed-gas species and chemisorbed species. Such an approach is based on kinetic equations for gas particles interacting with a potential field of surface particles [105; 106]. Additionally, there exist numerous phenomenological models of heterogeneous processes, e.g. [70; 107; 108]. However, most of them do not account for detailed vibrational kinetics. An exception is the Barbato model, developed in [109; 110]. The latter model was applied to investigate the influence of heterogeneous recombination on stagnation-line flow parameters [28; 32; 72; 111].

To account for the coupled effect of heterogeneous reactions and surface particle scattering in slip boundary conditions, there have been attempts to include these processes in theoretical methods within the one-temperature approximation [43; 82; 93; 94]. Nevertheless, the developed techniques were not accurately implemented and generalized for state-specific models, as stated in [90; 112]. This work presents that novel approach, which addresses known challenges in modeling surface reactions.

The key points of the present study are: 1) to summarize problems in known theoretical approaches for slip boundary conditions in non-equilibrium flows with surface reactions; 2) to develop a new self-consistent approach for deriving slip boundary conditions in gas mixtures with gas-phase state-to-state vibrational-chemical kinetics and heterogeneous processes; 3) to derive macroscopic boundary conditions on a partially catalytic wall; 4) to implement the new model to the computational fluid-dynamic code and assess the influence of different slip condition models on the air flow along the stagnation line, in particular, to evaluate the coupled effect of temperature jump and heterogeneous reaction models on the air flow kinetics, dynamics and heat transfer.

General characteristics and structure of work

Relevance of the topic lies in the necessity for accurate and self-consistent models that capture effects of non-equilibrium rarefied gas flows interaction with solid surfaces. These models are crucial for entry of space vehicles into planetary atmospheres and modeling gas flows in microchannels problems. Furthermore, the models are required in situations where accounting for non-equilibrium heterogeneous processes, such as wall catalyticity, ablation, and ionization effects during interaction with a solid body is essential. Rigorously developed models can accurately capture the influence of rarefaction effects, as well as both homogeneous and heterogeneous processes on gas flow characteristics near the surface, including the heat flux. The accuracy of the latter is crucial, as it can significantly impact the design of thermal protection systems for re-entry vehicles.

The aim and objectives of the research:

1. Construction of the approach that allows to obtain slip boundary conditions for fluid-dynamic variables within the frame of the state-to-state approach. Derivation of slip conditions, considering specific models of particles scattering by solid wall.
2. Comparison of the approach with other known theoretical, such as the Grad technique and the Patterson–Shidlovskiy method. Identification of benefits of the developed approach.
3. Further extension of the approach to accurately incorporate the influence of heterogeneous processes, including adsorption/desorption, vibrational excitation/deactivation and chemical reactions on the boundary conditions.
4. Validation of the advanced approach involving the theoretical comparison of wall mass fluxes with reliable phenomenological models and the comparison of the obtained effective heterogeneous recombination rates with those from *ab initio* molecular dynamics simulations.
5. Implementation of the developed models of slip boundary conditions to the fluid-dynamic solver for modeling dynamics and state-to-state air kinetics in the boundary layer near stagnation point.
6. Analysis of the impact of gas rarefaction, along with different types of slip conditions and wall catalytic effects on the boundary layer flow parameters.

Reliability of the results is ensured by the use of rigorous theoretical models within the frame of kinetic theory. The slip conditions are derived from the kinetic boundary condition constructed from first principles for the distribution function. Besides that, a rigorous comparison with other known slip conditions is provided, and it is proven that the general form of the conditions within the advanced approach is compatible with some phenomenological models and those obtained from accurate theoretical techniques; the latter can be obtained as limit cases of our general approach. The validity of the derived conditions is further confirmed by comparing the obtained air flow parameters in the boundary layer in the vicinity of the stagnation point with the results from other calculations. Furthermore, under the conditions of this air flow, the effective recombination rates derived within the framework of the developed generalized approach exhibit the best agreement with the coefficients obtained from MD simulations.

The scientific value of the dissertation is as follows:

— The approach that enables the derivation of state-specific slip boundary conditions for an arbitrary case of particle scattering by a solid wall, capturing the influence of non-equilibrium heterogeneous processes, is formulated.

— The analysis of well-known models for heterogeneous processes is conducted, emphasizing a general expression that ensures the accurate implementation of these processes.

— The impact of heterogeneous recombination models on silica surface, as well as the influence of gas rarefaction on the air flow parameters in the boundary layer are examined.

— The effects of diffusion model in the boundary conditions and the accommodation coefficient in the specular-diffusive scattering kernel on the mixture composition and the transport properties are investigated.

Practical value of the dissertation is as follows:

— Slip conditions are presented for specific cases of particles scattering by a solid wall, and the methods for their implementation into computational fluid dynamics (CFD) codes are discussed.

— Recommendations regarding the choice of the boundary conditions model, which includes the implementation or neglect of the temperature jump, are provided.

— The influence of the models on the total heat flux is discussed in detail, and the recommendation to avoid using phenomenological models of the flux is given, which is supported by numerical calculations.

The main results of the research are as follows:

1. Self-consistent and rigorous approach for obtaining slip boundary conditions from the developed kinetic boundary condition is formulated ([88], pp. 9—12).
2. Problems associated with the inclusion of heterogeneous reactions in known theoretical techniques are identified through theoretical analysis ([90], pp. 2—4). The problems are in the fact that the mass fluxes on the wall do not take into account the contributions of particles of different species. The latter is also confirmed by numerical calculations ([112], pp. 10—16).
3. The extension of the kinetic boundary condition, which includes the loss and gain in the number of particles due to heterogeneous processes is constructed ([90], pp. 2—4; [112], pp. 4—5).
4. State-specific slip boundary conditions, which are velocity slip, temperature jump, and expressions for species wall mass fluxes, are derived based on Maxwell and Cercignani–Lampis models of particles scattering by the surface ([88], pp. 11—14; [90], pp. 6—9; [112], pp. 5—7).
5. The dependence of the derived slip boundary conditions on the diagonal terms of the stress tensor — the bulk viscosity and relaxation pressure, capturing rapid inelastic translational-rotational energy exchange during particles interaction with the solid surface ([88], pp. 5—8; [89], pp. 4—6).
6. Influence of gas rarefaction, heterogeneous recombination models, and temperature jump on the air flow parameters in the boundary layer near stagnation point is examined. It is demonstrated that temperature jump significantly affects fluid-dynamic parameters and surface heat flux, while the impact of heterogeneous reactions on the silica surface is weaker ([112], pp. 10—16).
7. The effects of various diffusion velocity models in the slip boundary conditions are studied. It is shown that models influence particles concentrations and heat flux near the surface ([113], pp. 9—15).

Provisions to be defended:

1. Kinetic boundary condition for the distribution function modified to the state-to-state approach. Formulation of the method to obtain slip boundary

conditions using this modification. Verification of the equivalence of the proposed method to the Grad and Patterson–Shidlovskiy techniques in the one-temperature approximation.

2. Extension of the kinetic boundary condition and normalization condition for an arbitrary scattering kernel to account for the loss and gain in the number of particles resulting from adsorption/desorption, vibrational excitation/deactivation processes and heterogeneous chemical reactions.
3. Expressions for slip boundary conditions within the framework of the developed approach and its modification for Maxwell and Cercignani–Lampis scattering kernels. Demonstration of the independence of the boundary conditions for species number fluxes on the scattering model.
4. Identification of the general form of expression for mass fluxes on the surface that allows to capture correctly the influence of specified heterogeneous processes. Based on this statement, verification of the incapability of the other approaches to capture these processes.
5. Results of numerical simulations of air flow in the boundary layer in the vicinity of stagnation point. Assessment of the influence of different wall catalyticity models, supporting conclusions regarding the use of developed self-consistent extension.
6. Results of the study of the effects of gas rarefaction, diffusion model and accommodation coefficient on the air flow in the boundary layer. Estimation of the necessity to include temperature jump for different Knudsen numbers. Investigation of different processes contributions to the total wall heat flux.

Publications. The results presented in the dissertation are published in papers [1*–12*] of which 1 is in journal included in the list of peer-reviewed scientific journals recommended by the Higher Attestation Commission, 4 — in peer-reviewed publications indexed in the international citation databases Web of Science and Scopus, 7 — in conference proceedings indexed in the RSCI. The personal contribution of the author to the preparation of publications is described in the Appendix A.

Approbation of work. The results of work on the dissertation were reported at the All-Russian and international conferences:

1. XXII International Conference on Computational Mechanics and Modern Applied Software Systems CMMASS'2021 (Alushta, 2021);

2. 32nd International Symposium on Rarefied Gas Dynamics RGD32 (Seoul, South Korea);
3. 21st International Conference on the Methods of Aerophysical Research ICMAR-2022 (Novosibirsk, 2022);
4. XXIV International Conference on Applied Mathematics and Mechanics in the Aerospace Industry AMMAI'2022 (Alushta, 2022)
5. All-russian Scientific Symposium on Problems of Aeromechanics and Gas Dynamics, Dedicated to the 100th Anniversary of the Birth of Academician G. G. Cherny (Moscow, 2023);
6. XIII All-russian Congress on Theoretical and Applied Mechanics (St. Petersburg, 2023);
7. XXIII International Conference on Computational Mechanics and Modern Applied Software Systems CMMASS'2023 (Divnomorskoe, 2023).

Structure and scope of work. The dissertation work consists of an introduction, 3 chapters a conclusion, a bibliography of 153 entries and 1 appendix The total volume of the dissertation is 120 pages, including 44 figures and 6 tables.

Chapter 1. State-specific slip boundary conditions

In this chapter, the boundary conditions for fluid-dynamic parameters of strongly non-equilibrium multi-component gas mixture flows in slip regime are derived systematically by two different approaches. The first theoretical approach uses the technique proposed by Grad whereas the second one is based on the kinetic boundary condition. In the case of specular-diffusive scattering by solid wall it is shown that the two approaches are equivalent. At the same time, the approach based on the kinetic boundary condition provides more rigorous mathematical description of the problem and can be easily applied for other scattering kernels and gas-surface interaction models. The expressions for slip boundary conditions are given for two common types of scattering kernels, Maxwell, or specular-diffusive, and Cercignani–Lampis. The results provided in this chapter are published in [88; 89].

The chapter is organized as follows. First, the set of governing equations for a multi-component reacting gas mixture flow is presented in Sec. 1.1. The boundary conditions for velocity, temperature and number densities are obtained by the Grad's approach in Sec. 1.2 and by the approach, based on the kinetic boundary condition, in Sec. 1.3. In Sec. 1.3 the equivalence of both methods is shown and advantages of the second approach are discussed. Further simplifications of the obtained equations are presented in Sec. 1.4.

1.1 Governing equations for a non-equilibrium flow in the state-to-state approach

Kinetic equation

In this work, we consider the mixture of gases with translational, rotational, vibrational degrees of freedom and take into account internal energy transitions and chemical reactions. The distribution function $f_{cij}(\mathbf{r},\mathbf{u},t)$ is introduced for chemical species c, vibrational level i, and rotational level j ($\mathbf{r}$ is coordinate, $\mathbf{u}$ is the particle velocity, t is the time). The electronic excitation is neglected.

Neglecting the influence of mass and electromagnetic forces, the Boltzmann kinetic equations for distribution functions $f_{cij}(\mathbf{r},\mathbf{u},t)$ can be written in the Wang Chang–Uhlenbeck form [9]:

$$\begin{gathered}\frac{\partial f_{cij}}{\partial t} + \mathbf{u}_c \cdot \nabla f_{cij} = J_{cij}, \\ c = 1,\dots,L, \quad i = 0,\dots,N_c, \quad j = 0,\dots,N_{ci},\end{gathered} \tag{1.1}$$

where $\nabla = \partial/\partial\mathbf{r}$, L is the number of chemical species, N_c is the number of vibrational levels for c species, N_{ci} is the number of rotational levels of molecules c on the vibrational level i. J_{cij} is the integral operator responsible for the variation of the distribution function resulting from collision. In the general case, J_{cij} includes contributions of elastic and inelastic collisions, and chemical reactions:

$$J_{cij} = J_{cij}^{\mathrm{el}} + J_{cij}^{\mathrm{int}} + J_{cij}^{\mathrm{react}}. \tag{1.2}$$

Under strong nonequilibrium conditions, the collision operator can be split to the operators of rapid and slow processes [9]

$$J_{cij} = J_{cij}^{\mathrm{rap}} + J_{cij}^{\mathrm{sl}}. \tag{1.3}$$

To approximately solve the integro-differential equations, first, the corresponding dimensionless kinetic equations need to be written, and their form is as follows:

$$\frac{\partial f_{cij}}{\partial t} + \mathbf{u}_c \cdot \nabla f_{cij} = \frac{1}{\varepsilon} J_{cij}^{\mathrm{rap}} + J_{cij}^{\mathrm{slow}}, \tag{1.4}$$

where ε is the small parameter specified by the ratio of characteristic times of rapid and slow processes, $\varepsilon \approx \tau_{\mathrm{rap}}/\tau_{\mathrm{slow}}$.

In this study, the generalized Chapman-Enskog method developed in [9] is applied. The distribution function is represented as a generalized Chapman–Enskog series in the small parameter ε:

$$f_{cij} = \sum_r \varepsilon^r f_{cij}^{(n)} \left(\mathbf{u}, \rho_\lambda(\mathbf{r},t), \nabla\rho_\lambda(\mathbf{r},t), \nabla^2\rho_\lambda(\mathbf{r},t), \dots\right). \tag{1.5}$$

Here, r is the order ($r = 0,1,\dots$) and $\rho_\lambda(\mathbf{r},t)$ are the macroscopic gas parameters, required for a closed flow description (their number is defined by independent collision invariants). To obtain the equations for unknown functions, the expansion (1.5) needs to be substituted into Eq. (1.4).

In order to develop a closed macroscopic fluid-dynamic model, it is necessary to establish first the kinetic scaling.

State-to-state kinetic scaling and collision invariants

The gas mixture flow from here on is described in the framework of the state-to-state model for coupled detailed vibrational and chemical kinetics. However, all the assumption suggested can be as well applied for less detailed one- and multi-temperature approximations.

The main peculiarity of the state-to-state approach is that gas dynamics, mass and energy transport are fully coupled to non-equilibrium vibrational and chemical kinetics since the characteristic time scale of vibrational energy transitions τ_{vibr} and chemical reactions τ_{react} is the same as the fluid-dynamic time scale θ:

$$\tau_{\text{tr}} \sim \tau_{\text{rot}} \ll \tau_{\text{vibr}} \sim \tau_{\text{react}} \sim \theta, \tag{1.6}$$

where τ_{tr}, τ_{rot} are the characteristic times of translational and rotational relaxation.

According to this kinetic scaling, the collisional operator is divided into rapid and slow processes as following:

$$J_{cij}^{\text{rap}} = J_{cij}^{\text{tr}} + J_{cij}^{\text{rot}}; \qquad J_{cij}^{\text{sl}} = J_{cij}^{\text{vibr}} + J_{cij}^{\text{react}}. \tag{1.7}$$

Taking into account considered characteristic time scale (1.6), the scalar collision invariants of rapid processes in the state-to state approach $\psi_{cij}^{(\nu)}$ [9], are the momentum and particle total energy:

$$\psi_{cij}^{(\nu)} = m_c \mathbf{u}_c,\ \frac{m_c u_c^2}{2} + \varepsilon_j^{ci} + \varepsilon_i^c + \varepsilon_c,\ \ \nu = 1,2,3,4; \tag{1.8}$$

along with additional invariants of the most frequent collisions:

$$\psi_{ci}^{(\nu+4)} = a_{ci},\ \ \nu = 1,\ldots,L,\ \ L = \sum_{c=1}^{L_M} N_c + L_A. \tag{1.9}$$

Here m_c, $\mathbf{u}_c$ is the mass of chemical species c, ε_j^{ci}, ε_i^c, ε_c are the rotational, vibrational energy and the energy of formation. L_M, L_A are the numbers of molecular and atomic species, L is the number of gas mixture chemical components. The last set of invariants (1.9) appears because vibrational energy transitions and chemical reactions are frozen in the rapid processes time scale.

The formal kinetic theory for the STS approach is developed in [7; 9] in the framework of the generalized Chapman–Enskog method. The model includes

extended fluid-dynamic equations and their closure based on the zero- and first-order distribution functions as well as algorithms for the transport coefficients evaluation. A brief discussion of this developed theory will be provided in this section.

Definitions of macroscopic parameters and transport terms

First of all, it is necessary to specify parameters of the gas flows at the macroscopic scale. These macroscopic parameters are defined as the moments of the distribution functions [9]. The main parameters necessary for a comprehensive description of non-equilibrium gas flows are introduced below.

The population (number density) of molecular species c for the vibrational level i per unit volume, n_{ci}:

$$n_{ci}(\mathbf{r},t) = \sum_j \int f_{cij}(\mathbf{r},\mathbf{u},t)\,\mathrm{d}\mathbf{u}_c, \tag{1.10}$$

where the integration is performed in particles velocity phase space. The total number density of the gas mixture is defined as a sum of n_{ci}:

$$n(\mathbf{r},t) = \sum_{cij} \int f_{cij}(\mathbf{r},\mathbf{u},t)\,\mathrm{d}\mathbf{u}_c = \sum_{ci} n_{ci}. \tag{1.11}$$

The macroscopic velocity, $\mathbf{v}(\mathbf{r},t)$, of the gas flow is introduced by the following moment of the distribution function:

$$\rho\mathbf{v}(\mathbf{r},t) = \sum_{cij} m_c \int \mathbf{u}_c f_{cij}(\mathbf{r},\mathbf{u},t)\,\mathrm{d}\mathbf{u}_c, \tag{1.12}$$

where ρ is the mixture density, $\rho = \sum_{ci} m_c n_{ci}$.

The specific total internal energy, $U(\mathbf{r},t)$, of the mixture components is defined as the sum of energies:

$$U(\mathbf{r},t) = E_{\mathrm{tr}} + E_{\mathrm{rot}} + E_{\mathrm{vibr}} + E_{\mathrm{f}}, \tag{1.13}$$

which are the specific translational energy, E_{tr}:

$$\rho E_{\mathrm{tr}} = \sum_{cij} \int \frac{m_c c_c^2}{2} f_{cij}(\mathbf{r},\mathbf{u},t)\,\mathrm{d}\mathbf{u}_c; \tag{1.14}$$

the specific rotational energy, $E_{\rm rot}$:

$$\rho E_{\rm rot} = \sum_{cij} \varepsilon_j^{ci} \int f_{cij}(\mathbf{r}, \mathbf{u},t)\, \mathrm{d}\mathbf{u}_c; \tag{1.15}$$

the specific vibrational energy, $E_{\rm vibr}$:

$$\rho E_{\rm vibr} = \sum_{cij} \varepsilon_i^{c} \int f_{cij}(\mathbf{r}, \mathbf{u},t)\, \mathrm{d}\mathbf{u}_c = \sum_{ci} \varepsilon_i^{c} n_{ci}; \tag{1.16}$$

and the specific formation energy, $E_{\rm f}$:

$$\rho E_{\rm f} = \sum_{cij} \varepsilon_c \int f_{cij}(\mathbf{r}, \mathbf{u},t)\, \mathrm{d}\mathbf{u}_c = \sum_{c} \varepsilon_c n_c. \tag{1.17}$$

In the above relations $\mathbf{c}_c$ is the peculiar velocity of the c-th species, $\mathbf{c}_c = \mathbf{u}_c - \mathbf{v}$, n_c is the number density of chemical species c, $n_c = \sum\limits_i n_{ci}$. The values $\rho E_{\rm tr}$, $\rho E_{\rm rot}$, $\rho E_{\rm vibr}$, and $\rho E_{\rm f}$ represent the corresponding energy per unit volume.

Note that under nonequilibrium conditions, the specific internal energy (1.13) is a function of not only temperature but also depends on additional macroscopic parameters that differ for various deviations from equilibrium. In the state-to-state approach U is a function of T and n_{ci}. Therefore, the gas cannot be treated as calorically perfect.

The transport terms required in the state-to-state approach include the diffusion velocity of molecular species c on the vibrational level i, $\mathbf{V}_{ci}(\mathbf{r},t)$, the stress tensor, $\mathbf{P}(\mathbf{r},t)$, and the total heat flux, $\mathbf{q}(\mathbf{r},t)$, defined as follows:

$$n_{ci}\mathbf{V}_{ci}(\mathbf{r},t) = \sum_{j} \int \mathbf{c}_c f_{cij}(\mathbf{r}, \mathbf{u},t)\, \mathrm{d}\mathbf{u}_c; \tag{1.18}$$

$$\mathbf{P}(\mathbf{r},t) = \sum_{cij} \int m_c \mathbf{c}_c \mathbf{c}_c \mathbf{c}_c f_{cij}(\mathbf{r}, \mathbf{u},t)\, \mathrm{d}\mathbf{u}_c; \tag{1.19}$$

$$\mathbf{q}(\mathbf{r},t) = \sum_{cij} \int \left(\frac{m_c c_c^2}{2} + \varepsilon_j^{ci} + \varepsilon_i^{c} + \varepsilon_c \right) \mathbf{c}_c f_{cij}(\mathbf{r}, \mathbf{u},t)\, \mathrm{d}\mathbf{u}_c. \tag{1.20}$$

The heat flux is convenient to represent as the sum of several terms [9]:

$$\mathbf{q} = q_{\rm F} + q_{\rm TD} + q_{\rm MD} + q_{\rm DVE}. \tag{1.21}$$

The first term is the heat conduction (Fourier) flux due to the transfer of translational and rotational energy, $q_{\rm F}$, the second one is the thermal diffusion flux,

q_{TD}, the third one includes contributions of mass diffusion flux, q_{MD}, and the last term — vibrational energy transferred by excited molecules diffusion flux, q_{DVE}. These latter terms can be written explicitly only in the case of binary mixtures. While q_{F}, q_{TD} and q_{MD} appear also in both one-temperature and multi-temperature formulations, the term q_{DVE} is a particular feature of the state-to-state approach [25].

State-to-state zero- and first-order distribution functions

Omitting the details of the technique for obtaining the distribution functions [9], here, the first two terms — zero- and first-order — in the expansion (1.5) are presented. The other terms are not taken into account since their influence is relatively small in the considered slip flow regime.

In the zero-order approximation, the distribution function couples the Maxwell distribution over velocities and the Boltzmann distribution over rotational energy levels j multiplied by non-equilibrium number densities of vibrational states n_{ci} [9]:

$$f_{cij}^{(0)} = \frac{n_{ci}}{Z_{\mathrm{rot},ci}} \left(\frac{m_c}{2\pi k T} \right)^{3/2} s_j^{ci} \exp\left(-\frac{m_c c_c^2}{2kT} - \frac{\varepsilon_j^{ci}}{kT} \right), \tag{1.22}$$

where k is the Boltzmann constant, $Z_{\mathrm{rot},ci}$ is the rotational partition function depending on the vibrational state i, s_j^{ci} is the statistical weight for a molecule c on the j-th rotational and i-th vibrational levels.

The first-order distribution function is obtained as a linear combination of gradients of fluid-dynamic variables with unknown coefficients $\mathbf{A}_{cij}$, $\mathbf{D}_{cij}^{dk}$, $\mathbf{B}_{cij}$, F_{cij}, G_{cij} depending on the peculiar velocity and, implicitly, on the macroscopic flow parameters [9]:

$$\begin{aligned} f_{cij} = f_{cij}^{(0)} + \frac{f_{cij}^{(0)}}{n} \Bigg(& - \mathbf{A}_{cij} \cdot \nabla \ln T - \sum_{dk} \mathbf{D}_{cij}^{dk} \cdot \mathbf{d}_{dk} - \mathbf{B}_{cij} : \nabla \mathbf{v} \\ & - F_{cij} \nabla \cdot \mathbf{v} - G_{cij} \Bigg), \end{aligned} \tag{1.23}$$

where $\mathbf{d}_{ci}$ is the state-specific diffusive driving force for species ci,

$$\mathbf{d}_{ci} = \nabla(n_{ci}/n) + (n_{ci}/n - \rho_{ci}/\rho) \nabla \ln p, \tag{1.24}$$

$\rho_{ci} = n_{ci} m_c$ is the density of species ci and p is the pressure.

According to the generalized Chapman-Enskog method [9], unknown functions $\mathbf{A}_{cij}$, $\mathbf{D}^{dk}_{cij}$, $\mathbf{B}_{cij}$, F_{cij}, G_{cij} are found from linear integral equations complemented with constraints derived from the normalizing conditions for the distribution function. Solving the integral equations can be reduced to solving the systems of linear algebraic equations obtained by expanding the unknown functions in the series of orthogonal polynomials: Sonine polynomials $S^{(r)}_{\nu}\left(m_c c_c^2/2kT\right)$ over dimensionless velocity and Waldmann–Trübenbacher polynomials over discrete values of rotational energy $P^{(p)}_j\left(\varepsilon^{ci}_j/kT\right)$. Based on the integral equations, the following expansions are proposed [9]:

$$\mathbf{A}_{cij} = -\frac{m_c \mathbf{c}_c}{2kT} \sum_{rp} a_{ci,rp} S^{(r)}_{3/2} P^{(p)}_j, \tag{1.25}$$

$$\mathbf{D}^{dk}_{cij} = \frac{m_c \mathbf{c}_c}{2kT} \sum_{r} d^{dk}_{ci,rp} S^{(r)}_{3/2}, \tag{1.26}$$

$$\mathbf{B}_{cij} = \frac{m_c}{2kT} \left(\mathbf{c}_c \mathbf{c}_c - \frac{1}{3} c_c^2 \mathbf{I} \right) \sum_{r} b_{ci,r} S^{(r)}_{5/2}, \tag{1.27}$$

$$F_{cij} = \sum_{rp} f_{ci,rp} S^{(r)}_{1/2} P^{(p)}_j, \tag{1.28}$$

$$G_{cij} = \sum_{rp} g_{ci,rp} S^{(r)}_{1/2} P^{(p)}_j. \tag{1.29}$$

In the above relations, $a_{ci,rp}$, $d^{dk}_{ci,rp}$, $b_{ci,r}$, $f_{ci,rp}$, $g_{ci,rp}$ are the expansion coefficients. It is worth noting that different polynomial systems for different unknown functions in the first-order correction are used, even for the functions of the same tensor order. The set of polynomials is chosen accordingly to the right-hand sides of corresponding integral equations, see [9]. For instance, integral equations for vector functions $\mathbf{A}_{cij}$ include rotational energy whereas equations for $\mathbf{D}^{dk}_{cij}$ do not. This allows one to use solely Sonine polynomials in the expansion of $\mathbf{D}^{dk}_{cij}$ which is not possible for $\mathbf{A}_{cij}$, whose expansion requires the product of the Sonine and Waldmann–Trübenbacher polynomials. Such an approach is equivalent to choosing double polynomial sets for both $\mathbf{A}_{cij}$ and $\mathbf{D}^{dk}_{cij}$, but provides more straightforward derivation of linear transport systems for the multi-component diffusion coefficients.

Retaining only the first non-vanishing terms in expansions (1.25)–(1.29), the distribution function can be written in the form

$$
\begin{aligned}
f_{cij} = f_{cij}^{(0)} \Bigg[1 + \frac{m_c}{2nkT}\, \mathbf{c}_c \cdot \nabla \ln T \Big(& a_{ci,00} S_{3/2}^{(0)} P_j^{(0)} + a_{ci,10} S_{3/2}^{(1)} P_j^{(0)} \\
& + a_{ci,01} S_{3/2}^{(0)} P_j^{(1)} \Big) - \frac{m_c}{2nkT} \sum_{dk} d_{ci,0}^{dk} \mathbf{c}_c \cdot \mathbf{d}_{dk} S_{3/2}^{(0)} \\
& - \frac{m_c}{2nkT}\, b_{ci,0} S_{5/2}^{(0)} \left(\mathbf{c}_c \mathbf{c}_c : \nabla \mathbf{v} - \tfrac{1}{3}\, c_c^2 \nabla \cdot \mathbf{v} \right) \\
& - \frac{1}{n} \left(f_{ci,10} S_{1/2}^{(1)} P_j^{(0)} + f_{ci,01} S_{1/2}^{(0)} P_j^{(1)} \right) \nabla \cdot \mathbf{v} \\
& - \frac{1}{n} \left(g_{ci,10} S_{1/2}^{(1)} P_j^{(0)} + g_{ci,01} S_{1/2}^{(0)} P_j^{(1)} \right) \Bigg],
\end{aligned}
\tag{1.30}
$$

with

$$
S_{\boldsymbol{\nu}}^{(0)} = P_j^{(0)} = 1, \quad S_{\boldsymbol{\nu}}^{(1)} = 1 + \boldsymbol{\nu} - \frac{m_c c_c^2}{2kT}, \quad P_j^{(1)} = \left\langle \frac{\varepsilon_j^{ci}}{kT} \right\rangle_{\mathrm{rot}} - \frac{\varepsilon_j^{ci}}{kT}. \tag{1.31}
$$

Here $\langle \dots \rangle_{\mathrm{rot}}$ denotes averaging over rotational energy with local equilibrium Boltzmann distribution.

Governing equations for fluid-dynamic variables

The set of governing equations for the unknown STS-specific macrospocic parameters is obtained multiplying the Boltzmann equation (1.1) by the collision invariants (1.8)–(1.9), integrating over velocities and summing over c, i, j (for the additional invariants, summation is carried out only over the rotational states j). Thus, extended fluid-dynamic equations take the form [9]:

$$
\frac{dn_{ci}}{dt} + n_{ci} \nabla \cdot \mathbf{v} + \nabla \cdot (n_{ci} \mathbf{V}_{ci}) = R_{ci}^{\mathrm{vibr}} + R_{ci}^{\mathrm{react}}, \tag{1.32}
$$

$$
\rho \frac{d\mathbf{v}}{dt} + \nabla \cdot \mathbf{P} = 0, \tag{1.33}
$$

$$
\rho \frac{dU}{dt} + \nabla \cdot \mathbf{q} + \mathbf{P} : \nabla \mathbf{v} = 0. \tag{1.34}
$$

Here, $i = 0, \dots, N_c$, $c = 1, \dots, L$, R_{ci}^{vibr} and R_{ci}^{react} are state-specific production terms due to vibrational-vibrational (VV), vibrational-translational (VT) transitions

and chemical reactions. The closure of the above set of equations depends on the one-particle distribution function $f_{cij}(\mathbf{r},\mathbf{u},t)$ (see Eqs. (1.22), (1.30)).

Transport terms

Substituting distribution function (1.22) into the transport term definitions (1.18)–(1.20) yields zero heat flux and diffusion velocities ($\mathbf{q} = \mathbf{V}_{ci} = 0$), and the stress tensor in the form $\mathbf{P} = p\mathbf{I}$, with the pressure p and the unit tensor $\mathbf{I}$. The set of governing equations is reduced to the Euler equations coupled to the equations of chemical-vibrational kinetics for each vibrational state population.

The closure of governing equations (1.32)–(1.34) in the first-order approximation of the generalized Chapman–Enskog method is carried out substituting distribution function (1.30) into the definitions of the transport and production terms. Thus, the following constitutive relations are obtained [9]:

$$\mathbf{P} = (p - \zeta\nabla\cdot\mathbf{v} - p_{\rm rel})\mathbf{I} - 2\mu\mathbf{S}, \tag{1.35}$$

$$\mathbf{V}_{ci} = -\sum_{dk} D_{cidk}\mathbf{d}_{dk} - D_{T,ci}\nabla\ln T, \tag{1.36}$$

$$\mathbf{q} = -\lambda'\nabla T - p\sum_{ci} D_{T,ci}\mathbf{d}_{ci} + \sum_{ci} n_{ci}\mathbf{V}_{ci}\left(\frac{5}{2}kT + \langle\varepsilon_j^{ci}\rangle_{\rm rot} + \varepsilon_i^c + \varepsilon_c\right), \tag{1.37}$$

where μ and ζ are shear and bulk viscosity coefficients, $p_{\rm rel}$ is the relaxation (dynamic) pressure, $\mathbf{S}$ is the traceless symmetric part of the strain rate tensor, λ' is the partial thermal conductivity coefficient of translational and rotational degrees of freedom, D_{cidk} and $D_{T,ci}$ are multi-component state-specific diffusion and thermal diffusion coefficients. The peculiarity of mass and energy transfer in the STS approach is that diffusion of vibrational energy is governed by the gradients of vibrational level populations and thus does not rely on any quasi-stationary vibrational distributions. Thermal conductivity and bulk viscosity coefficients include contributions of rotational energy but do not depend on the vibrational energy, whose transport is driven by the diffusion of vibrational states.

Using expansions (1.25)–(1.29) one can rewrite the above constitutive relations in terms of the expansion coefficients:

$$\mathbf{P} = p\mathbf{I} - kT\sum_{ci}\frac{n_{ci}}{n}\left[b_{ci,0}\mathbf{S} - (f_{ci,10}\nabla\cdot\mathbf{v} + g_{ci,10})\mathbf{I}\right], \tag{1.38}$$

$$\mathbf{V}_{ci} = -\frac{1}{2n}\left(\sum_{dk} d^{dk}_{ci,0}\mathbf{d}_{dk} - a_{ci,00}\nabla\ln T\right), \tag{1.39}$$

$$\begin{aligned}\mathbf{q} = -\sum_{ci}\frac{n_{ci}}{n}\Bigg[&\left(\frac{5}{4}ka_{ci,10} + \frac{m_c}{2}c_{\mathrm{rot},ci}a_{ci,01}\right)\nabla T - \frac{p}{2n_{ci}}a_{ci,00}\mathbf{d}_{ci}\\ &+\frac{1}{2}\left(\sum_{dk} d^{dk}_{ci,0}\mathbf{d}_{dk} - a_{ci,00}\nabla\ln T\right)\left(\frac{5}{2}kT + \langle\varepsilon^{ci}_j\rangle_{\mathrm{rot}} + \varepsilon^c_i + \varepsilon_c\right)\Bigg].\end{aligned} \tag{1.40}$$

In the above expressions, $c_{\mathrm{rot},ci}$ is the rotational specific heat depending on the vibrational state. Note that the first-order production terms in Eq. (1.32) are also connected to the normal mean stress and can be expressed in terms of the expansion coefficients $f_{ci,rp}$ and $g_{ci,rp}$, see [114; 115].

The transport coefficients are functions of the expansion coefficients:

$$D_{cidk} = \frac{1}{2n}d^{dk}_{ci,0}; \tag{1.41}$$

$$D_{T,ci} = -\frac{1}{2n}a_{ci,00}; \tag{1.42}$$

$$\begin{aligned}\lambda' &= \sum_{ci}\frac{n_{ci}}{n}\left(\frac{5}{4}ka_{ci,10} + \frac{m_c}{2}c_{\mathrm{rot},ci}a_{ci,01}\right)\\ &= \sum_{ci}\frac{n_{ci}}{n}\left(\lambda'_{ci,\mathrm{tr}} + \lambda_{ci,\mathrm{rot}}\right) = \sum_{ci}\frac{n_{ci}}{n}\lambda'_{ci};\end{aligned} \tag{1.43}$$

$$\mu = \sum_{ci}\frac{n_{ci}}{n}\frac{kT}{2}b_{ci,0} = \sum_{ci}\frac{n_{ci}}{n}\mu_{ci}; \tag{1.44}$$

$$\zeta = -\sum_{ci}\frac{n_{ci}}{n}kTf_{ci,10} = \sum_{ci}\frac{n_{ci}}{n}\zeta_{ci}; \tag{1.45}$$

$$p_{rel} = -\sum_{ci}\frac{n_{ci}}{n}kTg_{ci,10} = \sum_{ci}\frac{n_{ci}}{n}p_{\mathrm{rel},ci}. \tag{1.46}$$

For the convenience, the effective transport coefficients λ'_{ci}, μ_{ci}, ζ_{ci}, $p_{\mathrm{rel},ci}$ have been defined here, which are not the true mixture transport coefficients but are needed

to facilitate physical interpretation of the boundary conditions. Note that thermal diffusion coefficients $D_{T,ci}$ can be expressed also in terms of coefficients $d^{dk}_{ci,1}$ instead of $a_{ci,00}$; both formulations are equivalent [116].

The procedure for evaluating expansion coefficients $a_{ci,rp}$, $d^{dk}_{ci,r}$, $b_{ci,r}$, $f_{ci,rp}$, $g_{ci,rp}$ is described in detail in [9], where the transport linear systems are derived. The efficient algorithms for evaluating these coefficients in dilute polyatomic gas mixtures using advanced computational methods can be found in [117]. Solution of these systems requires knowledge of the collision integrals depending on the cross sections of rapid processes and rotational energy relaxation times. State-resolved algorithms developed in [9; 41] are implemented in the software KAPPA [118] for air species and therefore, in further derivation, it will be assumed that the expansion coefficients are known functions of temperature, vibrational state, and mixture composition.

Concluding this section, it is worth emphasizing that at this step, a closed set of extended fluid-dynamic equations in both inviscid and viscous flow approximations, constitutive relations for the transport terms and expressions for the transport coefficients have been defined. These sets of governing equations at the present work are complemented by the thermally perfect gas equation of state ($p = nkT$) and calorically non-perfect gas model assuming explicit computation of the specific energy as a function of T and non-equilibrium vibrational level populations n_{ci} (1.13). The next step is to specify the boundary conditions for the set of macroscopic variables n_{ci}, $\mathbf{v}$, T.

1.2 Boundary conditions on a partially catalytic surface by the Grad's technique

In the present section, the boundary conditions on the external edge of the Knudsen layer are obtained using Grad's technique. Initially, the technique has been proposed for a singe-component gas without internal degrees of freedom and non-equilibrium chemical reactions [80]. In the study performed by Zade *et al.* [82] the approach has been applied for a multi-component gas mixture. Here the approach is applied for a gas mixture with internal degrees of freedom and STS coupled vibrational-chemical kinetics. In the present section, the specular-diffusive scattering model of particles interaction with the solid wall is considered as well. The calculation

procedure for the slip/jump equations is considered in detail, which allows one to apply the technique for other models of the gas flows.

In order to apply the technique, the distribution function of reflected particles f^+ should be expressed in terms of the distribution function of incident particles f^-. For the Maxwell model and in the case of partial catalytic wall, f^+ can be written as [88]:

$$f^+_{cij}(\mathbf{r},\mathbf{u}_c,t) = (1-\sigma_{ci})f^-_{cij}(\mathbf{r},\mathbf{u}_c - 2u_{cn}\mathbf{n},t) + (\sigma_{ci}-\gamma_{ci})f^{(0),w}_{cij}, \tag{1.47}$$

$$f^{(0),w}_{cij} = \frac{n^w_{ci}s^{ci}_j}{Z_{\mathrm{rot},ci}}\left(\frac{m_c}{2\pi k T^w}\right)^{3/2}\exp\left(-\frac{m_c u_c^2}{2kT^w} - \frac{\varepsilon^{ci}_j}{kT^w}\right). \tag{1.48}$$

Here $f^+_{cij}(\mathbf{r},\mathbf{u}_c,t)$, $f^-_{cij}(\mathbf{r},\mathbf{u}_c,t)$ are distribution functions of incident and reflected particles; $\mathbf{u}_c$ is the velocity of reflected particle; u_{cn} is the normal component of velocity ($u_{cn} > 0$); $\mathbf{n}$ is the normal to the surface; T^w is the wall temperature; n^w_{ci} is the number density of molecules of species ci prior to chemical reactions on the surface; γ_{ci} is the state-resolved extended recombination coefficient for the formation of a chemical species c in the vibrational state i; σ_{ci} is the accommodation coefficient for ci species, which represents the fraction of particles of ci species that are diffusely reflected. Relation (1.47), when reduced to the one-temperature approximation, corresponds to those in works [80; 82]. In Eq. (1.47), coordinates $\mathbf{r}$ of distribution functions of reflected and incident particles are assumed to be positioned at the external edge of the Knudsen layer.

The extended recombination coefficient γ_{ci} of ci species is defined as the fractions that are involved in recombination ($\gamma_{ci} < 0$), dissociation ($\gamma_{ci} > 0$) reactions or VT and VV energy transitions on the wall. The formal naming of this coefficient as the "recombination coefficient"follows from works of Scott [43; 93], and work [82], where this coefficient also describes heterogeneous recombination and dissociation. However, in the present study γ_{ci} is responsible not only for chemical reactions but also for the vibrational energy transitions. The coefficient can be written in terms of the normal to the surface mass flux of recombining/dissociating (involved in vibrational deactivation/excitation) reflected molecules of ci species F^w_{ci} and the normal to the surface mass flux of incident molecules of ci species F'_{ci}:

$$\gamma_{ci} = \frac{F^w_{ci}}{F'_{ci}}. \tag{1.49}$$

The first term in the f^+ expression (1.47) is responsible for specular reflection, whereas the second is associated with diffusive reflection with the local equilibrium

Maxwell–Boltzmann distribution (1.48). Because of the mechanism of specular-diffusive particles reflection, it is assumed that only diffusely reflected particles can react on the surface.

1.2.1 Technique description

To obtain the boundary conditions using the Grad's approach, one should multiply the distribution function of reflected particles by the corresponding microscopic characteristics and integrate over the half-space $u_{cn} > 0$. The procedure is conducted under the assumption that the distribution function variations are small in the Knudsen layer, thus the fluxes of mass, momentum and energy are constant. The microscopic characteristics are connected with the independent collision invariants of rapid processes (1.8), (1.9). The obtained equations represent the balance of mass, momentum and energy normal fluxes near the solid surface. Here, the distribution function in the form of Eq. (1.47) is considered and the summation over internal energy levels and chemical species (or rotational states, for the vibrational level populations) is carried out.

Before rigorously applying the procedure, it is necessary to include some discussion regarding the positioning of distribution functions in Eq. (1.47), and, consequently, the slip boundary conditions, at the outer boundary of the Knudsen layer. In the procedure, the first-order generalized Chapman–Enskog method distribution function is applied. This distribution function cannot describe the particles distribution in the layer due to non-equilibrium gas behavior and the nonlinear stress/strain-rate relation. Nevertheless, the first-order distribution can be considered in the bulk outer flow, and near the external edge of the layer for gases in the slip regime. Furthermore, in the presence of heterogeneous reactions, the incident and reflected particles distributions cannot be assumed to be the same in the layer. However, outside the layer, the distribution of gas species resulting from surface recombination/dissociation and vibrational deactivation/excitation can be considered as a local non-equilibrium.

All of these restrictions make it impossible to apply the Grad's technique in the case of the above-mentioned assumptions and heterogeneous processes. Nonetheless, if the spatial coordinates in Eq. (1.47) are taken outside the Knudsen layer, then the

technique can be applied, and the resulting slip boundary conditions will capture the physical effects of gas-surface interactions and heterogeneous reactions.

In the Grad's approach it is assumed that the normal component of the macroscopic velocity, v_n, is equal to zero near the solid wall [80]. To obtain the relations for the wall number densities n_{ci}^w, it is assumed that prior to chemical reactions, the fraction of recombining/deactivating particles is equal to zero, which is equivalent to recombination coefficients being equal to zero. The latter assumption leads to zero values of normal components of diffusion velocity:

$$\begin{aligned} n_{ci}V_{ci,n} =& \sum_j \int (u_{cn} - v_n) f_{cij} \mathrm{d}\mathbf{u}_c = \sum_j \int\limits_{u_{cn}>0} u_{cn} f_{cij}^{+}(\mathbf{u}_c) \mathrm{d}\mathbf{u}_c \\ &+ \sum_j \int\limits_{u'_{cn}<0} u'_{cn} f_{cij}^{-}(\mathbf{u}'_c) \mathrm{d}\mathbf{u}_c = -\sum_j (1-\sigma_{ci}) \int\limits_{u'_{cn}<0} u'_{cn} f_{cij}^{-} \mathrm{d}\mathbf{u}'_c \\ &+ \sum_j \sigma_{ci} \int\limits_{u_{cn}>0} u_{cn} f_{cij}^{(0),w} \mathrm{d}\mathbf{u}_c + \sum_j \int\limits_{u'_{cn}<0} u'_{cn} f_{cij}^{-} \mathrm{d}\mathbf{u}_c \\ &= \sum_j \sigma_{ci} \int\limits_{u'_{cn}<0} u'_{cn} f_{cij}^{-} \mathrm{d}\mathbf{u}'_c + \sum_j \sigma_{ci} \int\limits_{u_{cn}>0} u_{cn} f_{cij}^{(0),w} \mathrm{d}\mathbf{u}_c \\ &= \sigma_{ci} \left[\sum_j \int\limits_{u'_{cn}<0} u'_{cn} f_{cij}^{-} \mathrm{d}\mathbf{u}'_c + n_{ci}^w \sqrt{\frac{kT^w}{2\pi m_c}} \right] = 0, \end{aligned} \tag{1.50}$$

where $\mathbf{u}'_c$ is the velocity of incident particle. From the above relation the expression for the wall number density of ci species n_{ci}^w can be written as follows

$$n_{ci}^w = -\sqrt{\frac{2\pi m_c}{kT^w}} \sum_j \int\limits_{u'_{cn}<0} u'_{cn} f_{cij}^{-} \mathrm{d}\mathbf{u}'_c. \tag{1.51}$$

The above equation for n_{ci}^w is similar to the common expression [44; 80] for the case when internal degrees of freedom are not considered (summation over j is additional).

The number densities on the wall coincide with the number densities of incident particles n'_{ci}, if normal component of the incident diffusion velocity is equal to zero and normal component of macroscopic incident velocity $\mathbf{v}'$ ($v'_n < 0$) is the mean

thermal velocity with the wall temperature:

$$v'_n = -\sqrt{\frac{kT^w}{2\pi m_c}}; \tag{1.52}$$

$$V'_{ci,n} = 0. \tag{1.53}$$

1.2.2 Concentration jump

When considering chemical reactions on the surface, the typical mass flux equal to zero relations for each species are no longer valid. Consequently, the boundary conditions for number densities that can capture the influence of heterogeneous reactions are required. Such conditions are commonly referred to as the «concentration jump». Quantitatively it can be represented through the ratio of number densities n_{ci} on the external edge of the Knudsen layer and the number densities on the wall n^w_{ci}, n_{ci}/n^w_{ci}, and the transport coefficients along with the gradients of macroscopic parameters [93]. Following the described technique, with corresponding microscopic characteristic as the normal component of momentum $m_c u_{cn}$, the general equation for the concentration jump of ci species for the Maxwell model of gas-surface interaction is derived:

$$\begin{aligned}\sum_j \int\limits_{u_{cn}>0} u_{cn} f^+_{cij}(\mathbf{u}_c)\mathrm{d}\mathbf{u}_c = &-(1-\sigma_{ci})\sum_j \int\limits_{u'_{cn}<0} u'_{cn} f^-_{cij}(\mathbf{u}_c)\mathrm{d}\mathbf{u}'_c \\ &+ (\sigma_{ci}-\gamma_{ci})\sum_j \int\limits_{u_{cn}>0} u_{cn} f^{(0),w}_{cij}\mathrm{d}\mathbf{u}_c.\end{aligned} \tag{1.54}$$

Another common way to obtain the concentration jump equation is connected with the net mass flux F_{ci} of reflected particles [43; 82; 93]. In the state-to-state approach it can be written as:

$$F_{ci} = \sum_j m_c \int\limits_{u_{cn}>0} u_{cn}\left(f^+_{cij}(\mathbf{u}_c) - f^-_{cij}(\mathbf{u}_c - 2u_{cn}\mathbf{n})\right)\mathrm{d}\mathbf{u}_c. \tag{1.55}$$

F_{ci} represents the mass flux of recombined/dissociated or vibrationally excited/deactivated molecules of ci species. For gas particles that are not involved in recombination/dissociation reactions or VT and VV energy transitions ($\gamma_{ci} = 0$)

it turns to zero. On the other hand, F_{ci} can be determined as a normal component of the diffusion flux $\rho_{ci}\mathbf{V}_{ci}\cdot\ \mathbf{n}$. Thus, another form of the concentration jump equation for ci species can be written as follows:

$$\sum_j \int\limits_{u_{cn}>0} u_{cn}\left(f^+_{cij}(\mathbf{u}_c) - f^-_{cij}(\mathbf{u}_c - 2u_{cn}\mathbf{n})\right)\mathrm{d}\mathbf{u}_c = n_{ci}\mathbf{V}_{ci}\cdot\ \mathbf{n}. \tag{1.56}$$

Based on the above expression for the distribution function (1.30) and first-order diffusion velocity in the STS approach (1.39), both equations (1.54) and (1.56) can be written in terms of the expansion coefficients in the following form:

$$\begin{aligned}\frac{n^w_{ci}}{n_{ci}}\sqrt{\frac{T^w}{T}} =& \frac{\sigma_{ci}}{\sigma_{ci}-\gamma_{ci}}\left(1 - \frac{1}{2n}b_{ci,0}\,S_{nn} + \frac{1}{2n}\left(f_{ci,10}\nabla\cdot\mathbf{v} + g_{ci,10}\right)\right)\\ &+ \frac{2-\sigma_{ci}}{2(\sigma_{ci}-\gamma_{ci})n}\sqrt{\frac{\pi m_c}{2kT}}\left(a_{ci,00}\frac{\partial \ln T}{\partial n} - \sum_{dk} d^{dk}_{ci,0}\mathbf{d}_{dk}\cdot\mathbf{n}\right),\end{aligned} \tag{1.57}$$

here $c = 1,\ldots,L$, $i = 0,\ldots,N_c$ and $S_{nn} = \frac{\partial v_n}{\partial n} - \frac{\nabla\cdot\mathbf{v}}{3}$.

The analysis of the above equations shows that all the expansion coefficients in (1.38)–(1.40), except for those, that are connected with the thermal conductivity, contribute to the equations for number densities on the surface, as well as the temperature jump T/T^w. The first part in the right-hand side of the above equations corresponds to the contribution of the shear and normal mean stress (viscosity, bulk viscosity and relaxation pressure), while the second part is proportional to the diffusion velocity. The terms $f_{ci,10}$ and $g_{ci,10}$ connected with the effective bulk viscosity and relaxation pressure coefficients have been found in the concentration jump for the first time. It is also worth mentioning that these terms depend on the effects of slow processes on transport properties in the gas phase, confirming the development of a closed problem statement.

1.2.3 Velocity slip

The expression for the macroscopic velocity in the direction $\boldsymbol{\tau}_1$ in the tangent plane can be found by multiplying (1.47) by $m_c u_{cn} c_{c\tau_1}$; integrating over the half-space of the velocity $u_{cn} > 0$; and summing over rotational and vibrational energy

levels and chemical species:

$$\sum_{cij} m_c \int\limits_{u_{cn}>0} u_{cn} c_{c\tau_1} f^{+}_{cij}(\mathbf{u}_c)\mathrm{d}\mathbf{u}_c = -\sum_{cij} m_c(1-\sigma_{ci}) \int\limits_{u'_{cn}<0} u'_{cn} c_{c\tau_1} f^{-}_{cij}(\mathbf{u}_c)\mathrm{d}\mathbf{u}'_c + \sum_{cij} m_c(\sigma_{ci}-\gamma_{ci}) m_c \int\limits_{u_{cn}>0} u_{cn} c_{c\tau_1} f^{(0),w}_{cij}\mathrm{d}\mathbf{u}_c. \tag{1.58}$$

Substituting the distribution function (1.23) into above expression, the velocity slip v_1 (velocity component in the direction $\boldsymbol{\tau_1}$) is obtained in the form:

$$\sqrt{\frac{T^w}{T}} \sum_{ci} n^w_{ci} \sqrt{m_c}(\sigma_{ci}-\gamma_{ci}) v_1 = \sum_{ci} \frac{n_{ci}}{2n} \left[(2-\sigma_{ci}) \sqrt{\frac{\pi k T}{2}}\, b_{ci,0}\, S_{1n} - \sigma_{ci}\sqrt{m_c} \left(\frac{2a_{ci,00} - a_{ci,10}}{2} \frac{\partial \ln T}{\partial \tau_1} - \sum_{dk} d^{dk}_{ci,0} \mathbf{d}_{dk} \cdot \boldsymbol{\tau}_1 \right) \right]. \tag{1.59}$$

The left-hand side of the above relation represents the analogy of the mass flux of diffusely reflected and recombined/dissociated particles with macroscopic gas velocity v_1. The first term in the right-hand side is connected with the shear viscosity and is proportional to the component of the deformation rate tensor $S_{1n} = \frac{\partial v_1}{\partial n} + \frac{\partial v_n}{\partial \tau_1}$. The second term is the analogy of the $\boldsymbol{\tau}_1$ component of diffusion mass flux and the term, connected with translational thermal conductivity λ'_{tr}, associated with the elastic collisions energy exchanges. Rotational thermal conductivity coefficient λ_{rot}, responsible for the energy transfer associated with inelastic translational-rotational (TR) and rotational-rotational (RR) energy exchanges, does not contribute to the velocity slip expression.

Equation (1.59) can be simplified, if number densities on the wall are excluded. Taking into account (1.57), the following expression for the velocity component in the direction $\boldsymbol{\tau}_1$ is obtained:

$$v_1 = \frac{\sqrt{\frac{\pi k T}{2}} \sum\limits_{ci} (2-\sigma_{ci}) \frac{n_{ci}}{2n} b_{ci,0} S_{1n} - \sum\limits_{ci} \sigma_{ci} \frac{n_{ci}}{2n} \sqrt{m_c}\, \boldsymbol{X}_{ci,1} \cdot \boldsymbol{\tau}_1}{-\sqrt{\frac{\pi}{2kT}} \sum\limits_{ci} (2-\sigma_{ci}) \frac{m_c n_{ci}}{2n} \left(a_{ci,00} \frac{\partial \ln T}{\partial n} - \sum\limits_{dk} d^{dk}_{ci,0} \mathbf{d}_{dk} \cdot \boldsymbol{n} \right) + X_2}, \tag{1.60а}$$

$$\boldsymbol{X}_{ci,1} = \left(a_{ci,00} - \tfrac{a_{ci,10}}{2} \right) \nabla \ln T - \sum_{dk} d^{dk}_{ci,0} \mathbf{d}_{dk}; \tag{1.60б}$$

$$X_2 = \sum_{ci} \sigma_{ci} \tfrac{n_{ci}\sqrt{m_c}}{2n} \left(2n - b_{ci,0} S_{nn} + f_{ci,10} \nabla \cdot \mathbf{v} + g_{ci,10} \right). \tag{1.60в}$$

Similarly, the expression for v_2 (velocity component in the direction $\boldsymbol{\tau_2}$) can be derived:

$$v_2 = \frac{\sqrt{\frac{\pi kT}{2}} \sum\limits_{ci} (2 - \sigma_{ci}) \, \frac{n_{ci}}{2n} b_{ci,0} S_{2n} - \sum\limits_{ci} \sigma_{ci} \, \frac{n_{ci}}{2n} \sqrt{m_c} \, \boldsymbol{X}_{ci,1} \cdot \boldsymbol{\tau}_2}{-\sqrt{\frac{\pi}{2kT}} \sum\limits_{ci} (2 - \sigma_{ci}) \, \frac{m_c n_{ci}}{2n} \left(a_{ci,00} \frac{\partial \ln T}{\partial n} - \sum\limits_{dk} d^{dk}_{ci,0} \mathbf{d}_{dk} \cdot \boldsymbol{n} \right) + X_2}. \tag{1.61}$$

It can be seen that velocity slip expressions (1.60) and (1.61), unlike the concentration jump, do not explicitly depend on the recombination coefficients. Both Eqs. (1.60) and (1.61) depend on the shear and bulk viscosity coefficients, relaxation pressure, diffusion velocity of vibrational states and the component of the heat flux responsible for the transport of translational energy.

1.2.4 Temperature jump

The expression for the gas temperature T on the external edge of the Knudsen layer can be obtained by the similar procedure. The microscopic characteristic is represented by the total energy of a particle $u_{cn}(m_c c_c^2/2 + \varepsilon_j^{ci} + \varepsilon_i^c + \varepsilon_c)$. Following the Grad's technique:

$$\begin{aligned} &\sum_{cij} \int\limits_{u_{cn}>0} \left(\frac{m_c c_c^2}{2} + \varepsilon_j^{ci} + \varepsilon_i^c + \varepsilon_c \right) u_{cn} f_{cij}^{+} \mathrm{d}\mathbf{u}_c \\ &\qquad = -\sum_{cij} (1 - \sigma_{ci}) \int\limits_{u'_{cn}<0} \left(\frac{m_c c_c^2}{2} + \varepsilon_j^{ci} + \varepsilon_i^c + \varepsilon_c \right) u'_{cn} f_{cij}^{-} \mathrm{d}\mathbf{u}'_c \\ &\qquad\quad + \sum_{cij} (\sigma_{ci} - \gamma_{ci}) \int\limits_{u_{cn}>0} \left(\frac{m_c c_c^2}{2} + \varepsilon_j^{ci} + \varepsilon_i^c + \varepsilon_c \right) u_{cn} f_{cij}^{(0),w} \mathrm{d}\mathbf{u}_c. \end{aligned} \tag{1.62}$$

The above equation accounts for the influence of the internal energy on the temperature jump. For the first-order distribution function, with excluded number

densities on the wall, the following relation is obtained:

$$\frac{T}{T^w} = \frac{\sum\limits_{ci}(2-\sigma_{ci})\,\frac{n_{ci}}{n}\left(1+\frac{m_c v^2}{4kT^w}\right)\left(a_{ci,00}\frac{\partial \ln T}{\partial n} - \sum\limits_{dk} d^{dk}_{ci,0}\mathbf{d}_{dk}\cdot\mathbf{n}\right) + \sqrt{\frac{2kT}{\pi}}Y_1}{\sum\limits_{ci}\frac{5(2-\sigma_{ci})n_{ci}}{4n}\left(a_{ci,00}\frac{\partial \ln T}{\partial n} - \sum\limits_{dk} d^{dk}_{ci,0}\mathbf{d}_{dk}\cdot\mathbf{n}\right) - \frac{Y_3}{k}\frac{\partial \ln T}{\partial n} + \sqrt{\frac{2kT}{\pi}}(Y_2+Y_4)}, \tag{1.63а}$$

$$Y_1 = \sum_{ci}\sigma_{ci}\,\frac{n_{ci}}{n\sqrt{m_c}}\left(1+\frac{m_c v^2}{4kT^w}\right)\cdot(2n - b_{ci,0}S_{nn} + f_{ci,10}\nabla\cdot\mathbf{v} + g_{ci,10})\,; \tag{1.63б}$$

$$Y_2 = \sum_{ci}\sigma_{ci}\,\frac{n_{ci}}{n}\,\sqrt{m_c}\,\frac{c_{\mathrm{rot},ci}}{k}(f_{ci,01}\nabla\cdot\mathbf{v} + g_{ci,01}); \tag{1.63в}$$

$$Y_3 = \sum_{ci}(2-\sigma_{ci})\,\frac{n_{ci}}{2n}\left(\frac{5}{2}\,k a_{ci,10} + m_c c_{\mathrm{rot},ci} a_{ci,01}\right); \tag{1.63г}$$

$$Y_4 = \sum_{ci}\frac{3\sigma_{ci}n_{ci}}{n\sqrt{m_c}}\left(\frac{2n}{3} - \frac{b_{ci,0}}{2}S_{nn} + f_{ci,10}\nabla\cdot\mathbf{v} + g_{i,10}\right). \tag{1.63д}$$

The temperature jump, as well as the velocity slip, depend on the accommodation coefficients and does not include recombination coefficients. The expression also depend on all the expansion coefficients in (1.38)–(1.40). Thus, the contribution of surface reactions to the velocity slip and temperature jump is not explicit. Such implicit dependence on heterogeneous processes in the temperature and velocity expressions at the wall is connected to the fact that these macroparameters are defined by rapid processes, forming local equilibrium. Otherwise, the macroparameters would depend explicitly on heterogeneous processes.

The appearance of term (1.63в) and the second part of the term (1.63г) is associated with included rotational energy. The vibrational energy and the energy of formation do not explicitly contribute to the temperature jump. It is worth noting that the first attempt to account for the influence of the internal degrees of freedom for the multi-component gas mixture was made in Ref. [82]. In order to account for such an influence, the additional terms were included to the fluxes of translational energy. The additional terms consisted of mass fluxes of incident (or reflected) species, multiplied by the average internal energy carried by each molecule. However, it was done inconsistently since the contributions of internal energy appear neither in the first-order distribution function nor in the heat flux and normal stress. Therefore, no internal thermal conductivity and bulk viscosity arise in the temperature jump.

1.2.5 Discussion of the obtained slip/jump equations

The boundary conditions for number densities, velocity and temperature outside the Knudsen layer are obtained for the Maxwell model of particles scattering by the solid wall. The equations can be reduced to previously obtained expressions [43; 82; 93], if internal states of particles and slow processes are not taken into account. In this case the first-order distribution function for the particles of c chemical species can be written in the conventional form [116]:

$$f_c = f_c^{(0)} \left[1 - \frac{1}{n} \left[\mathbf{A}_c \cdot \nabla \ln T + \sum_d \mathbf{D}_c^d \cdot \mathbf{d}_d + \mathbf{B}_c : \nabla \mathbf{v} \right] \right], \tag{1.64}$$

$$f_c^{(0)} = n_c \left(\frac{m_c}{2\pi k T} \right)^{3/2} \exp\left(-\frac{m_c c_c^2}{2kT} \right). \tag{1.65}$$

For the functions $\mathbf{A}_c$, $\mathbf{D}_c^d$, $\mathbf{B}_c$ the following expansions in the series of Sonine polynomials $S_\nu^{(r)}$ are proposed [9]:

$$\mathbf{A}_c = -\frac{m_c \mathbf{c}_c}{2kT} \sum_r a_{c,r} S_{3/2}^{(r)}, \tag{1.66}$$

$$\mathbf{D}_c^d = \frac{m_c \mathbf{c}_c}{2kT} \sum_r d_{c,r}^d S_{3/2}^{(r)}, \tag{1.67}$$

$$\mathbf{B}_c = \frac{m_c}{2kT} \left(\mathbf{c}_c \mathbf{c}_c - \frac{1}{3} c_c^2 \mathbf{I} \right) \sum_r b_{c,r} S_{5/2}^{(r)}. \tag{1.68}$$

Considering only the first terms in the above expansions, the distribution function (1.64) is in the form

$$\begin{aligned} f_c = f_c^{(0)} \Bigg[1 + \frac{m_c \mathbf{c}_c}{2nkT} \cdot \left(a_{c,0} + a_{c,1} \left(\frac{5}{2} - \frac{m_c c_c^2}{2kT} \right) \right) \nabla T \\ - \frac{m_c \mathbf{c}_c}{2nkT} \cdot \sum_d d_{c,0}^d \mathbf{d}_d - \frac{m_c b_{c,0}}{2nkT} \left(\mathbf{c}_c \mathbf{c}_c : \nabla \mathbf{v} - \frac{1}{3} c_c^2 \nabla \cdot \mathbf{v} \right) \Bigg]. \end{aligned} \tag{1.69}$$

For the distribution function (1.69), the set of equations (1.57), (1.60), (1.61) and (1.63) can be rewritten in the form:

$$\begin{aligned}\frac{n_c^w}{n_c}\sqrt{\frac{T^w}{T}} =& \frac{\sigma_c}{\sigma_c-\gamma_c}\left(1-\frac{1}{2n}b_{c,0}S_{nn}\right)\\ &+\frac{2-\sigma_c}{2(\sigma_c-\gamma_c)n}\sqrt{\frac{\pi m_c}{2kT}}\left(a_{c,0}\frac{\partial \ln T}{\partial n}-\sum_{dk} d_{c,0}^{dk}\mathbf{d}_{dk}\cdot\mathbf{n}\right).\end{aligned} \tag{1.70}$$

$$v_l = \frac{\sqrt{\frac{\pi kT}{2}}\sum\limits_c (2-\sigma_c)\,\frac{n_c}{2n}b_{c,0}S_{ln} - \bar{\mathbf{X}}_1\cdot\boldsymbol{\tau}_l}{\sqrt{\frac{\pi}{2kT}}\sum\limits_c \sigma_c\,\frac{m_c n_c}{2n}\left(a_{c,0}\frac{\partial \ln T}{\partial n}-\sum\limits_d d_{c,0}^d\mathbf{d}_{dk}\cdot\boldsymbol{n}\right)+\bar{X}_2},\quad l=1,2, \tag{1.71а}$$

$$\bar{\mathbf{X}}_1 = \sum_c \sigma_c\,\frac{n_c}{2n}\sqrt{m_c}\left(\left(a_{c,0}-\tfrac{a_{c,1}}{2}\right)\nabla\ln T-\sum_d d_{c,0}^d\mathbf{d}_d\right); \tag{1.71б}$$

$$\bar{X}_2 = \sum_c \sigma_c\,\frac{n_c}{2n}\sqrt{m_c}\,(2n-b_{c,0}S_{nn})\,. \tag{1.71в}$$

$$\frac{T}{T^w} = \frac{\sum\limits_c (2-\sigma_c)\,\frac{n_c}{n}\left(1+\frac{m_c v^2}{4kT^w}\right)\left(a_{c,0}\frac{\partial\ln T}{\partial n}-\sum\limits_d d_{c,0}^d\mathbf{d}_d\cdot\mathbf{n}\right)+\sqrt{\frac{2kT}{\pi}}\bar{Y}_1}{\sum\limits_c (2-\sigma_c)\,\frac{5n_c}{4n}\left(a_{c,0}\frac{\partial\ln T}{\partial n}-\sum\limits_d d_{c,0}^d\mathbf{d}_d\cdot\mathbf{n}\right)-\bar{Y}_2+\sqrt{\frac{2kT}{\pi}}\bar{Y}_3}, \tag{1.72а}$$

$$\bar{Y}_1 = \sum_c \sigma_c\,\frac{n_c}{n\sqrt{m_c}}\left(1+\frac{m_c v^2}{4kT^w}\right)\cdot(2n-b_{c,0}S_{nn})\,; \tag{1.72б}$$

$$\bar{Y}_2 = \sum_c (2-\sigma_c)\,\frac{5n_c}{4n}\,a_{c,1}\frac{\partial\ln T}{\partial n}; \tag{1.72в}$$

$$\bar{Y}_3 = \sum_c \sigma_c\,\frac{3n_{ci}}{2n\sqrt{m_c}}\,(4/3n-b_{c,0}S_{nn})\,. \tag{1.72г}$$

Here, $c = 1,\dots L$, and L is the number of chemical species. The equations (1.70)–(1.72) are written in the form, similar to the one, obtained in Ref. [82]. Differences appear only due to the chosen expansions of terms in distribution function (1.69) in the Sonine polynomials. Therefore, in the limit case of particles without internal modes and reactions, the approach yields the well-known solution.

The Grad's method provides a simple procedure to derive the slip/jump equations. Similar procedure can be carried out by the half-flux method, and the

slip conditions derived by both methods will be the same. However, the use of these methods leads to some issues. The first issue occurs due to including in the distribution function of reflected particles the number densities on the wall n_{ci}^w (or n_c^w). This terms have no clear physical meaning, and their calculation remains an open question. Additionally, these terms cause certain calculation difficulties when excluded from the velocity slip and the temperature jump expressions. Another issue is connected with the choice of velocity for microscopic characteristics. Common mistake is to chose peculiar velocity instead of particle velocity and opposite. Goniak and Duffa [119] have pointed out that in the half-flux method microscopic velocity $\mathbf{u}_c$ should be used in the definition of fluxes, while the reference velocity $\mathbf{c}_c$ should be used in Grad's technique. However, this mistake still can be found in recent works [95].

Both methods can be generalized for other models of particles scattering with solid surfaces if the distribution function of reflected particles allows expression in terms of distribution function of incident particles. For the processes accounting for surface inner geometry, such as adsorption and emission, the above procedure becomes rather complicated. In order to overcome these issues, a more rigorous approach based on the kinetic boundary condition is suggested. The following section is devoted to the formulation of the mentioned approach for the STS model.

1.3 Approach based on the kinetic boundary condition

In this section, the problem formulation for deriving slip conditions from kinetic boundary condition is introduced. The conditions are presented for the Maxwell scattering model.

1.3.1 Kinetic boundary condition in the STS approach

Assuming that a collision of a particle with the surface is a rapid process and, thereby, neglecting possible change in vibrational and chemical state, as a slow processes, the known kinetic boundary conditions for a gas mixture with rapid and

slow processes can be modified to the following form:

$$f^{+}_{cij}(\mathbf{r},\mathbf{u}_c,t)u_{cn}|_{u_{cn}>0} = -\sum_{l}\int\limits_{u'_{cn}<0} f^{-}_{cil}(\mathbf{r},\mathbf{u}'_c,t)u'_{cn}T^{cij}_{l}(\mathbf{u}_c,\mathbf{u}'_c)\mathrm{d}\mathbf{u}'_c, \tag{1.73}$$

where $T^{cij}_{l}(\mathbf{u}_c,\mathbf{u}'_c)$ is the scattering kernel, which represents the gas-solid body interaction model and is defined as a probability density function on the half-space $u_{cn} > 0$. $T^{cij}_{l}(\mathbf{u}_c,\mathbf{u}'_c)\mathrm{d}\mathbf{u}_c$ is the probability, that incident molecule in the cil state with $\mathbf{u}'_c$ velocity will be reflected in the cij state with $\mathbf{u}_c$ velocity in the interval $\mathrm{d}\mathbf{u}_c$. The spatial coordinate in the above kinetic boundary condition is assumed to be placed at the external edge of the Knudsen layer, as in the BC for distribution function of reflected particles (1.47).

The scattering kernel T^{cij}_{l} must satisfy the non-negativeness, reciprocity and normalization conditions [120; 121]. In the case of multi-component gas mixture with internal degrees of freedom the reciprocity and normalization conditions can be written as:

1. The reciprocity relation:

$$|u'_{cn}|f^{(0)}_{cil}(T^w)T^{cij}_{l}(\mathbf{u}_c,\mathbf{u}'_c) = |u_{cn}|f^{(0)}_{cij}(T^w)T^{cil}_{j}(-\mathbf{u}'_c,-\mathbf{u}_c). \tag{1.74}$$

The equation above states that if the gas mixture is in equilibrium with the surface, the incident and reflected molecules distribution is the local equilibrium Maxwell–Boltzmann distribution with the surface temperature T^w.

2. The normalization condition, which, without accounting for adsorption/desorption on the solid wall and, as well, processes with chemical reactions has the form:

$$\sum_{j}\int\limits_{u_{cn}>0} T^{cij}_{l}(\mathbf{u}_c,\mathbf{u}'_c)\mathrm{d}\mathbf{u}_c = 1. \tag{1.75}$$

If processes with chemical reactions are included, such as recombination/dissociation and VT/VV energy transitions, equation (1.75) is not valid. Similar expression can be introduced with the mentioned earlier extended recombination coefficient γ_{ci}:

$$\sum_{j}\int\limits_{u_{cn}>0} T^{cij}_{l}(\mathbf{u}_c,\mathbf{u}'_c)\mathrm{d}\mathbf{u}_c = 1-\gamma_{ci}. \tag{1.76}$$

From relation (1.76) it can be seen that the coefficient γ_{ci} should include all the processes that can change state of a particle of ci species. Therefore, the coefficient for each species is the sum of the coefficients γ^{p}_{ci} of surface processes ($\gamma_{ci} = \sum\gamma^{p}_{ci}$).

It is supposed that $\gamma_{ci}^{p} > 0$ if the particles of species ci change their vibrational or/and chemical state due to the p process; $\gamma_{ci}^{p} < 0$ if the particles of species ci are formed as a result of the p process.

Considering normalization condition (1.76) for the scattering kernel, the following relation for the normal component of macroscopic velocity is fulfilled

$$\begin{aligned}
\rho v_n &= \sum_{cij} m_c \int\limits_{u_{cn}>0} u_{cn} f_{cij}^{+} \mathrm{d}\mathbf{u}_c + \sum_{cij} m_c \int\limits_{u_{cn}<0} u_{cn} f_{cij}^{-} \mathrm{d}\mathbf{u}_c \\
&= -\sum_{cij} m_c \int\limits_{u_{cn}>0} \sum_{l} \int\limits_{u'_{cn}<0} u'_{cn} f_{cil}^{-} T_l^{cij} \mathrm{d}\mathbf{u}'_c + \sum_{cij} m_c \int\limits_{u_{cn}<0} u_{cn} f_{cij}^{-} \mathrm{d}\mathbf{u}_c \\
&= -\sum_{cil} m_c (1-\gamma_{ci}) \int\limits_{u'_{cn}<0} u'_{cn} f_{cil}^{-} \mathrm{d}\mathbf{u}'_c + \sum_{cil} m_c \int\limits_{u'_{cn}<0} u'_{cn} f_{cil}^{-} \mathrm{d}\mathbf{u}'_c \\
&= \sum_{cil} m_c \gamma_{ci} \int\limits_{u'_{cn}<0} u'_{cn} f_{cil}^{-} \mathrm{d}\mathbf{u}'_c.
\end{aligned} \tag{1.77}$$

One can notice that in the case of wall catalyticity being neglected, the velocity normal component is equal to zero. In the case of heterogeneous reactions, similarly to the Grad's approach, it is assumed that $v_n = 0$, which leads to the following expression:

$$\sum_{cil} m_c \gamma_{ci} \int\limits_{u'_{cn}<0} u'_{cn} f_{cil}^{-} \mathrm{d}\mathbf{u}'_c = 0. \tag{1.78}$$

The latter expression is valid, e.g., if the diffusion velocity normal component of all the incident particles along with the directed to the surface normal macroscopic velocity component are equal to zero. It can also be approximated as zero if these normal components are small, and the solid surface is a low-catalytic material. Nonetheless, this relation does not offer a clear physical interpretation. A more appropriate expression will be introduced in the subsequent chapter as a part of the extension of the present approach .

Boundary conditions for fluid-dynamic parameters can be obtained by the approach, similar to the generalized Chapman–Enskog method [9; 116]. For the gas with internal degrees of freedom in slip regime, kinetic boundary condition (1.73) is multiplied by the independent collision invariants $\psi_{cij}^{(\nu)}$ (1.8)–(1.9), then integrated over the half-space $u_{cn} > 0$ and summed over c,i,j. Summation for $\psi_{cij}^{(\nu+4)}$ (1.9) is only carried out over rotational energy levels j. The collision invariants depend on

the velocity of the particle $\mathbf{u}_c$, while corresponding microscopic characteristics in the Grad's approach on the peculiar velocity $\mathbf{c}_c$.

1.3.2 Specular-diffusive scattering kernel

For the specular-diffusive, or Maxwell, model of particle interaction with solid wall the scattering kernel has the following form:

$$T_l^{cij}(\mathbf{u}_c,\mathbf{u}_c') =(1-\sigma_{ci})\delta_{lj}\delta(\mathbf{u}_c'-\mathbf{u}_c+2u_{cn}\mathbf{n})+(\sigma_{ci}-\gamma_{ci}) \times\frac{2}{\pi}\left(\frac{m_c}{2kT}\right)^2\frac{s_j^{ci}}{Z_{\mathrm{rot},ci}(T^w)}\exp\left(-\frac{m_c u_c^2}{2kT^w}-\frac{\varepsilon_j^{ci}}{kT^w}\right)u_{cn}. \tag{1.79}$$

The first part of the kernel is responsible for the specular reflection, whereas the second corresponds to the diffusive reflection with the local equilibrium distribution. The kernel (1.79) satisfies relations (1.74) and (1.76).

It should be noted that expression (1.79), despite being appropriate generalization, still has a disadvantage in being unable to describe various mechanisms of rotational state change of a molecule due to the wall impinging. One of the possible ways to overcome this is to introduce the probabilities of rotational state change due to specular and diffusive scattering, depending on the wall temperature and solid wall characteristics.

Substituting scattering kernel (1.79) into kinetic boundary condition (1.73) divided by u_{cn}, and considering expression (1.51) for the wall number densities, the same expression for f^+ as in Eq. (1.47) is obtained.

1.3.3 Boundary conditions for number densities

In order to find the expressions for n_{ci}, the generalized Chapman—Enskog method for boundary condition (1.73) with the additional invariants of the most frequent collisions a_{ci} (1.9) is applied. As one can see, the approach provides the

relation for number densities independent of scattering model :

$$\begin{aligned}\sum_j \int\limits_{u_{cn}>0} u_{cn} f_{cij}^{+} \mathrm{d}\mathbf{u}_c &= -\sum_{j,l} \int\limits_{u_{cn}>0} \int\limits_{u'_{cn}<0} u'_{cn} f_{cil}^{-}(\mathbf{r},\mathbf{u}'_c,t) T_l^{cij}(\mathbf{u}_c,\mathbf{u}'_c)\mathrm{d}\mathbf{u}'_c \\ &= -(1-\gamma_{ci})\sum_l \int\limits_{u'_{cn}<0} u'_{cn} f_{cil}^{-}(\mathbf{r},\mathbf{u}'_c,t)\mathrm{d}\mathbf{u}'_c.\end{aligned} \tag{1.80}$$

Eq. (1.80) was obtained due to the normalization condition for kernel (1.76).

However, for a thorough comparison with the Grad's technique in the case of specular scattering, it is essential to employ the procedure that takes into account kernel form (1.79). This will lead to the following integral relation

$$\begin{aligned}\sum_j \int\limits_{u_{cn}>0} u_{cn} f_{cij}^{+} \mathrm{d}\mathbf{u}_c &= -(1-\sigma_{ci})\sum_j \int\limits_{u'_{cn}<0} u'_{cn} f_{cij}^{-}\mathrm{d}\mathbf{u}'_c \\ &\quad -(\sigma_{ci}-\gamma_{ci})\sum_l \int\limits_{u'_{cn}<0} u'_{cn} f_{cil}^{-}\mathrm{d}\mathbf{u}'_c.\end{aligned} \tag{1.81}$$

Substituting in the right-hand side of the above equations the number densities on the wall n_{ci}^w given by relations (1.51), as expected, Eq. (1.54) is derived:

$$\sum_l \int\limits_{u'_{cn}<0} u'_{cn} f_{cil}^{-}\mathrm{d}\mathbf{u}'_c = -n_{ci}^w\sqrt{\frac{kT^w}{2\pi m_c}} = -\sum_j \int\limits_{u_{cn}>0} u_{cn} f_{cij}^{(0),w}\mathrm{d}\mathbf{u}_c. \tag{1.82}$$

Thus the concentration jump, obtained by the second approach, can be written in the form (1.57). However, as is mentioned above, the equations with included number densities on the wall are not convenient for practical simulations. In order to exclude them, the same terms in the right hand side of (1.81) should be reduced, which obviously leads to Eq. (1.80). Substituting the distribution function to (1.80) yields the following boundary condition for number density of *ci* species:

$$\begin{aligned}\left(1-\frac{\gamma_{ci}}{2}\right)\frac{n_{ci}}{2n}\left(a_{ci,00}\frac{\partial \ln T}{\partial n} - \sum_{dk} d_{ci,0}^{dk}\mathbf{d}_{dk}\cdot\mathbf{n}\right) &= -\gamma_{ci} n_{ci}\sqrt{\frac{kT}{2\pi m_c}} \\ &\quad \times\left(1-\frac{1}{2n}b_{ci,0}S_{nn}+\frac{1}{2n}\left(f_{ci,10}\nabla\cdot\mathbf{v}+g_{ci,10}\right)\right).\end{aligned} \tag{1.83}$$

The above equation can also be derived from expression (1.57) with n_{ci}^w calculated from Eq. (1.51). The second approach gives the relations with no need for further

simplifications, connected with n_{ci}^w. It is obvious that similar situation occurs for both the velocity slip and temperature jump expressions. Equation (1.83) in the one-temperature approach correspond to relations previously obtained in studies [43; 82; 93]. In [82], the concentration jump equations are reduced to the expressions for number densities n_{ci} in terms of the expansion coefficients. The expressions are not valid due to the incorrect determination of the diffusion coefficients in terms of the expansion coefficients. The other two works report expressions similar to (1.83).

One can notice, that n_{ci} can be eliminated from (1.83). However, this expression can still be referred to as the boundary condition for number density due to the dependence of the diffusive driving force, $\mathbf{d}_{cik}$, on this macroparameter gradient. Besides that, n_{ci} is not excluded since the LHS of Eq. (1.83) includes the mass flux of ci species. As already mentioned, it is conventional to express the species boundary conditions in terms of these mass fluxes, and this would be done later in Sec. 1.4.

Thus, the inclusion of the ratio n_{ci}^w/n_{ci} with no exact physical meaning in (1.83) has been eliminated. As a result, designation of boundary conditions for number densities as the concentration jump equations is no longer appropriate. The conditions should be treated as the relations for number or mass fluxes of species, expressed in terms of molar fractions n_{ci}/n, temperature T, and velocity $\mathbf{v}$, along with their gradients.

1.3.4 Velocity slip and temperature jump

Expression for the velocity in the direction $\boldsymbol{\tau}_1$ can be derived when the independent collision invariant $m_c u_{c1}$ (1.8) is applied in the procedure. For the Maxwell model (1.79):

$$\sum_{cij} m_c \int\limits_{u_{cn}>0} u_{cn} u_{c1} f_{cij}^{+} \mathrm{d}\mathbf{u}_c = -\sum_{cij} m_c (1-\sigma_{ci}) \int\limits_{u'_{cn}<0} u'_{cn} u_{c1} f_{cij}^{-} \mathrm{d}\mathbf{u}'_c. \tag{1.84}$$

Despite the differences between the equations (1.58) and (1.84) for the velocity slip, expression (1.84) can be reduced to Eq. (1.58):

$$\begin{aligned}\sum_{cij} m_c \int\limits_{u_{cn}>0} u_{cn} c_{c1} f_{cij}^{+} \mathrm{d}\mathbf{u}_c + v_1 \sum_{cij} m_c \int\limits_{u_{cn}>0} u_{cn} f_{cij}^{+} \mathrm{d}\mathbf{u}_c \\ = -\sum_{cij} m_c (1-\sigma_{ci}) \int\limits_{u'_{cn}<0} u'_{cn} c_{c1} f_{cij}^{-} \mathrm{d}\mathbf{u}'_c \\ - v_1 \sum_{cij} m_c (1-\sigma_{ci}) \int\limits_{u'_{cn}<0} u'_{cn} f_{cij}^{-} \mathrm{d}\mathbf{u}'_c.\end{aligned} \tag{1.85}$$

Substituting expression (1.80) to the right-hand side of the above equation yields

$$\begin{aligned}\sum_{cij} m_c \int\limits_{u_{cn}>0} u_{cn} c_{c1} f_{cij}^{+} \mathrm{d}\mathbf{u}_c = v_1 \sum_{cij} m_c (\sigma_{ci} - \gamma_{ci}) \int\limits_{u'_{cn}<0} u'_{cn} f_{cij}^{-} \mathrm{d}\mathbf{u}'_c \\ - \sum_{cij} m_c (1-\sigma_{ci}) \int\limits_{u'_{cn}<0} u'_{cn} c_{c1} f_{cij}^{-} \mathrm{d}\mathbf{u}'_c.\end{aligned} \tag{1.86}$$

Due to relation (1.51), equation (1.86) coincides with (1.58). Another way to show that the expressions for velocity slip coincide is to integrate equation (1.84). When carrying out such a procedure, the expression (1.60) is obtained.

The relation for the velocity slip in the direction $\boldsymbol{\tau}_2$ can be obtained in the same way. The above procedure with $m_c u_{cn}$ as the independent collision invariant gives the boundary condition for pressure p. Since p is not in the set of independent fluid-dynamic variables required for a closed flow description, the pressure jump is not considered here.

Boundary condition for the gas temperature can be obtained from the following equation:

$$\begin{aligned}\sum_{cij} \int\limits_{u_{cn}>0} \left(\frac{m_c u_c^2}{2} + \varepsilon_j^{ci} + \varepsilon_i^c + \varepsilon_c \right) u_{cn} f_{cij}^{+} \mathrm{d}\mathbf{u}_c \\ = -\sum_{cij} (1-\sigma_{ci}) \int\limits_{u'_{cn}<0} \left(\frac{m_c u_c^2}{2} + \varepsilon_j^{ci} + \varepsilon_i^c + \varepsilon_c \right) u'_{cn} f_{cij}^{-} \mathrm{d}\mathbf{u}'_c \\ - \sum_{cij} (\sigma_{ci} - \gamma_{ci}) \left(2kT^w + \langle \varepsilon^{ci} \rangle_{rot} + \varepsilon_i^c + \varepsilon_c \right) \int\limits_{u'_{cn}<0} u'_{cn} f_{cij}^{-} \mathrm{d}\mathbf{u}'_c.\end{aligned} \tag{1.87}$$

Integration of the above equation yields (1.63). Another way to obtain the same expression is to reduce the equation (1.87) to (1.62). The procedure is the same as for the velocity slip expressions.

Therefore, the equivalence between the two approaches for the Maxwell model has been demonstrated. However, establishing a general equivalence for an arbitrary scattering kernel is complicated due to the unknown distribution function of reflected particles.

1.4 Further discussion and simplifications

In the previous sections it was shown that the obtained boundary conditions for the set of macroscopic parameters under some assumptions can be reduced to the ones obtained for a multi-component gas mixture in the one-temperature approach. Nonetheless, for practical applications considerable simplifications still have to be done. The initial step in this direction is to write the expressions in a more physical form.

1.4.1 Expressions in terms of transport coefficients

First, it is useful to rewrite equations (1.60), (1.61), (1.63) and (1.83) in terms of the effective transport coefficients and transport terms. Taking into account expressions (1.35)–(1.37) and (1.41)–(1.46), the boundary conditions can be rewritten in the following form

$$\mathbf{V}_{ci} \cdot \mathbf{n} = \frac{-\gamma_{ci}}{(2-\gamma_{ci}) n \sqrt{2\pi m_c k T}} \left(2p - 2\mu_{ci} S_{nn} - \zeta_{ci} \nabla \cdot \mathbf{v} - p_{\mathrm{rel},ci}\right), \tag{1.88}$$

$$v_l = \frac{\sqrt{\frac{2\pi}{kT}} \sum\limits_{ci} \frac{(2-\sigma_{ci})n_{ci}}{n} 2\mu_{ci} S_{ln} + X_1}{\sqrt{\frac{2\pi}{kT}} \sum\limits_{ci} \frac{\sigma_{ci} m_c n_{ci}}{2} \mathbf{V}_{ci} \cdot \mathbf{n} + \sum\limits_{ci} \frac{\sigma_{ci}\sqrt{m_c} n_{ci}}{2nkT} \left(2p - 2\mu_{ci} S_{nn} - \zeta_{ci} \nabla \cdot \mathbf{v} - p_{\mathrm{rel},ci}\right)}, \tag{1.89а}$$

$$X_1 = \sum_{ci} \sigma_{ci} n_{ci} \sqrt{m_c} \left(\left(D_{Tci} + \frac{\lambda'_{\mathrm{tr},ci}}{5kn} \right) \frac{\partial \ln T}{\partial \tau_l} + \sum_{dk} D_{cidk} \mathbf{d}_{dk} \cdot \boldsymbol{\tau}_l \right), \tag{1.89б}$$

$$\frac{T}{T^w} = \frac{\sum\limits_{ci} (2 - \sigma_{ci})\, n_{ci} \left(1 + \frac{m_c v^2}{4kT^w}\right) \mathbf{V}_{ci} \cdot \mathbf{n} + \sqrt{\frac{2}{\pi kT}} Y_1}{\sum\limits_{ci} (2 - \sigma_{ci})\, \frac{5n_{ci}}{4} \mathbf{V}_{ci} \cdot \mathbf{n} - \frac{Y_3}{2k} \frac{\partial \ln T}{\partial n} + \sqrt{\frac{2}{\pi kT}} (Y_2 + Y_4)}, \tag{1.90а}$$

$$Y_1 = \sum_{ci} \sigma_{ci}\, \frac{n_{ci}}{2n\sqrt{m_c}} \left(1 + \frac{m_c v^2}{4kT^w}\right) \left(2p - 2\mu_{ci} S_{nn} - \zeta_{ci} \nabla \cdot \mathbf{v} - p_{\mathrm{rel},ci}\right); \tag{1.90б}$$

$$Y_2 = \sum_{ci} \sigma_{ci}\, \frac{3n_{ci}}{2n\sqrt{m_c}} \left(2/3p - \mu_{ci} S_{nn} - \zeta_{ci} \nabla \cdot \mathbf{v} - p_{\mathrm{rel},ci}\right); \tag{1.90в}$$

$$Y_3 = \sum_{ci} (2 - \sigma_{ci})\, \frac{n_{ci}}{n} \left(\lambda'_{\mathrm{tr},ci} + \lambda_{\mathrm{rot},ci}\right); \tag{1.90г}$$

$$Y_4 = T \sum_{ci} \sigma_{ci}\, \frac{n_{ci}}{2n} \sqrt{m_c}\, \frac{c_{\mathrm{rot},ci}}{k} (f_{ci,01} \nabla \cdot \mathbf{v} + g_{ci,01}). \tag{1.90д}$$

Here, $c = 1,\ldots,L$, $i = 0,\ldots,N_c$, $l = 1,2$. From the above expressions, one can clearly see the contribution of various transport processes to the boundary conditions. It also should be noted that the expressions reduce to the common expressions in the zero-order approximation: $v = 0$, $T = T^w$ (in this case all the transport coefficients vanish).

It is common to express the boundary conditions for species concentrations in terms of the mass fluxes of the mixture component ci, $\mathbf{J}_{ci}$, which can be written in terms of the diffusion velocity:

$$\mathbf{J}_{ci} = \rho_{ci} \mathbf{V}_{ci}. \tag{1.91}$$

In such a case, the expression (1.88) for each species is transformed into the following formula:

$$\mathbf{J}_{ci} \cdot \mathbf{n} = \frac{-\gamma_{ci} \rho_{ci}}{(2 - \gamma_{ci}) n \sqrt{2\pi m_c kT}} \left(2p - 2\mu_{ci} S_{nn} - \zeta_{ci} \nabla \cdot \mathbf{v} - p_{\mathrm{rel},ci}\right). \tag{1.92}$$

Assuming that the accommodation coefficients are independent of the vibrational level and chemical species of a particle, the velocity slip (1.89) and temperature jump (1.90) equations can be written as follows

$$v_l = \frac{\sqrt{\frac{2\pi}{kT}}\frac{2-\sigma}{\sigma}\,2\mu S_{ln} - \sum\limits_{ci} n_{ci}\sqrt{m_c}\,\mathbf{V}_{ci}\cdot\boldsymbol{\tau}_l + \sum\limits_{ci}\frac{n_{ci}\sqrt{m_c}}{5kn}\lambda'_{\mathrm{tr},ci}\frac{\partial \ln T}{\partial \tau_l}}{\frac{1}{kT}\sum\limits_{ci}\frac{n_{ci}}{2n}\sqrt{m_c}\,(2p - 2\mu_{ci}S_{nn} - \zeta_{ci}\nabla\cdot\mathbf{v} - p_{\mathrm{rel},ci})}, \tag{1.93}$$

$$\frac{T}{T^w} = \frac{(2-\sigma)\sum\limits_{ci} n_{ci}\mathbf{V}_{ci}\cdot\mathbf{n} + \sigma\sqrt{\frac{2}{\pi kT}}Y_1}{(2-\sigma)\sum\limits_{ci}\frac{5n_{ci}}{4}\mathbf{V}_{ci}\cdot\mathbf{n} - \frac{(2-\sigma)\lambda'}{2k}\frac{\partial \ln T}{\partial n} + \sigma\sqrt{\frac{2}{\pi kT}}(Y_2+Y_4)}, \tag{1.94а}$$

$$Y_1 = \sum_{ci}\frac{n_{ci}}{2n\sqrt{m_c}}\left(1+\frac{m_c v^2}{4kT^w}\right)(2p - 2\mu_{ci}S_{nn} - \zeta_{ci}\nabla\cdot\mathbf{v} - p_{\mathrm{rel},ci})\,; \tag{1.94б}$$

$$Y_2 = \sum_{ci}\frac{3n_{ci}}{2n\sqrt{m_c}}(2/3p - \mu_{ci}S_{nn} - \zeta_{ci}\nabla\cdot\mathbf{v} - p_{\mathrm{rel},ci})\,; \tag{1.94в}$$

$$Y_4 = T\sum_{ci}\frac{n_{ci}}{2n}\sqrt{m_c}\,\frac{c_{\mathrm{rot},ci}}{k}(f_{ci,01}\nabla\cdot\mathbf{v} + g_{ci,01}). \tag{1.94г}$$

The above relations are more practical than Eqs. (1.89), (1.90) since there is a general lack of data for the accommodation coefficient depending on c,i and even on the chemical species.

For a non-catalytic surface, the wall mass flux and temperature jump expressions (velocity slip does not change in this case) take the form:

$$\mathbf{J}_{ci}\cdot\mathbf{n} = 0, \tag{1.95}$$

$$\frac{T}{T^w} = \frac{\sqrt{\frac{2}{\pi kT}}\sum\limits_{ci}\frac{n_{ci}}{2n\sqrt{m_c}}\left(1+\frac{m_c v^2}{4kT^w}\right)(2p - 2\mu_{ci}S_{nn} - \zeta_{ci}\nabla\cdot\mathbf{v} - p_{\mathrm{rel},ci})}{-\frac{2-\sigma}{\sigma}\frac{\lambda'}{2k}\frac{\partial \ln T}{\partial n} + \sqrt{\frac{2}{\pi kT}}(Y_2+Y_4)}. \tag{1.96}$$

The set of equations for a fully catalytic wall case (all the atoms that reach the wall are a part of surface recombination process) can be obtained similarly. In this case γ_{ci} are assumed to be equal to unity in (1.92).

1.4.2 Slip/jump equations for a single-component gas

In this section, a single-component gas under the strongly non-equilibrium conditions is considered as a particular case of the obtained boundary conditions.

In this case, the set of equations (1.92), (1.93)–(1.94) is following:

$$\mathbf{J}_i \cdot \mathbf{n} = \frac{-\gamma_i \rho_i}{(2-\gamma_i) n \sqrt{2\pi m k T}} \left(2p - 2\mu_i S_{nn} - \zeta_i \nabla \cdot \mathbf{v} - p_{\mathrm{rel},i}\right), \tag{1.97}$$

$$v_l = \frac{\sqrt{\frac{2\pi}{mkT}} \frac{2-\sigma}{\sigma} 2\mu S_{ln} + \frac{1}{5k} \lambda'_{\mathrm{tr}} \frac{\partial \ln T}{\partial \tau_l}}{\frac{1}{2kT}\left(2p - 2\mu S_{nn} - \zeta \nabla \cdot \mathbf{v} - p_{\mathrm{rel}}\right)}, \tag{1.98}$$

$$\frac{T}{T^w} = \frac{-\sqrt{\frac{2}{\pi k T}} \left(1 + \frac{m v^2}{4 k T^w}\right) \left(2p - 2\mu S_{nn} - \zeta \nabla \cdot \mathbf{v} - p_{\mathrm{rel}}\right)}{\frac{(2-\sigma)\sqrt{m}\lambda'}{\sigma k} \frac{\partial \ln T}{\partial n} - \sqrt{\frac{2}{\pi k T}} \left(2p - 3\mu S_{nn} - \frac{3(\zeta \nabla \cdot \mathbf{v} + p_{\mathrm{rel}})}{2}\right)}, \tag{1.99}$$

where $i = 1, \ldots, N_M$ and N_M is the number of vibrational states of the gas molecule and γ_i is the vibrational deactivation/excitation coefficient. The expression (1.99) is simplified with the use of the following relation [9]:

$$\begin{aligned} \sum_i \frac{m n_i}{n} c_{\mathrm{rot},i} (f_{i,01} \nabla \cdot \mathbf{v} + g_{i,01}) &= -\sum_i \frac{m n_i}{n} c_{\mathrm{tr}} (f_{i,10} \nabla \cdot \mathbf{v} + g_{i,10}) \\ &= -k \sum_i \frac{3 n_i}{2n} (f_{i,10} \nabla \cdot \mathbf{v} + g_{i,10}). \end{aligned} \tag{1.100}$$

It can be observed that, in the considered gas case, the expressions explicitly depend on the transport coefficients without the necessity of defining effective ones.

If internal states of particles and slow processes are not taken into the account, the velocity slip and temperature jump are returned to the following relations

$$v_l = \frac{\sqrt{\frac{2\pi}{mkT}} \frac{2-\sigma}{\sigma} 2\mu S_{ln} + \frac{1}{5k} \lambda' \frac{\partial \ln T}{\partial \tau_l}}{\frac{1}{2kT}\left(2p - 2\mu S_{nn}\right)}, \tag{1.101}$$

$$\frac{T}{T^w} = \frac{\sigma \sqrt{\frac{2}{\pi k T}} \left(1 + \frac{m v^2}{4 k T^w}\right) \cdot \left(2p - 2\mu S_{nn}\right)}{-(2-\sigma)\sqrt{m} \frac{\lambda'}{k} \frac{\partial \ln T}{\partial n} + \sigma \sqrt{\frac{2}{\pi k T}} \left(2p - 3\mu S_{nn}\right)}. \tag{1.102}$$

Assuming that only $\partial v_l / \partial n$ (l = 1,2) derivatives of the velocity components are not equal to zero, it is found that

$$v_l = \frac{2-\sigma}{\sigma} \sqrt{\frac{2\pi}{mkT}} \frac{\mu}{n} \frac{\partial v_l}{\partial n} + \frac{\lambda'}{5kn} \frac{\partial \ln T}{\partial \tau_l}, \tag{1.103}$$

$$T - T^w = \frac{2-\sigma}{2\sigma} \sqrt{\frac{\pi m}{2kT}} \frac{\lambda'}{nk} \frac{\partial T}{\partial n} + \frac{m v^2}{4k}. \tag{1.104}$$

The velocity derivative $\partial v_n / \partial \tau_l$ can be neglected if the effects of surface curvature and roughness are not considered. The above equations are the well-known

expressions for velocity slip and temperature jump for a single-component gas in the case of specular-diffusive scattering [50; 122].

1.4.3 Cercignani-Lampis model of particles interaction with a wall

In this section, the conditions are presented for another commonly applied model of particles interaction with the solid wall, the Cercignani-Lampis (CL) model [47]. Generalization of the CL kernel for the case of reacting gas flows with rapid and slow processes can be introduced by the following relation:

$$\begin{aligned} T^{cij}_{l,\mathrm{CL}}(\mathbf{u}_c,\mathbf{u}'_c) =& \frac{2}{\pi}\left(\frac{m_c}{2kT^w}\right)^2 \frac{s_j^{ci}}{Z_{\mathrm{rot},ci}(T^w)}\frac{1}{\alpha_n\alpha_\tau}u_{cn} \\ & \times I_0\left(\frac{2m_c\sqrt{1-\alpha_n}u_{cn}u'_{cn}}{2kT^w\alpha_n}\right)\exp\left(-\frac{m_c(u_{cn}^2+(1-\alpha_n)u_{cn}'^2)}{2kT^w\alpha_n}\right) \\ & \times \exp\left(-\frac{m_c(\mathbf{u}_{c\tau}-\sqrt{1-\alpha_\tau}\mathbf{u}'_{c\tau})^2}{2kT^w\alpha_\tau}\right)\exp\left(-\frac{\varepsilon_j^{ci}}{kT^w}\right), \end{aligned} \tag{1.105}$$

where $\mathbf{u}_{c\tau}$ is the tangential velocity and I_0 is the zeroth order modified Bessel function:

$$I_0(x) = \frac{1}{\pi}\int\limits_0^\pi e^{x\cos\theta}\,\mathrm{d}\theta. \tag{1.106}$$

The coefficients α_n, α_τ should be treated as the normal and tangential energy accommodation coefficients. The kernel also can be written in terms of normal and tangential momentum coefficients, but here for the convenience the first option is preferred. The coefficients in Eq. (1.105) are assumed to be independent of gas mixture species. This assumption is made once again since identifying the values of these coefficients for each species is extremely challenging in practical applications, and because the resulting form of the obtained slip conditions occurs too complicated. The above kernel, as the previous Maxwell one (1.79), is not capable to describe the change of rotational state of a molecule while it is scattered from the surface. Similarly, this issue may be resolved by introducing the probability of the vibrational state change.

The kernel does not include surface processes via the recombination probability, γ_{ci}. However, similar to the previous Maxwell model, these processes can be included by adding the diffusive kernel to Eq. (1.105), multiplied by $(-\gamma_{ci})$. The latter will allow the kernel to satisfy the normalization condition (1.76). The additional term here as well indicates that not all particles of the given species were reflected, some of them changed their species as a result of heterogeneous reactions, which also lead to the appearance of additional particles of the same species.

For the considered model of particles interaction with the solid wall (1.105), the boundary conditions should be obtained only for velocity and temperature since the wall mass fluxes remain the same regardless of scattering kernel considered. The procedure yields the same velocity slip as the Maxwell model (1.93), which is in agreement with other works [50; 95]. However, the temperature jump is different:

$$\left(\frac{T}{T^w}\right)_{\text{CL}} = \frac{(\alpha_\tau + \alpha_n)\sum\limits_{ci}\frac{n_{ci}}{2n}\mathbf{V}_{ci}\cdot\mathbf{n} + \sqrt{\frac{2}{\pi kT}}Z_1}{(10-2\alpha_\tau-3\alpha_n)\sum\limits_{ci}\frac{n_{ci}}{4n}\mathbf{V}_{ci}\cdot\mathbf{n} - Z_2 + \sqrt{\frac{2}{\pi kT}}(Z_3+Z_4) + Z_5}, \quad (1.107\text{a})$$

$$Z_1 = \sum_{ci}\frac{n_{ci}}{2n\sqrt{m_c}}\left(\frac{\alpha_\tau m_c v^2}{2kT^w} + \alpha_\tau + \alpha_n\right)\left(2p - 2\mu_{ci}S_{nn} - \zeta_{ci}\nabla\cdot\mathbf{v} - p_{\text{rel},ci}\right); \quad (1.107\text{б})$$

$$Z_2 = \frac{(10-2\alpha_\tau-3\alpha_n)\lambda'_{\text{tr}}+5\lambda'_{\text{rot}}}{5k}\frac{\partial\ln T}{\partial n}; \quad (1.107\text{в})$$

$$Z_3 = \sum_{ci}\frac{n_{ci}\sqrt{m_c}}{n}c_{\text{rot},ci}T(f_{ci,01}\nabla\cdot\mathbf{v} + g_{ci,01}); \quad (1.107\text{г})$$

$$Z_4 = \sum_{ci}\frac{n_{ci}}{2n\sqrt{m_c}}\left((\alpha_n+\alpha_\tau)(2p - 3\zeta_{ci}\nabla\cdot\mathbf{v} - 3p_{\text{rel},ci}) - 6\alpha_n\mu_{ci}S_{nn}\right); \quad (1.107\text{д})$$

$$Z_5 = \frac{\sqrt{1-\alpha_\tau}\mu}{kT}\left(S_{1n}v_1 + S_{2n}v_2\right). \quad (1.107\text{е})$$

The above expression is already written in terms of effective transport coefficients and transport terms. Contrary to the Maxwell model, the temperature jump for the CL scattering kernel depends on two accommodation coefficients, and due to that has more complex expression.

1.5 Conclusions of Chapter 1

In this chapter macroscopic slip boundary conditions are derived for the extended set of fluid-dynamic equations in the frame of the state-to-state model for fully coupled vibrational-chemical kinetics, gas dynamics and transport processes. The boundary conditions are obtained by taking into account the surface chemical and vibrational non-equilibrium processes. Two approaches are applied in order to obtain the slip conditions: the one proposed by Grad, generalized for reacting gases with both rapid and slow processes, and the approach developed in this thesis based on the kinetic boundary condition. For the Maxwell gas-surface interaction model it is shown that the resulting conditions are equivalent. Yet, the latter approach has multiple advantages. The approach based on the kinetic boundary condition provides a more rigorous mathematical description of the problem and can be easily generalized for other scattering kernels and gas-surface interaction models. This will allow taking into account more complex accommodation on the surface, including translational and different types of internal energy accommodation.

The obtained set of boundary conditions includes conditions for the mass fluxes of each species, accounting for molecular vibrational level populations and chemical number densities; velocity slip and temperature jump. All these quantities are expressed in terms of the effective state-specific transport coefficients: diffusion, thermal diffusion, thermal conductivity of translational and rotational degrees of freedom, shear and bulk viscosity, and relaxation pressure. The effect of the normal mean stress components (bulk viscosity and relaxation pressure) on the boundary conditions is shown for the first time. Under thermal equilibrium conditions, the derived expressions reduce to known relations obtained earlier in the one-temperature approach. It is worth noting that implementation of the new boundary conditions to simulations of non-equilibrium flows is straightforward since they depend on the same expansion coefficients as the transport coefficients, and therefore additional complexity in the numerical code is not required.

Slip boundary conditions were implemented as a program code module within the framework of project № 075-15-2024-544 «Mathematical models and numerical methods as the basis for the development of robotic systems, new materials and intelligent design technologies».

Chapter 2. Advanced approach for deriving boundary conditions accounting for surface processes

In the present chapter, a generalization of the theoretical approach developed in the previous chapter is proposed. Gaseous mixture here as well is described on the basis of the detailed state-to-state model. The proposed extension provides a more accurate representation of heterogeneous reactions and enables the derivation of boundary conditions in terms of macroparameters and transport coefficients, similar to the previous form of the approach. However, the new slip conditions depend on more physically appropriate processes probabilities, rather than empirical processes coefficients. Expressions for velocity slip, temperature jump, and mass fluxes of species on the wall are derived on the basis of the advanced kinetic boundary condition taking into account gain and loss of particles in surface processes. As in the previous chapter, the scattering models chosen are the ones of Maxwell and Cercignani–Lampis. Additionally, the comparison of theoretical and phenomenological expressions for the mass fluxes obtained in the frame of various approaches is performed. The outcomes discussed in this chapter have been published in [90; 112; 113].

The structure of the chapter is the following: after a brief formulation of challenges in the description of heterogeneous reactions in Section 2.1, the extension of the kinetic boundary condition approach in order to account for these reactions is proposed in Section 2.2. The slip conditions based on the new approach are presented in Section 2.3. Another variation of the kinetic boundary condition, designed to ensure the total mass flux conservation, is introduced in Sec. 2.4. The simplifications of the derived slip conditions, based on the two developed kinetic boundary conditions, can be found in 2.5. In Section 2.6, the mass fluxes on the surface derived in the frame of different approaches taking into account heterogeneous reactions are examined.

2.1 Limitations of known theoretical approaches for modeling surface processes

In the previous chapter, slip conditions based on the kinetic boundary condition for the distribution function were derived, and the advantages of this approach were demonstrated. The expressions were obtained in the case of the STS description of nonequilibrium flow dynamics fully coupled to vibrational-chemical kinetics. It was shown on the basis of specular-diffusive scattering that the proposed approach is equivalent to other commonly applied theoretical techniques such as the Grad [80] and Patterson–Shidlovsky half-flux [81; 87] methods. The main differences are in the form of the obtained conditions, which require no further simplifications, in more precise theoretical justification of the approach, and in its applicability to state-to-state flow simulations.

Nonetheless, the approach has an issue with correct accounting for the influence of chemical surface processes on gas dynamics. The effect of these processes on gas dynamics near the wall is introduced via the boundary conditions for species concentrations, written as the relations for the normal components of the mass fluxes near the wall. In the above mentioned approach, if recombination/dissociation and vibrational excitation/deactivation are considered, the corresponding conditions can be written in the form (1.92):

$$\mathbf{J}_{ci} \cdot \mathbf{n}|_s = -k_{ci}^w \rho_{ci}, \tag{2.1}$$

where $\mathbf{J}_{ci} \cdot \mathbf{n}|_s$ is the mass flux of a given species ci normal component on the external edge of the Knudsen layer, k_{ci}^w is the rate coefficient of wall heterogeneous processes affecting ci species. The latter relation means that the mass flux of the species ci depends solely on the density ρ_{ci} of that given species (and not densities of other species). Additionally, it is independent of the chosen model of particles interaction with the solid wall.

Equation (2.1) has a limited value in the case of heterogeneous processes, when different species may contribute to the mass flux of a given species. Additionally, this relation cannot account for the formation of particles resulting from surface non-equilibrium processes with initial zero concentration near the wall. Since the model developed in Section 1.3 is related to other known theoretical techniques [43; 80—82; 87; 93], the same problem arises for them either. Here an approach allowing to

overcome the mentioned issue will be presented. The main idea is in including to the kinetic boundary condition an additional term responsible for heterogeneous surface processes and by modifying the normalization condition for the scattering kernel.

2.2 Extension of the developed approach

First, it is essential to revisit the fundamentals of the approach developed in 1.3. In order to obtain the slip conditions, the kinetic boundary condition, i.e. the relation connecting the distribution functions of incident and reflected by solid wall particles, has to be specified. It can be expressed, after integration over the half-space $u_{cn} > 0$, as a relation between the number flux of reflected particles and the number flux of incident particles in the elementary area near the solid wall. This area distance from the surface in the normal direction is of the order of the mean free path (external edge of the Knudsen layer). For the STS approximation, if only scattering is taken into account, the kinetic boundary condition has the following form:

$$f^{+}_{cij} u_{cn}|_{u_{cn}>0} = -\sum_{l} \int\limits_{u'_{cn}<0} f^{-}_{cil}(\mathbf{r},\mathbf{u}'_c,t) u'_{cn} T^{cij}_{l}(\mathbf{u}_c,\mathbf{u}'_c) \mathrm{d}\mathbf{u}'_c. \tag{2.2}$$

The kernel $T^{cij}_{l}(\mathbf{u}_c,\mathbf{u}'_c)$, as the probability density, must satisfy a normalization condition, which in the state-specific form is written as follows:

$$\sum_{j} \int\limits_{u_{cn}>0} T^{cij}_{l}(\mathbf{u}_c,\mathbf{u}'_c) \mathrm{d}\mathbf{u}_c = 1. \tag{2.3}$$

Boundary conditions (2.2), (2.3) imply that during scattering, particles only change their velocities and rotational levels since scattering is a rapid process. The probability of such a transition is defined by the kernel. The generalization for heterogeneous processes can be included in the above relation (2.3). This can be done by modifying the right-hand side by the sum of mentioned earlier coefficients $\sum \gamma^{p}_{ci}$. It is supposed that $\gamma^{p}_{ci} > 0$ if particles of species ci change their vibrational or chemical state due to the surface process p; $\gamma^{p}_{ci} < 0$ if particles of species ci are formed as a result of the p process. These coefficients are an extension of the common recombination coefficients initially adapted in the slip conditions by Scott

[93]. The normalization condition (2.3) with such an assumption is rewritten as

$$\sum_{j} \int\limits_{u_{cn}>0} T_l^{cij}(\mathbf{u}_c,\mathbf{u}'_c)\mathrm{d}\mathbf{u}_c = 1 - \sum_{p} \gamma_{ci}^{p}. \tag{2.4}$$

However, as previously noted, this approach fails to accurately describe all types of non-equilibrium surface processes.

The next step is to present an alternative method for accounting for the loss and gain in the number of particles. The formulas below present such an alternative and include the modified kinetic BC:

$$\begin{aligned} f_{cij}^{+}(\mathbf{r},\mathbf{u}_c,t)u_{cn}|_{u_{cn}>0} = &- \sum_{l} \int\limits_{u'_{cn}<0} f_{cil}^{-}(\mathbf{r},\mathbf{u}'_c,t)u'_{cn}T_l^{cij}(\mathbf{u}_c,\mathbf{u}'_c)\mathrm{d}\mathbf{u}'_c \\ &+ \sum_{dk,dk\neq ci} \gamma_{dk}^{ci}\tilde{f}_{cij}^{+}(\mathbf{r},\mathbf{u}_c,t)u_{cn}|_{u_{cn}>0}, \end{aligned} \tag{2.5}$$

as well as the modified normalization condition for the scattering kernel T_l^{cij}:

$$\sum_{j} \int\limits_{u_{cn}>0} T_l^{cij}(\mathbf{u}_c,\mathbf{u}'_c)\mathrm{d}\mathbf{u}_c = 1 - \sum_{dk,dk\neq ci} \gamma_{ci}^{dk}. \tag{2.6}$$

Here, γ_{dk}^{ci} is the independent of the rotational state of a molecule probability that particle of chemical species d with vibrational level k changes its state to ci. The term on the LHS of the expression (2.5), after the integration over half-space, represents the number flux of particles reflected by the solid wall. Relation implies that this number flux consists of: 1) the number flux of scattered particles, transformed by the kernel T_l^{cij}; 2) the flux of particles obtained as a result of heterogeneous chemical reactions and vibrational deactivation/excitation due to the wall impinging. It is assumed that the latter particles are then desorbed into the gas phase with the known distribution function $\tilde{f}_{cij}^{+}(\mathbf{r},\mathbf{u}_c,t)$.

An obvious disadvantage of the proposed scheme (2.5), (2.6) is that it depends on the known distribution of reflected particles involved in surface reactions. This distribution might be obtained through rigorous and numerically expensive kinetic modelling, specific to a given set of gas mixture components and solid body surface structure. To avoid these challenges, the model distribution function can be applied. However, the latter would not account for the distribution of incident particles before their change of state. Furthermore, the proposed scheme cannot provide information on how the change of state of cij particles affects the number flux of reflected

particles of other species involved in surface chemical processes with cij particles. Additionally, the normal components of wall mass fluxes are written in the form similar to that presented in Eq. (2.1), i.e. the mass flux of a given species normal component near the wall, $\mathbf{J}_{ci} \cdot \mathbf{n}|_s$, depends solely on the density ρ_{ci} of a given species: $\mathbf{J}_{ci} \cdot \mathbf{n}|_s = -\tilde{k}^w_{ci}\rho_{ci}$. Here, the rate constants $\tilde{k}^w_{ci}$ differ from the ones, written for the initial scheme (2.2), (2.4). Thus, the problem of incorrect description of non-equilibrium surface processes remains.

The issue of independence from the distribution function of incident particles can be resolved by the following modification of (2.5):

$$\begin{aligned} f^+_{cij}(\mathbf{r},\mathbf{u}_c,t)u_{cn}|_{u_{cn}>0} = &- \sum_l \int\limits_{u'_{cn}<0} f^-_{cil}(\mathbf{r},\mathbf{u}'_c,t)u'_{cn}T^{cij}_l(\mathbf{u}_c,\mathbf{u}'_c)\mathrm{d}\mathbf{u}'_c \\ &- \sum_{dkl,dk\neq ci} \gamma^{ci}_{dk} \int\limits_{u'_{cn}<0} f^-_{cil}(\mathbf{r},\mathbf{u}'_d,t)u'_{cn}\tilde{T}^{cij}_l(\mathbf{u}_c,\mathbf{u}'_c)\mathrm{d}\mathbf{u}'_c, \end{aligned} \tag{2.7}$$

where kernels $\tilde{T}^{cij}_l$ and T^{cij}_l satisfy normalization conditions (2.3) and (2.6), correspondingly. The above scheme, with such assumptions, is equivalent to the initially considered (2.2), (2.4). However, it is evident that the second term in the right-hand side of equation (2.7) does not represent an actual increase in the number of particles of the given species because it considers the number flux of particles of the same species. This statement explains the reason why the initial approach provided above mentioned limitations for the wall mass fluxes expressions. Finally, to overcome the aforementioned issues with the schemes (2.5), (2.6) and (2.7), the kinetic boundary condition should be rewritten correspondingly:

$$\begin{aligned} f^+_{cij}(\mathbf{r},\mathbf{u}_c,t)u_{cn}|_{u_{cn}>0} = &- \sum_l \int\limits_{u'_{cn}<0} f^-_{cil}(\mathbf{r},\mathbf{u}'_c,t)u'_{cn}T^{cij}_l(\mathbf{u}_c,\mathbf{u}'_c)\mathrm{d}\mathbf{u}'_c \\ &- \sum_{dkl,dk\neq ci} \gamma^{ci}_{dk} \int\limits_{u'_{dn}<0} f^-_{dkl}(\mathbf{r},\mathbf{u}'_d,t)u'_{dn}\tilde{T}^{cij}_{dkl}(\mathbf{u}_c,\mathbf{u}'_d)\mathrm{d}\mathbf{u}'_d. \end{aligned} \tag{2.8}$$

In the scheme (2.8) the number flux of reflected particles of cij consists of the number flux of scattered particles, transformed by the kernel T^{cij}_l, and the fluxes of particles of different species that are transformed into particles of given species due to the wall chemical reactions or vibrational state change. The probability of such a transformation is γ^{ci}_{dk}, and subsequent reflection into the gas phase is described by the

kernel $\tilde{T}^{cij}_{dkl}$. From here on, it will be assumed that $\tilde{T}^{cij}_{dkl}(\mathbf{u}_c,\mathbf{u}'_d)$ is the diffusive kernel:

$$T^{cij}_{dkl}(\mathbf{u}_c,\mathbf{u}'_d) = \frac{2}{\pi}\left(\frac{m_c}{2kT^w}\right)^2 \frac{s^{ci}_j}{Z_{\mathrm{rot},ci}(T^w)} \exp\left(-\frac{m_c u_c^2}{2kT^w} - \frac{\varepsilon^{ci}_j}{kT^w}\right) u_{cn}, \tag{2.9}$$

with the below normalization condition:

$$\sum_j \int\limits_{u_{cn}>0} \tilde{T}^{cij}_{dkl}(\mathbf{u}_c,\mathbf{u}'_d)\mathrm{d}\mathbf{u}_c = 1. \tag{2.10}$$

The diffusive scattering model, chosen for its simplicity, can be justified by the fact that the particle, which is trapped by the surface before chemical reaction, spends some time on the surface and the consequent diffusive reflection occurs as a result of the energy accommodation [123]. The loss of the particles of given species is specified on the basis of normalization condition (2.6) for the kernel $T^{cij}_l(\mathbf{u}_c,\mathbf{u}'_c)$. Here as well it is connected with the fact that not all particles are scattered, some of them are involved in non-equilibrium surface processes — heterogeneous reactions and vibrational excitation/deactivation.

Is it worth noting that in the above approach, only binary collisions of gas particles near and on the solid wall are considered. This does not considerably affect its generality since both Eley–Rideal and Langmuir–Hinshelwood recombination mechanisms are based on binary collisions of atoms and adsorbed atoms.

The adsorption and desorption processes should also be considered, so the scheme could better capture the surface chemistry effect on gas dynamics. The first can be included on the basis of sticking coefficient $\mathtt{S}_{ci}$, described as the fraction of incident particles impinging on a surface that are really adsorbed [70]. Since adsorption initiates the loss of particles that might be scattered at the given time and position, then the process can be included via the normalization condition for the kernel

$$\sum_j \int\limits_{u_{cn}>0} T^{cij}_l(\mathbf{u}_c,\mathbf{u}'_c)\mathrm{d}\mathbf{u}_c = 1 - \sum_{dk,dk\neq ci} \gamma^{dk}_{ci} - \mathtt{S}_{ci}. \tag{2.11}$$

Desorption, on the opposite, initiates gain in the number of particles that are reflected, and can be included in condition (2.7) by introducing the desorption coefficient $\mathtt{D}^w_{ci}$, defined as the ratio of the number flux of desorbed particles to the number flux of incident particles. The distribution of desorbed into the gas phase particles at the given time can be, for example, considered as the local equilibrium

Maxwell-Boltzmann distribution $\tilde{f}^{+,M}_{cij}(\mathbf{r},\mathbf{u}_c,t)$ (1.22):

$$\begin{aligned} f^{+}_{cij}(\mathbf{r},\mathbf{u}_c,t)u_{cn}|_{u_{cn}>0} = &-\sum_{l}\int\limits_{u'_{cn}<0} f^{-}_{cil}(\mathbf{r},\mathbf{u}'_c,t)u'_{cn}T^{cij}_{l}(\mathbf{u}_c,\mathbf{u}'_c)\mathrm{d}\mathbf{u}'_c \\ &-\sum_{dkl,dk\neq ci}\gamma^{ci}_{dk}\int\limits_{u'_{dn}<0} f^{-}_{dkl}(\mathbf{r},\mathbf{u}'_d,t)u'_{dn}\tilde{T}^{cij}_{dkl}(\mathbf{u}_c,\mathbf{u}'_d)\mathrm{d}\mathbf{u}'_d \\ &+\mathtt{D}_{ci}\tilde{f}^{+,M}_{cij}(\mathbf{r},\mathbf{u}_c,t)u_{cn}|_{u_{cn}>0}. \end{aligned} \tag{2.12}$$

It is worth mentioning that the distribution of desorbed particles from the surface $\tilde{f}^{+,M}_{cij}(\mathbf{r},\mathbf{u}_c,t)$ depends on the wall temperature, but not on the one, considered on the external edge of the Knudsen layer.

The above relation does not consider the distribution of particles prior to their adsorption. Nevertheless, if necessary, this distribution can be accounted for. In such a case, the time particles spend on the surface must also be considered, leading to increased complexity in the expressions and required modification of the kinetic BC. In this section, the simplified approach (2.12) will be considered, which affects the surface balance equation.

It should be emphasized that the scheme considered here is noticeably different from the one, applied in the previous chapter. As is shown later, it allows one to overcome the mentioned issues in the wall mass fluxes description and obtain conditions that account for the complex surface mechanisms.

2.3 Slip conditions

In this section boundary conditions for the STS set of fluid-dynamic variables [9] will be obtained for two most widely used models, which are those proposed by Maxwell [44] and Cercignani–Lampis [47].

2.3.1 Expressions for the wall mass fluxes

The procedure described in Sec. 1.3 to obtain the slip conditions in the case of the new kinetic boundary condition (2.12) will be applied for the first-order state-specific distribution function (1.30). As in the initial approach, it is assumed that the velocity component along the normal, v_n, is zero in the vicinity of the surface. Such an assumption provides the following balance law at the wall:

$$\sum_{ci} n_{ci}\mathbf{V}_{ci}\cdot\mathbf{n} = \sum_{ci}\frac{\mathtt{S}_{ci}}{2}\left[n_{ci}\mathbf{V}_{ci}\cdot\mathbf{n} - \sqrt{\frac{kT}{2\pi}}\frac{n_{ci}}{n\sqrt{m_c}}\left(2n - b_{ci,0}S_{nn} + f_{ci,10}\nabla\cdot\mathbf{v} + g_{ci,10}\right)\right] + \sqrt{\frac{kT}{2\pi}}\sum_{ci}\mathtt{D}_{ci}\frac{n_{ci}}{\sqrt{m_c}}. \tag{2.13}$$

Here as well the notation that all the terms are taken on the external edge of the Knudsen layer, $|_s$, is omitted. When adsorption and desorption are neglected, a simplified relation is derived, which can be interpreted as the conservation of number flux near the wall within the introduced scheme (2.12):

$$\sum_{ci} n_{ci}\mathbf{V}_{ci}\cdot\mathbf{n} = 0. \tag{2.14}$$

The above expression significantly differs from the one obtained in the previous form of the approach (1.78). In the present case, expressions (2.13) and (2.14) provide a clear interpretation of the effects of heterogeneous processes and an understanding of how the considered form of the BC for the distribution function affects the total number flux near the wall.

The expressions for species wall number fluxes, as in the previous approach, are independent of the chosen model for the scattering kernel. They are influenced by the type of kinetic boundary condition and the considered approximation of the distribution function. Implementing the procedure from Chapter 1 for the particles

distribution (1.23) results in the following expressions for the new scheme (2.12):

$$\left(2-\sum_{dk,dk\neq ci}\gamma_{ci}^{dk}-\mathtt{S}_{ci}\right)\mathbf{J}_{ci}\cdot\mathbf{n}=-\frac{\left(\sum\limits_{dk,dk\neq ci}\gamma_{ci}^{dk}+\mathtt{S}_{ci}\right)\rho_{ci}}{n\sqrt{2\pi m_c kT}}\left(p+P_{nn,ci}\right)$$
$$+\sqrt{\frac{2kT}{\pi m_c}}\rho_{ci}\mathtt{D}_{ci}-\sum_{dk,dk\neq ci}\gamma_{dk}^{ci}\frac{m_c}{m_d}\mathbf{J}_{dk}\cdot\mathbf{n} \tag{2.15}$$
$$+\frac{1}{\sqrt{2\pi kT}}\sum_{dk,dk\neq ci}\gamma_{dk}^{ci}\frac{m_c\rho_{dk}}{n\sqrt{m_d^3}}\left(p+P_{nn,dk}\right),$$

where $c=1,\ldots,L$, $i=0,\ldots,N_c$. The expressions are presented in a more compact form already in terms of the mass fluxes, the effective transport coefficients and normal stresses for specific species ci, $P_{nn,ci}=p-2\mu_{ci}S_{nn}-\zeta_{ci}\nabla\cdot\mathbf{v}-p_{\mathrm{rel},ci}$. The difference from the expressions (1.92), is in the last three additional terms appearing in the RHS of Eq. (2.15) and the accounted fraction of particles loss before scattering $\sum\limits_{dk}\gamma_{ci}^{dk}+\mathtt{S}_{ci}$. This sum has replaced the sum of coefficients $\sum\gamma_{ci}^{p}$, which allowed to account for both loss and gain in the particles number (2.4). The obtained relation implies that the mass flux of particles of given species near the surface $\rho_{ci}\mathbf{V}_{ci}\cdot\mathbf{n}$ consists of: 1) the mass flux of desorbed particles with the mean non-slip velocity $\sqrt{\frac{2kT}{\pi m_c}}$; 2) the opposite mass flux of particles of given species that change their state due to surface processes; 3) fluxes of particles that are a part of ci species formation.

2.3.2 Maxwell model

In the case of the state-to-state approximation and in the frame of newly obtained normalization condition (2.11), the specular-diffusive kernel can be

expressed as follows:

$$\begin{aligned} T^{cij}_{l,\mathrm{M}}(\mathbf{u}_c,\mathbf{u}'_c) =&(1-\sigma_{ci})\delta_{lj}\delta(\mathbf{u}'_c-\mathbf{u}_c+2u_{cn}\mathbf{n}) \\ &+\left(\sigma_{ci}-\sum_{dk,dk\neq ci}\gamma^{dk}_{ci}-\mathbb{S}^{w}_{ci}\right)T^{cij}_{l,\mathrm{diff}}(\mathbf{u}_c,\mathbf{u}'_c), \end{aligned} \tag{2.16}$$

$$T^{cij}_{l,\mathrm{diff}}(\mathbf{u}_c,\mathbf{u}'_c) =\frac{2}{\pi}\left(\frac{m_c}{2kT^w}\right)^2\frac{s^{ci}_j u_{cn}}{Z_{\mathrm{rot},ci}(T^w)}\exp\left(-\frac{m_c u_c^2}{2kT^w}-\frac{\varepsilon^{ci}_j}{kT^w}\right). \tag{2.17}$$

In the above kernel, the detailed rotational state change is neglected. However, as mentioned in Sec. 1.3.2, this can be addressed by introducing probabilities of rotational state change. In the given kernel, the accommodation coefficients are species-dependent. Nonetheless, the boundary conditions will be derived without this assumption for the sake of simplification and comparison reasons.

The procedure to obtain the slip conditions, performed for the Maxwell scattering kernel $T^{cij}_{l,\mathrm{M}}$, yields the following boundary condition for velocity component v_l (l = 1,2):

$$v_l=\frac{(2-\sigma)\sqrt{\frac{\pi}{2kT}}\sum\limits_{ci}\frac{n_{ci}}{n}2\mu_{ci}S_{ln}+\sigma\sum\limits_{ci}n_{ci}\sqrt{m_c}\left(\frac{\lambda'_{\mathrm{tr},ci}}{5kn}\frac{\partial\ln T}{\partial\tau_l}-\mathbf{V}_{ci}\cdot\boldsymbol{\tau}_l\right)}{\sigma\sum\limits_{ci}\frac{n_{ci}}{2nkT}\sqrt{m_c}\,(p+P_{nn,ci})-\sum\limits_{ci}n_{ci}\sqrt{m_c}\mathbb{D}_{ci}}. \tag{2.18}$$

The difference in velocity slip, compared to the relation obtained from the initial form of the approach (1.93), is expressed by the denominator term associated with desorption coefficients. Therefore, if the desorption process is neglected, the velocity slip coincides with that derived in the frame of the initial scheme. When the desorption coefficient is non-zero, the term associated with this coefficient contributes to an increase in the velocity slip value.

The temperature jump in the context of the presented approach remains unchanged. However, this statement is no longer valid if the distribution of particles desorbed into the gas phase takes place at a temperature different from T^w.

2.3.3 Cercignani–Lampis model

Generalization of the CL kernel for the case of reacting gas flows with rapid and slow processes can be introduced by the following relation:

$$
\begin{aligned}
T^{cij}_{l,\mathrm{CL}}(\mathbf{u}_c,\mathbf{u}'_c) =& \frac{2}{\pi}\left(\frac{m_c}{2kT^w}\right)^2 \frac{s^{ci}_j}{Z_{\mathrm{rot},ci}(T^w)}\,\frac{u_{cn}}{\alpha_{n,ci}\alpha_{\tau,ci}}\,\exp\left(-\frac{\varepsilon^{ci}_j}{kT^w}\right)\\
&\times I_0\left(\frac{2m_c\sqrt{1-\alpha_{n,ci}}u_{cn}u'_{cn}}{2kT^w\alpha_{n,ci}}\right)\exp\left(-\frac{m_c(\mathbf{u}_{c\tau}-\sqrt{1-\alpha_{\tau,ci}}\mathbf{u}'_{c\tau})^2}{2kT^w\alpha_{\tau,ci}}\right)\\
&\times\exp\left(-\frac{m_c(u^2_{cn}+(1-\alpha_{n,ci})u'^2_{cn})}{2kT^w\alpha_{n,ci}}\right)-\left(\sum_{dk}\gamma^{dk}_{ci}+\mathrm{S}^w_{ci}\right)T^{cij}_{l,\mathrm{diff}}(\mathbf{u}_c,\mathbf{u}'_c),
\end{aligned}
\tag{2.19}
$$

where in the summation $dk \neq ci$ and $T^{cij}_{l,\mathrm{diff}}$ is defined from (2.17). The above kernel, as the previous Maxwell one, is not capable to describe the change of rotational state of a molecule while it is scattered from the surface. Similarly, this issue may be resolved by introducing the probability of the rotational state change. The CL kernel here is introduced similarly to the one of Chapter 1 — (1.105).

Within the framework of the initial approach, the velocity slip for the Cercignani–Lampis kernel coincides with the Maxwell kernel when replacing the energy accommodation coefficients with the tangential and normal momentum accommodation coefficients. This statement is also valid for the new approach, resulting in the velocity slip for the current kernel being governed by Eq. (2.18).

The expression for the temperature jump in the new approach is the same as that in the initial approach (1.107). This statement remains true only if the accommodation coefficients are the same for all gas mixture components.

Consequently, within the framework of the new kinetic boundary condition, both kernels yield the same temperature boundary conditions as those from the initial form of the kinetic BC. Nonetheless, as will be demonstrated below, the temperature conditions can be simplified in a manner that was not available in the previous approach.

2.4 Further extension of the technique to ensure the constraint of zero wall mass flux

The approach developed in this chapter ensures the total normal number flux conservation (2.14) at the external edge of the Knudsen layer, under the assumption of neglected adsorption and desorption processes, while considering only vibrational excitation/deactivation and heterogeneous chemical reactions. The relation implies that at the external edge, the number flux of incident particles to the surface coincides with the number flux of particles scattered by the surface. This is due to the assumption that these surface processes occur immediately for both the gas and surface particles, resulting in the equivalence of the mentioned fluxes. However, in most cases, only the conservation of mass flux is required, which can be achieved numerically within this approach but cannot be derived theoretically.

Therefore, it is useful to develop an approach that ensures mass flux conservation. Such an approach can be based on the following kinetic boundary condition:

$$\begin{aligned} m_c f^{+}_{cij}(\mathbf{r},\mathbf{u}_c,t)u_{cn}|_{u_{cn}>0} = -m_c \sum_{l} \int\limits_{u'_{cn}<0} f^{-}_{cil}(\mathbf{r},\mathbf{u}'_c,t)u'_{cn}T^{cij}_{l}(\mathbf{u}_c,\mathbf{u}'_c)\mathrm{d}\mathbf{u}'_c \\ - \sum_{dkl,dk\neq ci} m_d \gamma^{ci}_{dk} \int\limits_{u'_{dn}<0} f^{-}_{dkl}(\mathbf{r},\mathbf{u}'_d,t)u'_{dn}\tilde{T}^{cij}_{dkl}(\mathbf{u}_c,\mathbf{u}'_d)\mathrm{d}\mathbf{u}'_d. \end{aligned} \tag{2.20}$$

The normalization conditions for the kernels are the same. After integrating over the half-space, the left-hand side of Eq. (2.20) can be expressed as a relation in the elementary area near the solid wall, regarding the mass flux of reflected particles. This mass flux includes both the mass flux of scattered particles and the mass flux of particles that are transformed into the ci particles. One can easily notice that this kinetic boundary condition is similar to the one of the generalized approach of Section 2.2. The difference is that in Eq. (2.20), mass fluxes are considered instead of number fluxes.

Neglecting the normal velocity component near the wall results in the following balance law for this approach:

$$\sum_{ci} \rho_{ci}\mathbf{V}_{ci}\cdot\mathbf{n} = 0. \tag{2.21}$$

This balance law ensures the required conservation of the normal mass flux near the wall. However, in the presence of adsorption and desorption processes included in the scheme, it will no longer be valid.

The wall mass fluxes relations here as well are independent of the chosen model of particles scattering by the wall, defined by the kernel T_l^{cij}. Nevertheless, they depend on the selected reflection of particles affected by non-equilibrium surface processes, defined by the kernel T_{dkl}^{cij}, also assumed to be diffusive. The procedure described in Capter 1 yields the following relations for the mass fluxes:

$$\begin{aligned}\left(2-\sum_{dk,dk\neq ci}\gamma_{ci}^{dk}\right)\mathbf{J}_{ci}\cdot\mathbf{n}=&-\frac{\sum_{dk,dk\neq ci}\gamma_{ci}^{dk}\rho_{ci}}{n\sqrt{2\pi m_c kT}}\left(p+P_{nn,ci}\right)\\&-\sum_{dk,dk\neq ci}\gamma_{dk}^{ci}\mathbf{J}_{dk}\cdot\mathbf{n}+\frac{1}{\sqrt{2\pi kT}}\sum_{dk,dk\neq ci}\gamma_{dk}^{ci}\frac{\rho_{dk}}{n\sqrt{m_d}}\left(p+P_{nn,dk}\right).\end{aligned}\tag{2.22}$$

The above expression for ci species is written in a form similar to the one in which mass fluxes were given by the extended approach (2.15). The difference between these relations is given by the additional fraction of masses, m_c/m_d, appearing in the two last summation terms on the right-hand side of Eq. (2.15).

When considering only specular-diffusive scattering by the solid wall, it is demonstrated that the velocity slip is the same for both considered approaches. Temperature jump, on the other hand, is different, with the following form:

$$\frac{T}{T^w}=\frac{(2-\sigma)\sum_{ci}\rho_{ci}\mathbf{V}_{ci}\cdot\mathbf{n}+\sigma\sqrt{\frac{2}{\pi kT}}\sum_{ci}\frac{\rho_{ci}}{2n\sqrt{m_c}}\left(1+\frac{m_c v^2}{4kT^w}\right)\cdot\left(p+P_{ci,nn}\right)}{(2-\sigma)\sum_{ci}\frac{5\rho_{ci}}{4}\mathbf{V}_{ci}\cdot\mathbf{n}-(2-\sigma)\sum_{ci}\frac{\rho_{ci}}{n}\frac{\lambda'_{ci}}{2k}\frac{\partial\ln T}{\partial n}+\sigma\sqrt{\frac{2}{\pi kT}}\,Y},\tag{2.23а}$$

$$Y=\sum_{ci}\frac{3\rho_{ci}}{2n}\left(\frac{-\frac{p}{3}+\mu_{ci}S_{nn}+P_{ci,nn}}{\sqrt{m_c}}+\frac{\sqrt{m_c}c_{\mathrm{rot},ci}T(f_{ci,01}\nabla\cdot\mathbf{v}+g_{ci,01})}{3}\right).\tag{2.23б}$$

The difference here is in the presence of the species densities, ρ_{ci}, instead of the number densities, n_{ci}. As a result, only the effective thermal conductivity coefficients appear in the above relation, while the thermal conductivity coefficient, as in Eq. (1.94), is not present.

2.5 Simplifications of obtained expressions

In practical applications, the sticking coefficient, $\mathtt{S}_{ci}^{w}$, and the desorption coefficient, $\mathtt{D}_{ci}^{w}$, are often quite hard to determine. Despite the importance of modeling the desorption and adsorption processes, and their substantial influence on heterogeneous reactions, in this chapter and the following chapter, these processes will be neglected. Therefore, simplified boundary condition expressions for this case are required.

First, the temperature jump will be presented under the mentioned assumption. In the case of the approach based on the extended kinetic boundary condition 2.2, the expressions for the Maxwell and CL kernels are the following:

$$\left(\frac{T}{T^w}\right)_{\mathrm{M}} = \frac{\sigma\sqrt{\frac{2}{\pi kT}}\sum\limits_{ci}\frac{n_{ci}}{2n\sqrt{m_c}}\left(1+\frac{m_c v^2}{4kT^w}\right)\cdot\left(p+P_{ci,nn}\right)}{-\frac{(2-\sigma)\lambda'}{2k}\frac{\partial \ln T}{\partial n}+\sigma\sqrt{\frac{2}{\pi kT}}\sum\limits_{ci}\frac{3n_{ci}}{2n}\left(\frac{-\frac{p}{3}+\mu_{ci}S_{nn}+P_{ci,nn}}{\sqrt{m_c}}+\frac{\sqrt{m_c}c_{\mathrm{rot},ci}T(f_{ci,01}\nabla\cdot\mathbf{v}+g_{ci,01})}{3}\right)}, \tag{2.24}$$

$$\left(\frac{T}{T^w}\right)_{\mathrm{CL}} = \frac{\sqrt{\frac{2}{\pi kT}}\sum\limits_{ci}\frac{n_{ci}}{2n\sqrt{m_c}}\left(\alpha_\tau\frac{m_c v^2}{2kT^w}+\alpha_\tau+\alpha_n\right)\left(p+P_{nn,ci}\right)}{-\frac{(10-2\alpha_\tau-3\alpha_n)\lambda'_{\mathrm{tr}}+5\lambda'_{\mathrm{rot}}}{5k}\frac{\partial \ln T}{\partial n}+\sqrt{\frac{2}{\pi kT}}\left(Z_1+Z_2\right)+\frac{\sqrt{1-\alpha_\tau}\mu}{kT}\left(S_{1n}v_1+S_{2n}v_2\right)}, \tag{2.25а}$$

$$Z_1 = \sum_{ci}\frac{n_{ci}\sqrt{m_c}}{n}c_{\mathrm{rot},ci}T(f_{ci,01}\nabla\cdot\mathbf{v}+g_{ci,01}); \tag{2.25б}$$

$$Z_2 = \sum_{ci}\frac{n_{ci}}{2n\sqrt{m_c}}\left((\alpha_n+\alpha_\tau)(2p-3\zeta_{ci}\nabla\cdot\mathbf{v}-3p_{\mathrm{rel},ci})-6\alpha_n\mu_{ci}S_{nn}\right). \tag{2.25в}$$

The above equations were obtained from Eqs. (1.94), (1.107) under the assumption that desorption and adsorption processes are neglected (2.14). This can be done since the new approach provides the same BCs for temperature. However, the latter expressions in the frame of the previous approach could not be simplified to such a form, as the balance law (2.14) is only applicable in the context of the new approach.

In the case of the subsequent extension of the developed approach to ensure the mass flux conservation 2.4, the relation for the temperature at the external edge

of the Knudsen layer is as follows:

$$\left(\frac{T}{T^w}\right)_{\mathrm{M}} = \frac{\sigma\sqrt{\frac{2}{\pi kT}}\sum\limits_{ci}\frac{\rho_{ci}}{2n\sqrt{m_c}}\left(1+\frac{m_c v^2}{4kT^w}\right)\cdot(p+P_{ci,nn})}{-(2-\sigma)\sum\limits_{ci}\frac{\rho_{ci}}{n}\frac{\lambda'_{ci}}{2k}\frac{\partial \ln T}{\partial n}+\sigma\sqrt{\frac{2}{\pi kT}}\,Y}, \tag{2.26а}$$

$$Y = \sum_{ci}\frac{3\rho_{ci}}{2n}\left(\frac{-\frac{p}{3}+\mu_{ci}S_{nn}+P_{ci,nn}}{\sqrt{m_c}}+\frac{\sqrt{m_c}c_{\mathrm{rot},ci}T(\mathrm{f}_{ci,01}\nabla\cdot\mathbf{v}+\mathrm{g}_{ci,01})}{3}\right). \tag{2.26б}$$

The equation above was simplified using balance law (2.21).

As for boundary conditions for species densities (2.15), the expressions in the case of neglected adsorption and desorption processes are the following:

$$\begin{aligned}\left(2-\sum_{dk}\gamma_{ci}^{dk}\right)\mathbf{J}_{ci}\cdot\mathbf{n} = &-\frac{\sum\limits_{dk}\gamma_{ci}^{dk}\rho_{ci}}{n\sqrt{2\pi m_c kT}}(p+P_{nn,ci})-\sum_{dk}\gamma_{dk}^{ci}\frac{m_c}{m_d}\mathbf{J}_{dk}\cdot\mathbf{n}\\ &+\frac{1}{\sqrt{2\pi kT}}\sum_{dk}\gamma_{dk}^{ci}\frac{m_c\rho_{dk}}{n\sqrt{m_d^3}}(p+P_{nn,dk}),\end{aligned} \tag{2.27}$$

in the summations, terms where $dk \neq ci$ are omitted. The remaining probabilities, γ_{dk}^{ci}, within the framework of the STS approximation, are associated with either recombination/dissociation or vibrational excitation/deactivation. The latter process obviously influences only the mass fluxes of molecular components and are defined by the probabilities $\gamma_{M(i)}^{M(k)}$ ($M(i)$ corresponds to a molecule in the vibrational state i and the probability defines transition of this molecule from state i to state k). Neglecting surface chemical reactions for these mass fluxes yield the below expressions:

$$\begin{aligned}\mathbf{J}_{M(i)}\cdot\mathbf{n} = &-\frac{\sum_{k,k\neq i}\gamma_{M(i)}^{M(k)}\rho_{M(i)}}{\left(2-\sum_{k,k\neq i}\gamma_{M(i)}^{M(k)}\right)n\sqrt{2\pi m_M kT}}\left(p+P_{nn,M(i)}\right)\\ &-\frac{1}{2-\sum_{k,k\neq i}\gamma_{M(i)}^{M(k)}}\sum_{k,k\neq i}\gamma_{M(k)}^{M(i)}\mathbf{J}_{M(k)}\cdot\mathbf{n}\\ &+\frac{1}{\left(2-\sum_{k,k\neq i}\gamma_{M(i)}^{M(k)}\right)\sqrt{2\pi kT}}\sum_{k,k\neq i}\gamma_{M(k)}^{M(i)}\frac{\rho_{M(k)}}{n\sqrt{m_M}}\left(p+P_{nn,M(k)}\right),\end{aligned} \tag{2.28}$$

where $i = 0,\ldots,N_M$. To obtain the mass flux for a given species, one has to solve the system of linear equations.

It is important to mention that obtaining accurate probabilities of vibrational deactivation on the surface is extremely challenging, and the effect of such processes in the case of simplified models is found to be negligible [72]. Therefore, it is common practice to focus only on heterogeneous recombination/dissociation. In this case, the expressions for atomic and molecular mass fluxes for diatomic molecules are the following:

$$\begin{aligned}\mathbf{J}_A \cdot \mathbf{n} = &- \frac{\sum_{M,k} \gamma_A^{\mathrm{rec},M(k)} \rho_A}{\left(2 - \sum_{M,k} \gamma_A^{\mathrm{rec},M(k)}\right) n\sqrt{2\pi m_A kT}} \left(p + P_{nn,A}\right) \\ &- \frac{1}{2 - \sum_{M,k} \gamma_A^{\mathrm{rec},M(k)}} \sum_{M,k} \gamma_{M(k)}^{\mathrm{diss},A} \frac{m_A}{m_M} \mathbf{J}_{M(k)} \cdot \mathbf{n} \\ &+ \frac{1}{\left(2 - \sum_{M,k} \gamma_A^{\mathrm{rec},M(k)}\right) \sqrt{2\pi kT}} \sum_{M,k} \gamma_{M(k)}^{\mathrm{diss},A} \frac{m_A \rho_{M(k)}}{n\sqrt{m_M^3}} \left(p + P_{nn,M(k)}\right),\end{aligned} \tag{2.29}$$

$$\begin{aligned}\mathbf{J}_{M(i)} \cdot \mathbf{n} = &- \frac{\sum_A \gamma_{M(i)}^{\mathrm{diss},A} \rho_{M(i)}}{\left(2 - \sum_A \gamma_{M(i)}^{\mathrm{diss},A}\right) n\sqrt{2\pi m_M kT}} \left(p + P_{nn,M(i)}\right) \\ &- \frac{1}{2 - \sum_A \gamma_{M(i)}^{\mathrm{diss},A}} \sum_A \gamma_A^{\mathrm{rec},M(i)} \frac{m_M}{m_A} \mathbf{J}_A \cdot \mathbf{n} \\ &+ \frac{1}{\left(2 - \sum_A \gamma_{M(i)}^{\mathrm{diss},A}\right) \sqrt{2\pi kT}} \sum_A \gamma_A^{\mathrm{rec},M(i)} \frac{m_M \rho_A}{n\sqrt{m_A^3}} \left(p + P_{nn,A}\right).\end{aligned} \tag{2.30}$$

Here, $\gamma_A^{\mathrm{rec},M(i)}$ and $\gamma_{M(i)}^{\mathrm{diss},A}$ are the recombination and dissociation probabilities, respectively. In the first case, an atom A participates in a recombination reaction where a molecule M on the vibrational level i is formed. In the second case, the molecule $M(i)$ is decomposed into two atoms, one of which is the atom A. In this case, in order to obtain the expression for the mass flux of a given species, the system of linear equations must be solved as well.

In the present work, the focus is solely on recombination on the solid surface since, in practical applications, it is common to consider only this specific process.

The above expressions in such case can be rewritten in the form:

$$\mathbf{J}_A \cdot \mathbf{n} = -\frac{\sum_{M,k} \gamma_A^{\mathrm{rec},M(k)}}{2 - \sum_{M,k} \gamma_A^{\mathrm{rec},M(k)}} \frac{\rho_A}{n\sqrt{2\pi m_A kT}} \left(p + P_{nn,A}\right); \tag{2.31}$$

$$\begin{aligned} \mathbf{J}_{M(i)} \cdot \mathbf{n} = &-\sum_A \frac{\gamma_A^{\mathrm{rec},M(k)}}{2} \frac{m_M}{m_A} \mathbf{J}_A \cdot \mathbf{n} \\ &+ \frac{1}{\sqrt{2\pi kT}} \sum_A \frac{\gamma_A^{\mathrm{rec},M(k)}}{2} \frac{m_M \rho_A}{n\sqrt{m_A^3}} \left(p + P_{nn,A}\right), \end{aligned} \tag{2.32}$$

where $A = 1, \ldots, L_A$ and $M = 1, \ldots, L_M$, $i = 0, \ldots, N_M$. By substituting the atomic mass fluxes (2.31) into Eq. (2.32) and performing some simplifications, the above system is written in the form (2.37)-(2.38).

In the following section, the obtained BCs will be compared with those from the previous Chapter under the same simplifications and with some other phenomenological models.

2.6 Comparison of slip condition models with respect to heterogeneous reactions

In the frame of the present approach, non-equilibrium surface processes (except desorption) have explicit influence only on the boundary conditions for species concentrations. Such expressions are conventionally written in terms of normal components of mass fluxes near the wall. The latter, when calculated, can be included in the temperature jump and the velocity slip.

In this section slip boundary conditions for species concentrations are presented for a particular case when adsorption/desorption processes are neglected, and only recombination is taken into account. It should be emphasized that adsorption and desorption are neglected for the sake of simplification, due to high complexity of evaluating their rate coefficients and lack of available data. In practical applications, these processes can play an important role and, therefore, one should employ the general forms of the expression from this Chapter. Besides that, the above assumptions are made in order to compare the results with some phenomenological models, which in most cases are written with respect to the chosen heterogeneous process. In the frame of the present work three different models are considered: the

model developed initially in previous chapter 1.3, the present model 2.2, and the model proposed by Barbato in [109; 110].

2.6.1 Model, developed in previous chapter

When considering only recombination as a single heterogeneous process, the state-specific boundary conditions obtained within the framework of the approach developed in [88; 89] (reported in section 1.3) take the following form:

$$\mathbf{J}_A \cdot \mathbf{n} = - \frac{\sum_{M,i} \gamma_A^{\mathrm{rec},M(i)}}{2 - \sum_{M,k} \gamma_A^{\mathrm{rec},M(k)}} \frac{p + P_{nn,A}}{n\sqrt{2\pi m_A kT}} \rho_A, \tag{2.33}$$

$$\mathbf{J}_{M(i)} \cdot \mathbf{n} = \frac{\sum_A \gamma_A^{\mathrm{rec},M(i)}}{2 + \sum_A \gamma_A^{\mathrm{rec},M(i)}} \frac{p + P_{nn,M(i)}}{n\sqrt{2\pi m_M kT}} \rho_{M(i)}, \tag{2.34}$$

where $A = 1,\ldots,L_A$ and $M = 1,\ldots,L_M$, $i = 0,\ldots,N_M$. To compare with commonly used models, Eqs. (2.33) and (2.34) can be written in a conventional form using effective reaction rate constants, as shown below:

$$\mathbf{J}_A \cdot \mathbf{n} = - \sum_{M,i} \tilde{k}_{A,M(i)}^{w,\mathrm{rec}} \rho_A, \tag{2.35}$$

$$\mathbf{J}_{M(i)} \cdot \mathbf{n} = \sum_A \tilde{\tilde{k}}_{A,M(i)}^{w,\mathrm{rec}} \rho_{M(i)}. \tag{2.36}$$

Here, $\tilde{k}_{A,M(i)}^{w,\mathrm{rec}}$ and $\tilde{\tilde{k}}_{A,M(i)}^{w,\mathrm{rec}}$ are the effective wall recombination rate coefficients. The main drawback, as already specified above, is the dependence of the molecular component mass flux near the wall solely on the density of the same molecular component.

The formulas, when simplified to the one-temperature approximation with no internal degrees of freedom, are similar to other known theoretical expressions [43; 82; 93; 94]. Such conditions were derived in the frame of the Grad [80] or Patterson–Shidlovskiy [81; 87] methods, which in the present form do not provide correct implementation of heterogeneous reactions.

The model described here will be further referred to as «Model I».

2.6.2 Improved model

The technique introduced in the present chapter yields the normal particle flux in the form of Eq. (2.15), which under the above mentioned simplifications can be written as:

$$\mathbf{J}_A \cdot \mathbf{n} = - \frac{\sum_{M,k} \gamma_A^{\mathrm{rec},M(k)}}{2 - \sum_{M,k} \gamma_A^{\mathrm{rec},M(k)}} \frac{p + P_{nn,A}}{n\sqrt{2\pi m_A kT}} \rho_A, \tag{2.37}$$

$$\begin{aligned} \mathbf{J}_{M(i)} \cdot \mathbf{n} = & \frac{1}{\sqrt{2\pi kT}} \sum_A \frac{\gamma_A^{\mathrm{rec},M(i)}}{2} \frac{m_M}{m_A} \frac{p + P_{nn,A}}{n\sqrt{m_A}} \\ & \times \left[1 + \frac{\sum_{M,k} \gamma_A^{\mathrm{rec},M(k)}}{2 - \sum_{M,k} \gamma_A^{\mathrm{rec},M(k)}} \right] \rho_A. \end{aligned} \tag{2.38}$$

The above expressions are obtained by simplifying Eqs. (2.31)–(2.32). One can notice that the general form of atomic component mass flux (2.37) is the same as in the previous form (2.35). On the contrary, the molecular component mass fluxes differ from (2.36). Correspondingly, Eq. (2.38) can be rewritten as follows:

$$\mathbf{J}_{M(i)} \cdot \mathbf{n} = \sum_A \hat{k}_{A,M(i)}^{w,\mathrm{rec}} \rho_A. \tag{2.39}$$

The latter expression corresponds to the phenomenological one reported in [108; 124], and the theoretically derived one in [84]. Though in the developed approach there is an exact expression for the effective recombination rate coefficient. This rate coefficient can also be taken from phenomenological approximations or obtained from experiments.

This model will be called hereafter «Present model».

2.6.3 Barbato model

A simpler model adopted to take into account surface catalycity, without considering the rarefaction effects such as velocity slip and temperature jump, is the one commonly used in the literature [28; 32; 109; 110; 125]. In this model the surface derivatives of the molecular vibrational distributions and of atomic mass

fractions are written in the form:

$$\frac{\mathrm{d}y_A}{\mathrm{d}n} = \frac{\sum_{M,i}\gamma_A^{\mathrm{rec},M(i)}}{D_A}\sqrt{\frac{kT}{2\pi m_A}}\,y_A, \tag{2.40}$$

$$\frac{\mathrm{d}y_{M(i)}}{\mathrm{d}n} = -\sum_A \frac{\gamma_A^{\mathrm{rec},M(i)}}{D_A}\sqrt{\frac{kT}{2\pi m_A}}\,y_A, \tag{2.41}$$

where y_A,$y_{M(i)}$ are atomic and molecular species mass fractions, respectively ($y_c = \rho_c/\rho$). The above formulas can be approximately written in terms of mass fluxes if the Fick law ($\rho_{ci}\mathbf{V}_{ci} \approx -\rho D_{ci}\nabla y_c$) is applied for the diffusion velocity:

$$\mathbf{J}_A \cdot \mathbf{n} = -\sum_{M,i}\gamma_A^{\mathrm{rec},M(i)}\sqrt{\frac{kT}{2\pi m_A}}\,\rho_A = -\sum_{M,i}\bar{k}^{w,\mathrm{rec}}_{A,M(i)}\,\rho_A, \tag{2.42}$$

$$\mathbf{J}_{M(i)} \cdot \mathbf{n} = \sum_A \frac{\gamma_A^{\mathrm{rec},M(i)} D_{M(i)}}{D_A}\sqrt{\frac{kT}{2\pi m_A}}\,\rho_A = \sum_A \bar{\bar{k}}^{w,\mathrm{rec}}_{A,M(i)}\,\rho_A. \tag{2.43}$$

One can notice that the generic conventional form of Eqs. (2.42)–(2.43) is the same as that of developed extended approach (see Eqs. (2.37) and (2.38)). The effective recombination reaction rate constants are, however, different.

The above model will be further referred to as «Barbato model».

2.7 Conclusions of Chapter 2

In the present Chapter, the generalized approach allowing to obtain slip boundary conditions for the state-specific set of macroparameters, is developed in the viscous flow approximation. The proposed technique is based on the extension of the kinetic boundary condition, which enables to account for various surface non-equilibrium processes, such as adsorption-desorption, vibrational excitation-deactivation and heterogeneous reactions in a correct form, unlike the previous form of the approach. Besides that, the proposed scheme retains all the advantages of its initial form from the previous Chapter: 1) the slip conditions depend only on macroparameters, accommodation coefficients and probabilities of surface processes without required further simplification, as in half-flux and Grad's methods; 2) the approach should not cause any additional computational costs if all coefficients

of surface processes are known; 3) the procedure can be easily adapted for one- and multi-temperature approximations, and for the first one, the conditions can be already written based on the provided formulas.

Surface processes directly affect the boundary conditions for species concentrations. The general form of the latter in terms of the mass fluxes is in accordance with known phenomenological models, however, effective recombination coefficients are calculated theoretically. Slip boundary conditions were derived for the Maxwell and Cercignani–Lampis scattering kernels, and differences between them in the frame of the new scheme appear only in the temperature jump. Non-equilibrium surface processes do not affect explicitly velocity and temperature values near the wall, except for desorption, which appears in the velocity slip. Under the neglected adsorption assumption, the temperature and velocity boundary conditions are the same as those obtained in the case of the initial form of the approach.

Additionally, in this Chapter, another improved version of the kinetic boundary condition is proposed to ensure the conservation of the mass flux near the surface in the case of heterogeneous recombination reactions and vibrational energy transitions. Using this boundary condition and the Maxwell scattering kernel, wall mass fluxes, velocity slip, and temperature jump are derived. It is demonstrated that only the velocity slip remains unchanged under the considered scheme.

A system of boundary conditions in the one-temperature approximation was obtained and implemented within the framework of project № 075-15-2024-544 «Mathematical models and numerical methods as the basis for the development of robotic systems, new materials and intelligent design technologies».

Chapter 3. Air flow in a boundary layer in the vicinity of stagnation point

The models of slip boundary conditions developed in previous chapters are assessed in the present chapter. The set of boundary conditions is transformed using the Lees–Dorodnitsyn coordinate system to be implemented in the fluid-dynamic solver for modeling the dynamics and state-to-state air kinetics in the boundary layer near stagnation point. Several scenarios of various degree of gas rarefaction are considered. Recombination probabilities and effective reaction rates are calculated and compared to recent molecular-dynamic simulations. The influence of the slip boundary conditions model on the flow parameters is assessed by comparing the results of seven types of test cases. For each set, temperature jump is either neglected or accounted for, and one of the three different models of solid wall catalyticity is considered (see 2.6). The impact of the scattering model, diffusion model, and different types of approach generalizations (see 2.2 and 2.4) on the flow characteristics in the boundary layer is examined as well. The results of this chapter can be found in papers [112; 113]. This work was carried out in collaboration with Dr. Iole Armenise.

The chapter is structured in the following manner. Initially, the problem statement and kinetic schemes used in simulations are given in Sec. 3.1. Test cases description is provided in 3.2.1 subsection. The results 3.2 are organized as follows: first, the models are examined based on the distributions of fluid-dynamic variables along stagnation line 3.2.4; a detailed description of wall heat fluxes is presented in Section 3.2.5, including a comparison with some phenomenological models; the influence of the accommodation coefficient, diffusion model, and approaches based on different types of kinetic boundary conditions is analysed in 3.2.6 and 3.2.7.

3.1 Problem statement

Description of the rarefied gaseous mixture flow in a boundary layer near stagnation point of a body moving at supersonic speed can be reduced to a one-dimensional problem using Lees–Dorodnitsyn coordinates [125]. The transformation

formulas are following [39]:

$$\xi = \int_0^x \rho_e \mu_e v_e r^2 dx, \qquad \eta = \frac{v_e r}{\sqrt{2\xi}} \int_0^y \rho dy, \tag{3.1}$$

where ξ and η are the coordinates parallel and normal to the body surface; x and y are the initial Cartesian coordinates; r is the vertical coordinate measured from the centerline of an axisymmetric body; the subscript 'e' refers to the external edge of the boundary layer.

The coordinate ξ in Eq (3.1) represents the longitudinal direction, while η, depending on ξ, is the new transverse coordinate. The advantage of this transformation is that in the (ξ, η) reference system, the velocity component along the surface, v_n, only depends on the transverse coordinate, i.e., $v_n(\xi, \eta)$ becomes $v_n(\eta)$, so that the velocity profile along the normal to the surface, η, does not depend on the point on the surface in which it is observed. In the case of flow near the stagnation point of an axisymmetric body, additional simplifications can be made, and the dependence of all parameters on ξ vanishes [125]. Therefore, all the parameters in the boundary layer are assumed to be dependent only on the η coordinate.

3.1.1 Governing equations

The general system of state-to-state fluid-dynamic equations, given by Eqs. (1.32)–(1.34), for the hypersonic boundary layer of a body flying in a $N_2/N/O_2/O/NO$ mixture in the Lees-Dorodnitsyn coordinates, is as follows [39]:

$$\begin{aligned} \frac{\partial^2 y_i}{\partial \eta^2} + f\,\mathrm{Sc}\,\frac{\partial y_i}{\partial \eta} &= S_i, \qquad i = 1,...,L; \\ \frac{\partial^2 T/T_e}{\partial \eta^2} + f\,\mathrm{Pr}\,\frac{\partial T/T_e}{\partial \eta} &= S_T. \end{aligned} \tag{3.2}$$

The first L equations are 155 continuity equations, one for each species i, whose mass fraction is y_i; thus, there are one continuity equation for the atomic nitrogen, one for the atomic oxygen and 61, 44, 48 continuity equations for the vibrational levels of N_2, O_2 and NO, respectively. The last equation is the energy conservation equation, in which the unknown is the temperature T normalized to its value T_e

at the external boundary layer edge. On the left-hand side of the equations the Schmidt (Sc) and Prandtl (Pr) numbers appear as well as the stream function, $f = f(\eta)$ [125]. On the right-hand side S_i and S_T are the source terms corresponding to the gas-phase state-to-state vibrational and chemical kinetics. Two important parameters are included in these latter terms: the pressure, p_e, and the derivative of the external edge velocity component along the body surface with respect to the coordinate along the body surface itself, β, measuring the inverse of the residence time of a fluid element in a particular point of the boundary layer [125]. Details on this hypersonic boundary layer system and, in particular, on the construction of S_i and S_T are given in Ref. [39].

Starting from the temperature and species mass fractions, i.e. the atomic mass fractions and the mass fractions of the different molecular vibrational levels, unknowns of the system (3.2), the transport properties are obtained by means of the modified Chapman-Enskog theory [7; 8] (see also Section 1.1).

3.1.2 Non-equilibrium processes

Gas-phase reactions and state-resolved rates models

The gas-phase state-to-state vibrational and chemical kinetic processes considered in this study are: the vibrational-vibrational, VV, and vibrational-translational, VT_m, energy transitions due to the collisions between two molecules, that also include the dissociation-recombination reactions by means of the ladder climbing model and the assumption, in the dissociation rates calculation, of a vibrational level, representing the atoms, above the last bound molecular vibrational level [126—132]

$$\mathrm{N_2}(i_1) + \mathrm{N_2}(i_2) \rightleftharpoons \mathrm{N_2}(i_1 + 1) + \mathrm{N_2}(i_2 - 1), \tag{3.3}$$

$$\mathrm{O_2}(i_1) + \mathrm{O_2}(i_2) \rightleftharpoons \mathrm{O_2}(i_1 + 1) + \mathrm{O_2}(i_2 - 1), \tag{3.4}$$

$$\mathrm{N_2} + \mathrm{N_2}(i_1) \rightleftharpoons \mathrm{N_2} + \mathrm{N_2}(i_1 - 1), \tag{3.5}$$

$$\mathrm{O_2} + \mathrm{O_2}(i_1) \rightleftharpoons \mathrm{O_2} + \mathrm{O_2}(i_1 - 1); \tag{3.6}$$

the vibrational-translational, VT_a, energy transitions due to the collisions between an atom and a molecule [111; 132—135]

$$\mathrm{N} + \mathrm{N_2}(i_1) \rightleftharpoons \mathrm{N} + \mathrm{N_2}(i_2), \tag{3.7}$$

$$\mathrm{O} + \mathrm{O_2}(i_1) \rightleftharpoons \mathrm{O} + \mathrm{O_2}(i_2), \tag{3.8}$$

$$\mathrm{N} + \mathrm{O_2}(i_1) \rightleftharpoons \mathrm{N} + \mathrm{O_2}(i_2); \tag{3.9}$$

the direct dissociation caused by the collisions between an atom and a molecule [111; 132—134; 136]

$$\mathrm{N} + \mathrm{N_2}(i) \rightleftharpoons 3\mathrm{N}, \tag{3.10}$$

$$\mathrm{O} + \mathrm{O_2}(i) \rightleftharpoons 3\mathrm{O}, \tag{3.11}$$

$$\mathrm{O} + \mathrm{N_2}(i) \rightleftharpoons \mathrm{O} + 2\mathrm{N}, \tag{3.12}$$

$$\mathrm{N} + \mathrm{O_2}(i) \rightleftharpoons \mathrm{N} + 2\mathrm{O}; \tag{3.13}$$

and finally the exchange Zeldovich reactions [111; 132; 136]

$$\mathrm{O} + \mathrm{N_2}(i_1) \rightleftharpoons \mathrm{N} + \mathrm{NO}(i_2), \tag{3.14}$$

$$\mathrm{N} + \mathrm{O_2}(i_1) \rightleftharpoons \mathrm{O} + \mathrm{NO}(i_2). \tag{3.15}$$

State-specific rate coefficients of processes (3.4)–(3.15) are obtained using quasi-classical trajectory calculations performed in [111; 127—130; 132—136].

Heterogeneous reactions and recombination probabilities

Unlike the gas-phase processes, the heterogeneous state-to-state reactions considered in the present work are not directly included in the boundary layer system (3.2). Instead, they are incorporated in the boundary conditions at the surface, following various models of wall mass fluxes discussed in Section 2.6.

The reactions at the surface are recombination reactions according to the Eley–Rideal impact mechanism, where desorption of a newly obtained particle is

assumed to be a part of the mechanism:

$$\mathrm{N} + \mathrm{N}^* \xrightarrow{\gamma_{\mathrm{NN}}(i)} \mathrm{N}_2(i) + *, \tag{3.16}$$

$$\mathrm{O} + \mathrm{O}^* \xrightarrow{\gamma_{\mathrm{OO}}(i)} \mathrm{O}_2(i) + *, \tag{3.17}$$

$$\mathrm{O} + \mathrm{N}^* \xrightarrow{\gamma_{\mathrm{ON}}(i)} \mathrm{NO}(i) + *, \tag{3.18}$$

$$\mathrm{N} + \mathrm{O}^* \xrightarrow{\gamma_{\mathrm{NO}}(i)} \mathrm{NO}(i) + *, \tag{3.19}$$

where $*$ is an active adsorption site of the surface, N^* and O^* are nitrogen and oxygen adatoms, i.e. atoms adsorbed on the surface. Adsorption and desorption as separate processes are not included to the present work. It is worth noting that the heterogeneous recombination Eley–Rideal mechanism is chosen due to its simplicity.

The recombination coefficients $\gamma_{\mathrm{NN}}(i)$, $\gamma_{\mathrm{OO}}(i)$, $\gamma_{\mathrm{NO}}(i)$ and $\gamma_{\mathrm{ON}}(i)$, for a SiO_2 surface, are calculated at each iteration up to convergence [28] (see also 3.2.2) due to their dependence on both the surface properties and the impinging flux [109; 110]. To be precise, the global (i.e. independent of vibrational level) heterogeneous recombination coefficients are calculated, then they are uniformly spread on the corresponding molecule vibrational ladders. To argue the reason of this uniform spread is beyond the aim of the present work, however it was discussed in [111] based on the studies [103; 131; 137—140].

It is important to stress that in each model investigated in the present work, i.e. Model I, Present model and Barbato model (see Sec. 2.6), the recombination coefficients are calculated using the approach proposed in [109; 110]. The choice of the mentioned approach is due to its ability to account for the dependence of the recombination probability not only on the surface temperature but also on the flow characteristics.

3.1.3 Diffusion velocity models

All introduced in Sec. 2.6 boundary conditions for species mass fluxes depend on the diffusion velocity. The rigorous state-specific relation (1.36) requires the knowledge of numerous parameters. Moreover, in such a case, the boundary conditions will form a system of non-linear equations that must be solved at each iteration. For the sake of simplicity, it is preferable to employ simplified models for

the diffusion velocity. One of the commonly used models is the Fick law:

$$\rho_{ci}\mathbf{V}_{ci} = -\rho D_{ci}\nabla\cdot\left(\frac{\rho_{ci}}{\rho}\right), \qquad D_{ci} = \frac{1-n_{ci}/n}{\sum\limits_{dk} n_{dk}/(n\mathcal{D}_{cidk})}, \tag{3.20}$$

where D_{ci} is the effective diffusion coefficient, $\mathcal{D}_{cidk}$ are binary diffusion coefficients for each pair of chemical-vibrational species, ci and dk.

The Hirschfelder-Curtiss (HC) [141] approximation is another simplified model for the diffusion velocity, which can be used as an alternative to (3.20):

$$n_{ci}\mathbf{V}_{ci} = -nD^{*}_{ci}\mathbf{d}_{ci}, \qquad D^{*}_{ci} = \frac{1-\rho_{ci}/\rho}{\sum\limits_{dk,dk\neq ci} n_{dk}/(n\mathcal{D}_{cidk})}. \tag{3.21}$$

The Fick law is commonly used in fluid dynamics but originally it was limited to binary mixtures [142; 143]; expression (3.20) represents its generalization for the STS approach. However, it still neglects thermal and barodiffusion as well as cross-coupling between gradients of various species mass fractions. The Hirschfelder–Curtiss law partially overcomes these limitations since it includes species molar fractions and diffusive driving forces, similarly to initial definition (1.36). Thus, the HC law is treated here as more accurate. However, neither of these relations can provide the global mass conservation $\sum_{ci}\rho_{ci}\mathbf{V}_{ci} = 0$. This constraint can be satisfied by adding a correction to the diffusion velocity expressions [142].

3.2 Results and discussion

In this section, results of numerical modeling of a five-component air mixture flow in the boundary layer in the vicinity of the stagnation point are presented. Different models of slip boundary conditions are implemented and assessed.

For the readability of the following figures, it is useful to specify that coordinate η, when equal to 0, corresponds to the surface, and $\eta = \eta_{Max} = 8$ corresponds to the boundary layer external edge.

3.2.1 Test cases description

To numerically solve the system (3.2), the flow parameters at the external edge of the boundary layer need to be specified. The chosen datasets are presented in Table 1. The considered sets correspond to the parameters after the detached shock

Table 1 — External edge flow parameters and surface temperature.

Notation	T_e, K	T^w, K	p_e, Pa	β, 1/s
EP1 (85 km)	7000	1000	1000	5000
EP2 (60 km)	9500	1150	17600	3086

wave near a hypersonic re-entry vehicle. The altitudes for the considered cases are approximately equal to 85 km and 60 km, respectively. Mach number of the free steam flow for both sets is equal to 15. The varying parameters are the temperature T_e, the pressure p_e, and the parameter β, dependent on the vehicle nose radius. The air mixture composition at the external edge is 78.58% N_2+N, 21.38% O_2+O, 0.04% NO. Both nitrogen and oxygen at the boundary layer external edge are split between the respective molecules and atoms following the chemical equilibrium at the external temperature T_e, and the molecular vibrational distributions are the Boltzmann ones. The silica surface wall temperature values T^w are 1000 K and 1150 K, correspondingly to the chosen set of external edge parameters.

For the first set of parameters (EP1), the Knudsen number at the external edge is approximately 0.007. The other set of external flow conditions corresponds to a less rarefied gas scenario, with Kn estimated as 0.0006.

Numerical modeling for each set of external edge parameters is performed for different test cases of slip boundary conditions considered. The test cases are summarized in Table 2. Starting from this point, the subsequent assumptions are made: 1) the velocity slip is neglected in all the cases since its effect in the stagnation region is small; 2) the temperature jump is considered based on the specular-diffusive (Maxwell) kernel and is given by Eq. (1.94), the mass fluxes in the expression are calculated according to the models introduced in Table 2; the accommodation coefficient σ for the cases considered is set to 0.5 unless stated otherwise (its values will be varied later in Sec. 3.2.7); 3) the diffusion velocity is chosen according to

Table 2 — Test cases for considered catalytic model and temperature jump (TJ).

Notation	Description
TC0: Barbato	Eqs. (2.40)-(2.41), no temperature jump
TC1: TJ	Non-catalytic surface, temperature jump
TC2: Model I+TJ	Eqs. (2.33)-(2.34), temperature jump
TC3: Barbato+TJ	Eqs. (2.40)-(2.41), temperature jump
TC4: No-Slip	Non-catalytic surface, no temperature jump
TC5: Present+TJ	Eqs. (2.37)-(2.38), temperature jump
TC6: Present	Eqs. (2.37)-(2.38), no temperature jump

models described in 3.1.3, and for the test cases of Table 2, the Fick law is applied; however, another model is tested as well in Section 3.2.6.

3.2.2 Numerical scheme

Before reporting the outcomes of the modeling, it is essential to include some discussion about the numerical scheme used in this study. The numerical simulation of the considered problem was conducted in collaboration with Dr. I. Armenise (CNR ISTP, Bari) using the scheme reported in [39]. A brief overview of the method is provided below.

To solve the boundary layer system of equations (3.2), an iterative finite-difference numerical method is applied. The coordinate normal to the surface, η, is uniformly divided into 160 nodes of the grid (see below for the discussion of grid convergence). Then, the equations are discretized using central finite differences on this grid. The slip conditions are discretized accordingly. At the initial stage, the Gauss iterative method is employed to solve the system of discretized equations with a triangular matrix, using the initial conditions for the parameters y_i and $\theta = T/T_e$ at each grid node. This allows recalculating the parameter values, and these updated values are then inserted both into the coefficient matrix and the known vector. The system is then solved again to obtain new values of y_i and θ. This process is repeated until a steady-state flow is achieved.

As for slip BCs, simplified models for diffusion velocity are applied (see 3.1.3), eliminating the need to solve a system of equations for discretized boundary conditions. However, this is faithful since the square root of the temperature boundary value in species concentrations and temperature BCs is obtained from the previous iteration. Otherwise, solving a system of non-linear equations is required, which is even more complex when rigorous diffusion velocity models are applied. The latter will also be necessary in the case of finite-volume methods. In such cases, the values of macroscopic parameters in fictitious cells are obtained, and then the system of equations needs to be solved.

Grid convergence

The equations of system (3.2) are discretized by central differences on a uniform grid containing 160 nodes. The chosen number of grid nodes has been verified by repeating the calculations for EP1 conditions (see Table 1) and test case TC5 (see Table 2) on two finer grids of 320 and 640 nodes, respectively. By the results for different variables obtained for the three grids on the nodes corresponding to the 160-nodes grid, the Richardson Extrapolation has been performed and the corresponding values RE_n (n is the node number index) have been obtained. Such a technique was used in [144]. Finally, by comparing these extrapolated values with the values originally obtained on the 160 nodes grid, O_n, the χ^2 test has been calculated:

$$\chi^2 = \sum_{n=1}^{N} \frac{(O_n - RE_n)^2}{RE_n}. \tag{3.22}$$

To give some examples, the χ^2 values are 0.15 for the N_2 density, $1.28 \cdot 10^{-2}$ for the N density, $3.86 \cdot 10^{-6}$ for the O_2 density, $8.47 \cdot 10^{-3}$ for the O density and $4.13 \cdot 10^{-4}$ for the NO density, much less than $N = 160$. To summarize, a grid of 160 nodes returns a good approximation to the results.

3.2.3 Rates of heterogeneous reactions

Heterogeneous recombination probabilities that correspond to the surface processes (3.16)-(3.19), as is already mentioned, are calculated on the basis of the approach proposed in [28; 109]. Different values of the probabilities depending on the chosen test case of slip boundary conditions are presented in Table 3 for the first set of external edge parameters and the wall temperature value of 1000 K. Test cases

Table 3 — Recombination probabilities calculated for different test cases.

Test case	γ_{NN}	γ_{OO}	γ_{ON}	γ_{NO}
TC0: Barbato	1.955e-3	1.264e-2	4.236e-3	8.213e-3
TC2: Model I+TJ	6.875e-3	5.961e-3	1.49e-2	3.874e-3
TC3: Barbato+TJ	3.316e-3	1.079e-2	7.185e-3	7.013e-3
TC5: Present+TJ	6.607e-3	6.324e-3	1.432e-2	4.111e-3
TC6: Present	6.573e-3	6.371e-3	1.424e-2	4.141e-3

TC1 and TC4 corresponding to a non-catalytic surface are not included in this table. One can see that, according to the Barbato model, the maximum probabilities are obtained for heterogeneous oxygen recombination (3.17) and NO formation (3.19). For all other models, the dominating surface reaction is NO recombination (3.18) involving nitrogen adatoms and gas-phase oxygen atoms; recombination probabilities calculated for test cases 2, 5 and 6 are in close agreement. The effect of the temperature jump on recombination probabilities is weak; for the Present model its contribution is within 1%. The effect of the approach (Model I versus Present model) is also weak although the difference is slightly greater.

It is interesting to compare effective recombination coefficients obtained for various models. Table 4 presents the coefficient for oxygen recombination (3.17), which appears in different models for the molecular mass fluxes discussed in Section 2.6. One can notice that the expressions for effective reaction rate coefficients of the Model I and the Present model under the assumptions made in Section 3.2.1 are close to the ones of the Barbato model. However, upon closer examination, despite the similarities in their expressions, there exist noticeable differences in the actual values. These values were obtained from the TC5 simulations using the same

Table 4 — Effective rate coefficient for heterogeneous oxygen recombination (3.17).

Model	$k^{w,\mathrm{rec}}_{\mathrm{O},\mathrm{O}_2}$, cm/s, 85 km	$k^{w,\mathrm{rec}}_{\mathrm{O},\mathrm{O}_2}$, cm/s, 60 km
Model I	156.7	249.5
Present model	444.7	709.6
Barbato model	193.6	318.9
Molecular dynamics [145]	451.1	631.1

macroscopic parameters and recombination probabilities. The results are compared with recent molecular-dynamic (MD) simulations carried out in [145]. It is worth mentioning that the calculations were conducted on the basis of the simplified impact recombination mechanism since here the same mechanism 3.1.2 is considered, and the certain parameters associated with other mechanisms are unavailable.

One can see that the effective recombination rates are strongly affected by the model: the Barbato model and Model I yield a considerably lower value of $k^{w,\mathrm{rec}}_{\mathrm{O},\mathrm{O}_2}$ compared to the Present model. The best agreement with MD simulations [145] is provided by the Present model. This indicates the importance of correct evaluation of normal mass fluxes on the surface. Model I underestimates the mass flux since it does not take into account contribution of different molecular species to $\mathbf{J}_{M(i)}$. The phenomenological Barbato model does not account for rarefaction effects and uses simplified expressions for the mass flux. The Present model is based on a more reliable kinetic boundary condition and shows good accuracy. Based on this analysis, the results of TC5 simulations are chosen as benchmark for the further discussion.

In addition to the Present model mentioned here, the developed approach allowed for another extension, as discussed in Section 2.4. Its distinctive feature is the ability to ensure the total mass flux conservation near the wall in the case of neglected adsorption/desorption processes. It is worth noting that the approach was constructed synthetically, and conservation is not necessarily required at every moment in time due to the dependence of heterogeneous reactions on adsorption/desorption processes. The effective recombination coefficient, $k^{w,\mathrm{rec}}_{\mathrm{O},\mathrm{O}_2}$, for this model is two times smaller than that of the Present model, although it remains higher than those provided by Model I and Barbaro formulas. This difference arises from variations in their wall mass fluxes relations, given by equations (2.27) and (2.22). In the Present model (2.27), additional terms involving the ratio of particle

masses m_d/m_c are introduced. The observed value of the effective recombination coefficient also supports the choice of the Present model as a benchmark. However, due to extreme similarities in the models, an extended comparison is recommended, and this will be done in Section 3.2.6.

3.2.4 Fluid-dynamic variables

First of all, it is essential to compare the distributions of fluid-dynamic variables across the boundary layer.

Temperature

To start with, the temperature jump on the surface for different test cases need to be evaluated. In Table 5, the gas temperature near the surface (at $\eta = 0$) is given for several test cases taking into account temperature jump (TJ) and two sets of external flow conditions corresponding to a different rarefaction degree. All

Table 5 — The effect of temperature jump on T at $\eta = 0$.

Test case	$T(\eta = 0)$, K (85 km)	$T(\eta = 0)$, K (60 km)
TC4: No-Slip	1000	1150
TC1: TJ	1437	1368
TC2: Model I+TJ	1452	1379
TC3: Barbato+TJ	2590	1731
TC5: Present+TJ	1485	1390

models except the one of Barbato yield close values of the temperature jump. The latter model (TC3) considerably overpredicts the gas temperature near the surface; this is confirmed by DSMC [1] and viscous shock layer simulations [146] providing the TJ values similar to those obtained for the Present model. It is not surprising that for higher altitude (higher rarefaction), the temperature jump is larger. Thus,

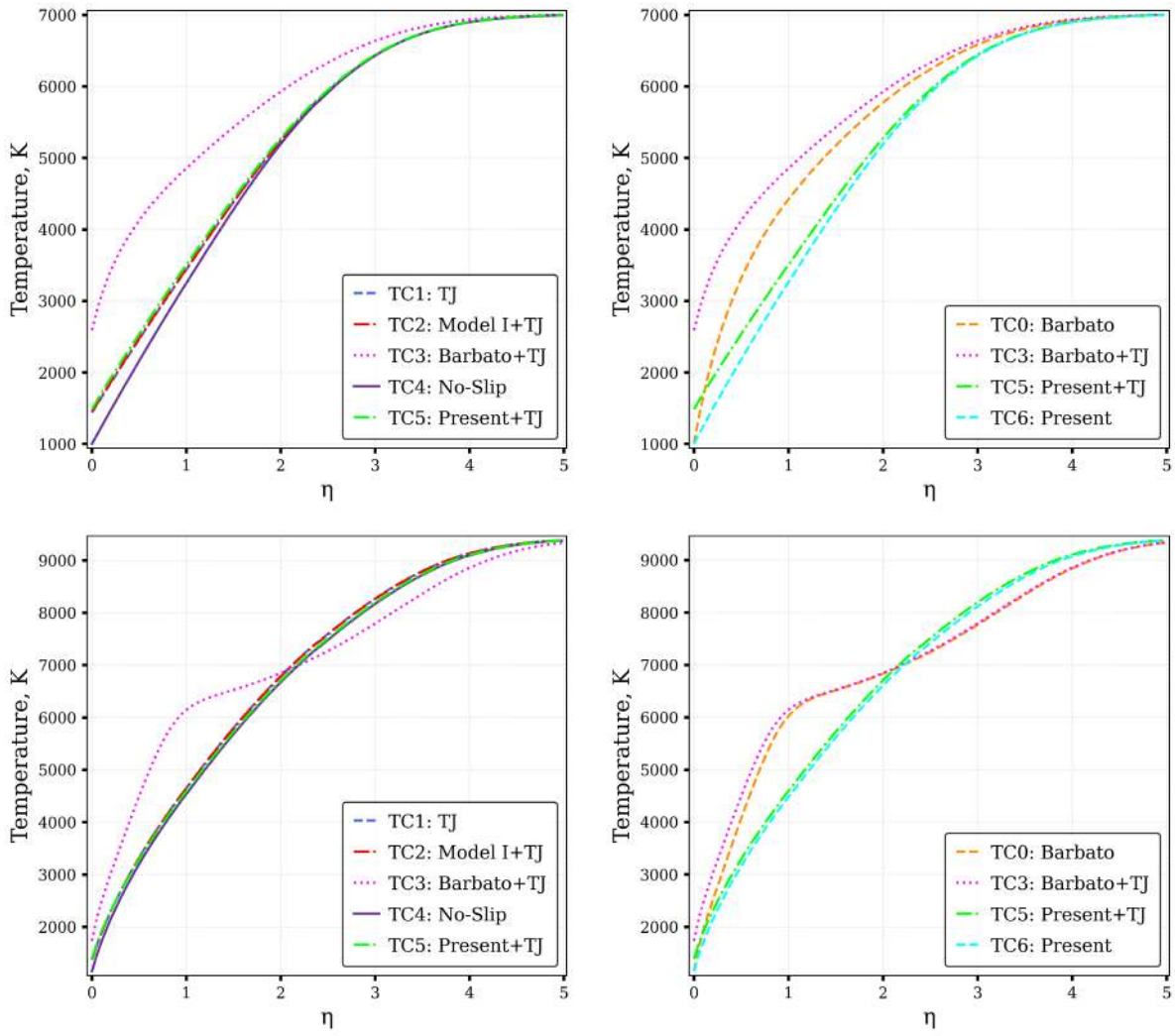

Figure 3.1 — Temperature profiles as functions of η. Top panel: case EP1 (85 km). Bottom panel: EP2 (60 km). Left plots: comparison between TC1–TC5; right plots: more detailed comparison between the Barbato and Present models.

for the altitude of 85 km the average gas temperature variation near the surface is about 45% of T^w whereas for 60 km, it is about 12%.

Temperature distributions as functions of η are reported in Fig. 3.1. For Model I and Present model, the temperature profiles are rather close, showing some discrepancy near the surface ($\eta < 1.5$) due to the temperature jump for the case EP1 (85 km); for the less rarefied gas (60 km), the effect of TJ and surface processes model is almost negligible. Situation is quite different for the Barbato model, which yields larger temperature jump, sharp increase in T near the surface and considerably higher temperature at $\eta < 2.5$, which alters gas-phase chemical reaction mechanisms. For the case EP2 (60 km), the shape of temperature distribution is non-uniform across the layer, with change of convexity in the middle

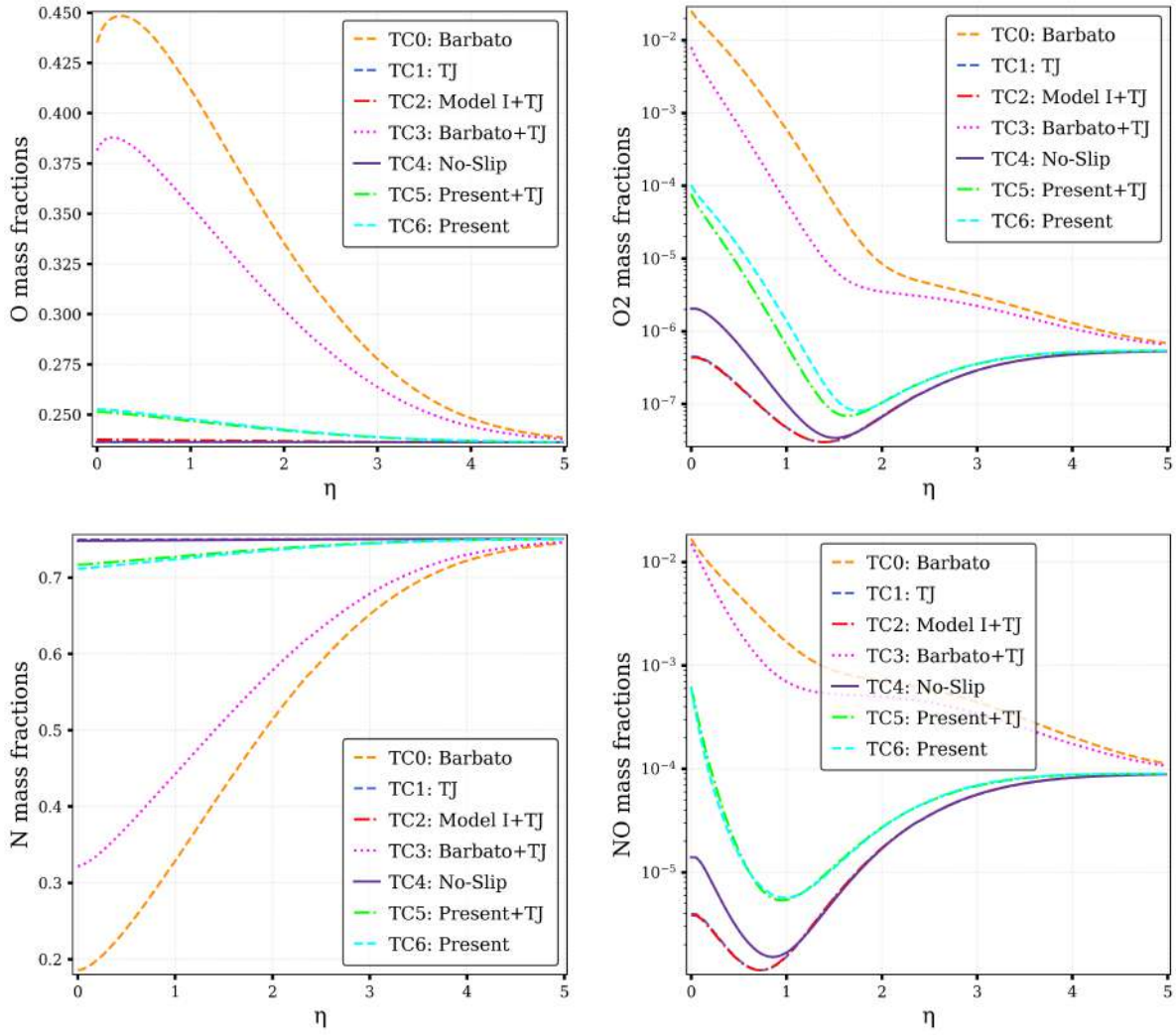

Figure 3.2 — Species mass fractions as functions of η. Case EP1 (85 km).

of the boundary layer. The reasons for such behaviour may be associated with strong coupling of fluid-dynamic and chemical processes and possibly mutual effect of gas-phase and heterogeneous reactions for this model.

Mass fractions

Mass fraction distributions across the boundary layer are plotted in Figs. 3.2–3.3. Whereas the mass fraction of nitrogen decreases monotonically from the external edge towards the surface, fractions of other species may behave non-monotonically, depending on the model and altitude. For the Barbato model, there is a strong competition between gas-phase and surface reactions; this explains

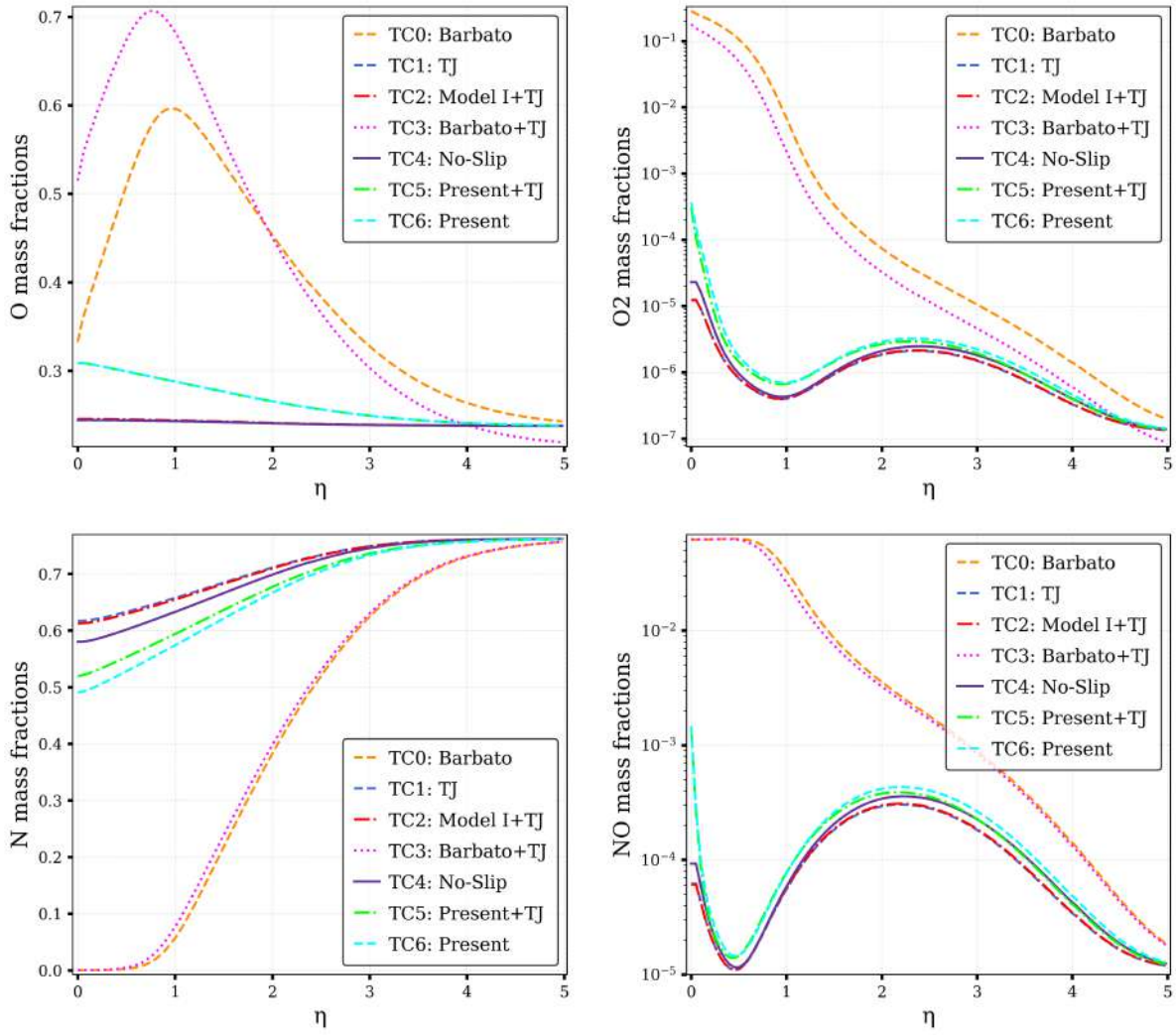

Figure 3.3 — Species mass fractions as functions of η. Case EP2 (60 km).

y_O maxima occurring at $\eta < 1$. Analysis of gas-phase reactions shows that for the Barbato model, the contribution of reaction (3.15) in the gas phase is high, which leads to a sharp decrease of y_N towards the wall with corresponding increase in the mass fractions of O and NO, partially compensated near the wall by surface recombination. Such a chemical mechanism is associated with the temperature distribution across the boundary layer, which, for the Barbato model significantly differs from other models. This effect is especially pronounced for lower altitude (case EP2, 60 km). All other models yield qualitatively similar distributions of the species mass fractions in the boundary layer, with a noticeable difference near the surface. The results obtained using the Model I are close to those for a non-catalytic wall. Therefore, this «weakly catalytic» model underpredicts the catalytic effects caused by the contributions of all molecules to the mass flux of a given molecular species. The effect of the temperature jump for the case EP2 (60 km) is small; it increases

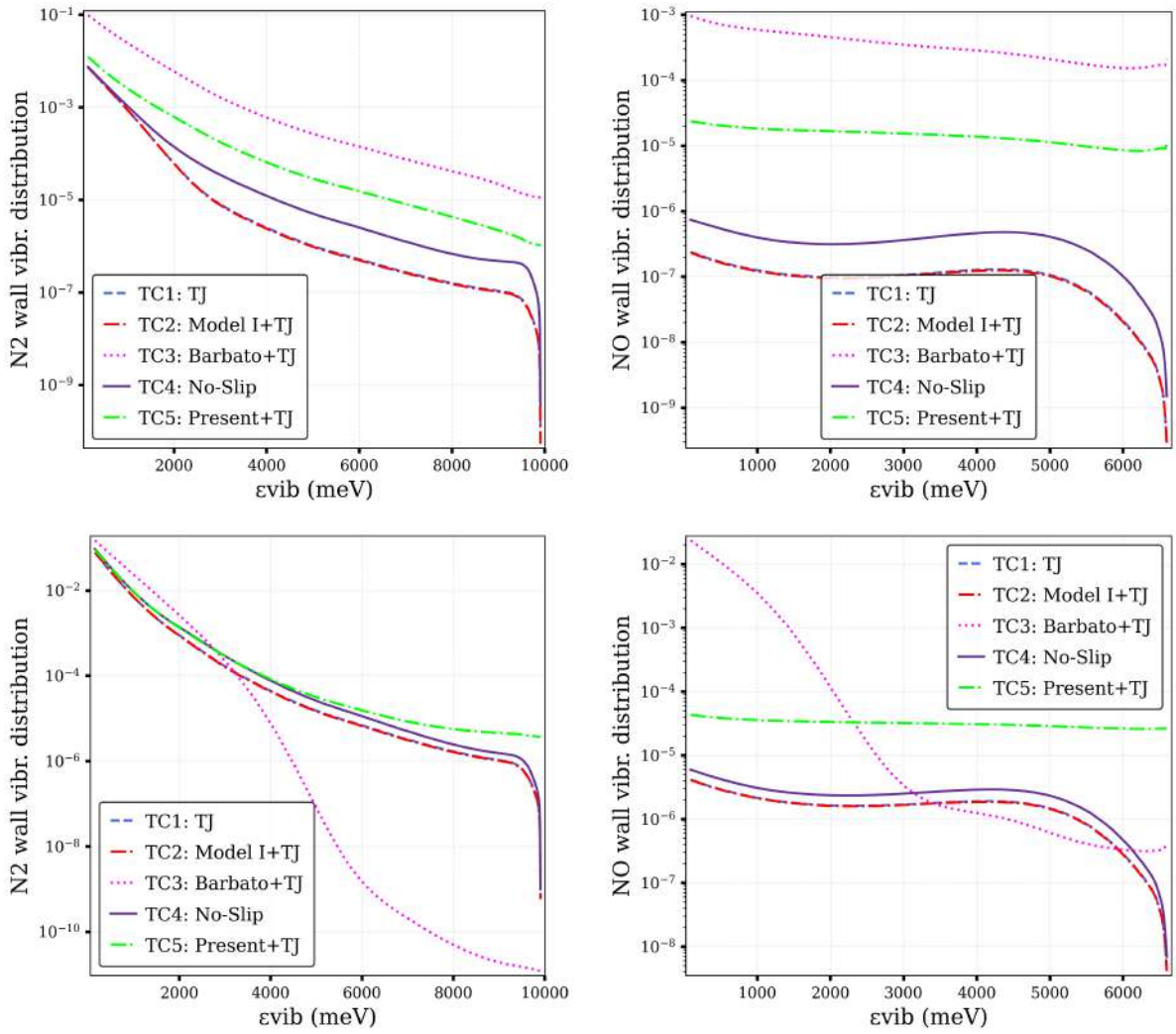

Figure 3.4 — N_2 and NO vibrational distributions at the wall ($\eta = 0$) as functions of vibrational energy. Top panel: case EP1 (85 km). Bottom panel: EP2 (60 km).

with the altitude and is expected to be much greater for lower Knudsen numbers. Note that for a non-catalytic wall, taking into account the temperature jump yields some decrease in the NO and O_2 surface mass fractions for the case EP1 (85 km).

Vibrational energy distributions

Molecular state-to-state vibrational distributions near the surface are reported in Fig. 3.4 for two sets of external flow parameters and different models of catalytic properties and slip boundary conditions. For the case EP1 (85 km), vibrational distributions of nitrogen show gradual decreasing with the energy. For a non-

catalytic surface and weakly catalytic Model I, one can see some perturbations and depopulation of high states due to gas-phase dissociation processes; these processes are compensated by heterogeneous reactions when the Barbato and Present model are used. For these models the distributions vary smoothly with the vibrational energy per molecule ε_{vib}. Oxygen vibrational distributions show similar behaviour as those of nitrogen. NO vibrational distributions for non-catalytic (TC1, TC4) and weakly catalytic (TC2) models have a more sophisticated shape with a kind of inversion of level populations at intermediate energies. For the catalytic models (TC3, TC5), higher levels are more populated due to more efficient surface recombination processes; for the Barbato model, additional contribution is from the gas-phase Zeldovich reaction. For the case EP2 (60 km) with lower rarefaction, vibrational distributions of O_2 keep the same qualitative behaviour, distributions of N_2 (except for the Barbato model) become close to each other at the low and intermediate states and show some discrepancy for high energy, when the Present model is used. For these models, NO distributions are qualitatively similar to those obtained in the EP1 case but are found to be higher. The Barbato model yields essentially different vibrational distributions for N_2 and NO, which are perturbed by the mutual effect of gas-phase and heterogeneous reactions. The temperature jump considerably affects the vibrational distributions (compare cases TC1 and TC4) for the case EP1 but weakly influences level populations for the EP2 case, which is in agreement with the results for the mixture composition discussed above.

3.2.5 Heat fluxes

In this subsection, the total heat flux values and the contributions of various transport processes to the energy flux across the boundary layer are discussed. Fig. 3.5 shows the total heat flux across the boundary layer calculated for two sets of external flow parameters and different models for boundary conditions. For both altitudes, the Barbato model overestimates the heat flux, both at the surface and in a flow, especially when the temperature jump is neglected. Including the temperature jump to the slip boundary conditions causes a significant decrease in the surface heat flux; the difference is larger for a more rarefied flow. A similar conclusion is drawn in [146]; some quantitative estimates are discussed hereafter in

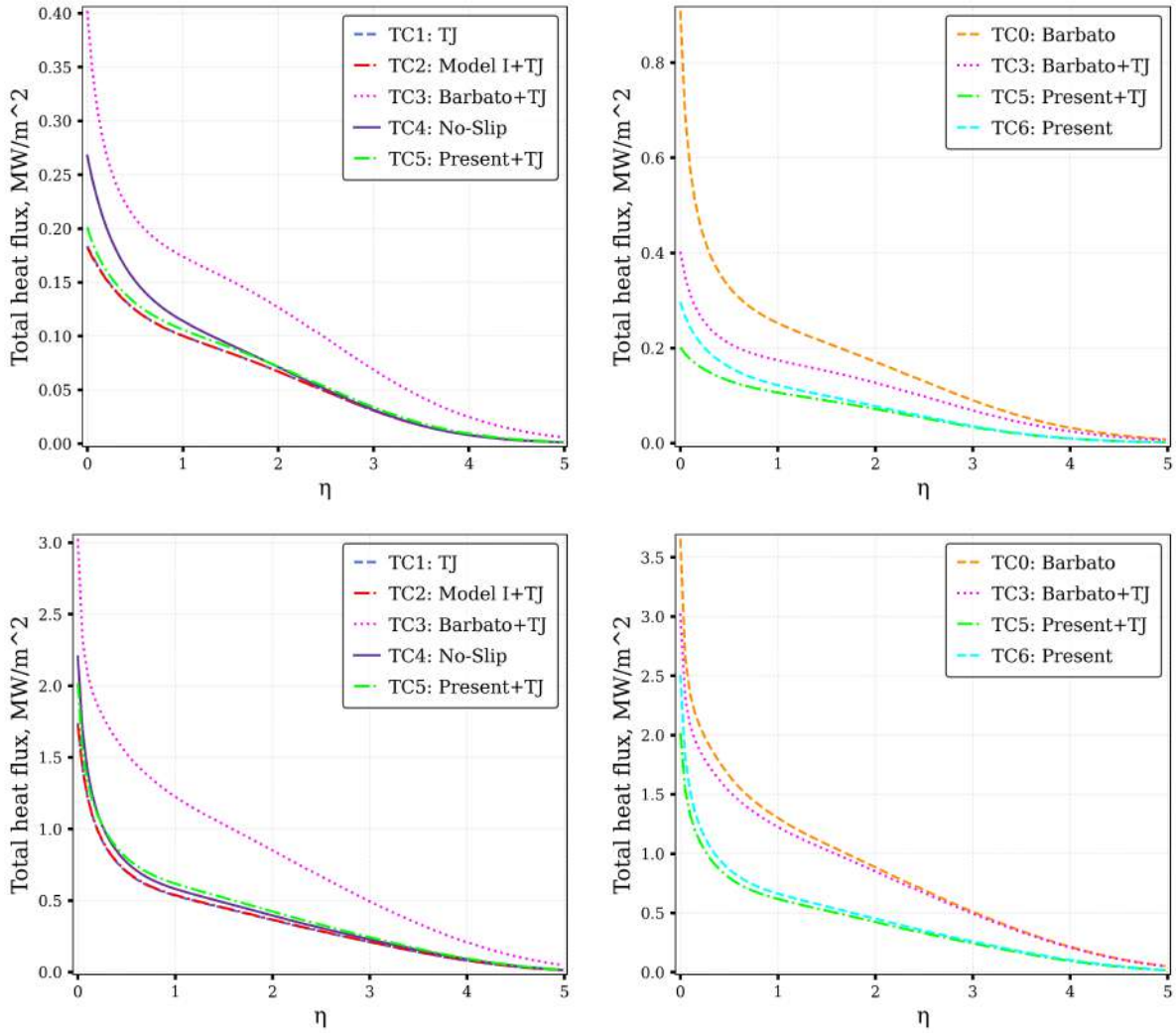

Figure 3.5 — Total heat flux as a function of η. Top panel: case EP1 (85 km). Bottom panel: EP2 (60 km). Left plots: comparison between TC1–TC5; right plots: more detailed comparison between the Barbato and Present models.

this section. The effect of surface catalyticity is not that high as expected (except for the Barbato model). The reason for such a small effect may be associated to the competition of mass diffusion and vibrational energy diffusion discussed hereafter.

Contributions of thermal conduction (Fourier), thermal diffusion (TD), mass diffusion (MD), and vibrational energy diffusion (DVE) to the total heat flux are plotted in Figs. 3.6 and 3.7 as functions of η for different test cases. Note that the latter process occurs only in the state-to-state approach; in the multi-temperature models it is rather connected with gradients of vibrational temperatures. As is shown in [26; 32], the contribution of thermal diffusion is of the same order as the Fourier flux; this process has to be taken into account in the stagnation line flow simulations. For the Barbato model, the mass diffusion flux is of the same order as the Fourier

flux for the EP2 case and about three times lower for the EP1 case. For other models, the MD contributions are found much lower compared to the Fourier flux. An interesting effect is that the contribution of vibrational energy diffusion is close to the MD contribution but has the opposite sign, which causes strong compensation effects for these two transport processes.

Table 6 — Stagnation point wall heat fluxes, obtained from the different test cases and some phenomenological models.

Model	EP1 (85 km) $\mathbf{q}^w$, MW/m^2	EP2 (60 km) $\mathbf{q}^w$, MW/m^2
TC0: Barbato	0.9084	3.654
TC1: TJ	0.1836	1.740
TC2: Model I+TJ	0.1822	1.726
TC3: Barbato+TJ	0.4021	3.025
TC4: No-Slip	0.2675	2.202
TC5: Present+TJ	0.2012	2.017
TC6: Present	0.2967	2.506
Fay-Riddel, non-catalytic [147]	0.2524	1.6997
Goulard [148]	0.6937	2.7210
Fenster [149]	0.0915	0.3545
Sutton-Graves [150]	1.2916	8.7795

In Table 6, the stagnation point surface heat fluxes calculated for different test cases are presented and compared with the results obtained on the basis of semi-empirical expressions widely used in the computational fluid dynamics. Approximate calculations of the heat flux were performed using the data of the benchmark TC5 case, and, as one can notice, show significant scatter in q^w values. The surface heat flux calculated using the Fay–Riddel formula for a non-catalytic wall [147] agrees well with the flux calculated for the non-catalytic surface without temperature jump (TC4) for both considered cases of gas rarefaction. The value provided by the formula is about 6% smaller for the more rarefied gas case, and in the case of high-enthalpy flow at 60 km altitude, the value differs by approximately 22%. Such results are consistent with the recent analysis of this expression [151]. The Fay-Riddel formula for a fully catalytic surface cannot be used in the present study since it is

limited to the case when the Lewis number is greater than unity; in the simulations performed, Le may be less than 1. The Goulard heat flux [148], representing an improvement of the Fay–Riddel formula by including the wall catalytic activity in more detail, overestimates the heat flux. For the set of EP1 parameters the Goulard formula provides a relatively high q^w value, comparable to the data provided by the Barbato model. In the less rarefied gas regime, it still yields a high value, but comparable to the result of TC6. The results of the other models by Fenster [149] and Sutton-Graves [150] yield extreme deviations in the heat flux values. Based on the above information, it is not recommended to use the mentioned formulas for heat fluxes when dealing with low-density gases and surfaces with small catalytic activity. Besides the mentioned phenomenological formulas and the exact solutions for heat fluxes from kinetic theory, there exist other theoretical approaches to find approximate heat flux expressions, e.g., within the framework of the viscous shock layer (VSL) and thin VSL theories [152; 153]. However, these expressions are provided for higher altitudes (from 90 km) of the Earth's atmosphere and are not compared here.

It is interesting to evaluate separately the contribution of the temperature jump (TJ) and heterogeneous reactions (HR) to q^w for the Present model (TC4–TC6). One can see that in the considered flow regimes, the TJ-effect is more important than that of HR, even for the case EP2 corresponding to the altitude of 60 km. Although formal inclusion of surface reactions increases q^w up to 10–15% (compare the results for TC4 and TC6), taking into account the temperature jump decreases the wall heat flux to a greater extent. Thus, for EP1 (85 km), the HR contribution of about 10% is compensated by about 30% decrease in q^w due to the temperature jump; the overall decrease in the wall heat flux is about 25% when both TJ and HR are included self-consistently. For the less rarefied case EP2, the HR positive contribution of about 14% is compensated by the negative effect of TJ (around 21%), which yields an overall decrease in q^w of about 8%. With rising Knudsen number, the contribution of weak surface chemistry decreases whereas the role of temperature jump becomes dominating.

It is worth emphasizing that the Present model used for TC5 simulations takes into account both TJ and HR effects self-consistently, and can be used in the continuum and slip flow regimes up to rather high $\mathrm{Kn} \sim 0{,}1 - 0{,}2$.

As for other models of heterogeneous reactions, it can be seen that the Model I underestimates the effect of surface chemistry. Contrarily, the Barbato

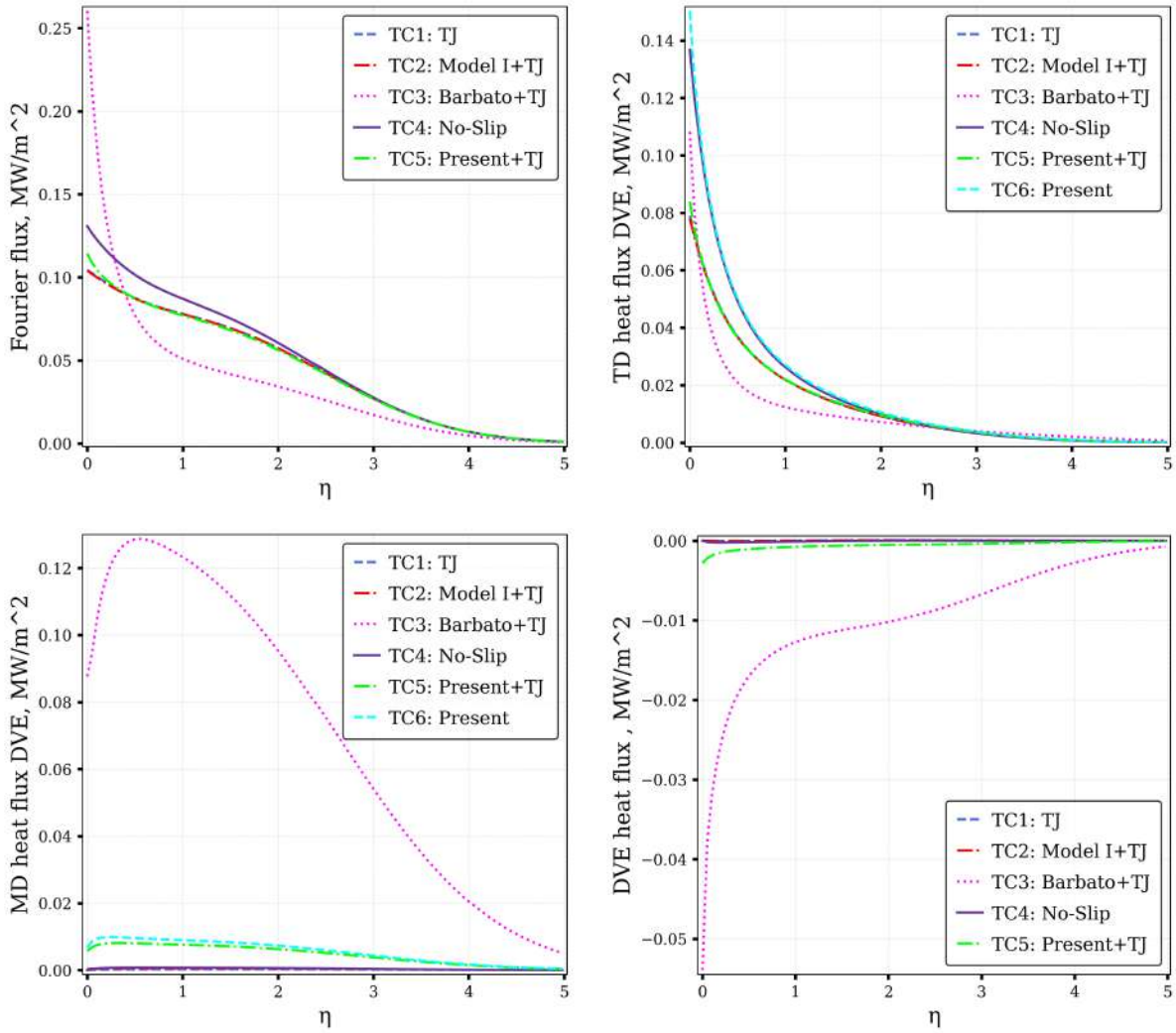

Figure 3.6 — Different contributions to the total heat flux as functions of η. Case EP1 (85 km).

model overpredicts the surface heat flux due to heterogeneous reactions. Such an important role of HR is not confirmed in flight experiments and other simulations based on the Scott recombination model [146]. In the latter work it was shown that for high altitudes, the results obtained for catalytic and non-catalytic surfaces become close, which is not the case for the Barbato model.

3.2.6 Influence of different formulations of slip BC

In this section, both Fick (3.20) and Hirschfelder–Curtiss (HC) (3.21) diffusion models are assessed. Additionally, different forms of the approach developed in

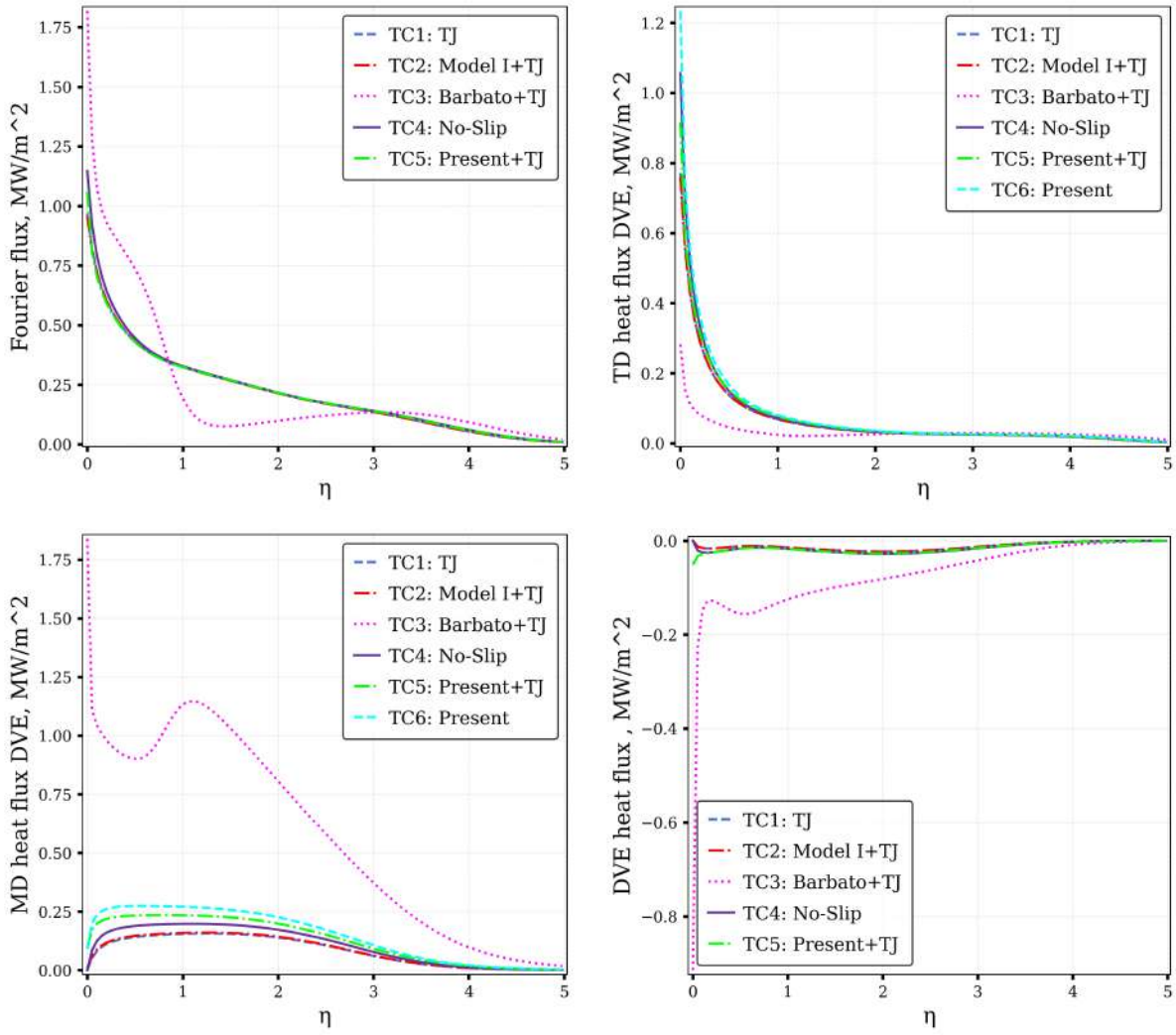

Figure 3.7 — Different contributions to the total heat flux as functions of η. Case EP2 (60 km).

Chapter 2 — extension I (Eqs. (2.27) and (2.24)) and extension II (Eqs. (2.22) and (2.23)) are examined in the boundary layer near stagnation point. The difference between these two developed extensions lies in fulfilling the balance laws when neglecting adsorption/desorption processes. The first one guarantees the conservation of the total number flux on the surface, while the second ensures the conservation of the total mass flux.

The velocity slip is neglected here as well, and the Maxwell model of particles scattering is chosen, with the accommodation coefficient set to 0.5. The notation is different from the previous sections: TC5 or TC6 from Sec. 3.2.1 correspond here for the extension I, but are denoted as I<Diffusion model>, <TJ case>; the similar notation is also applied for the extension II.

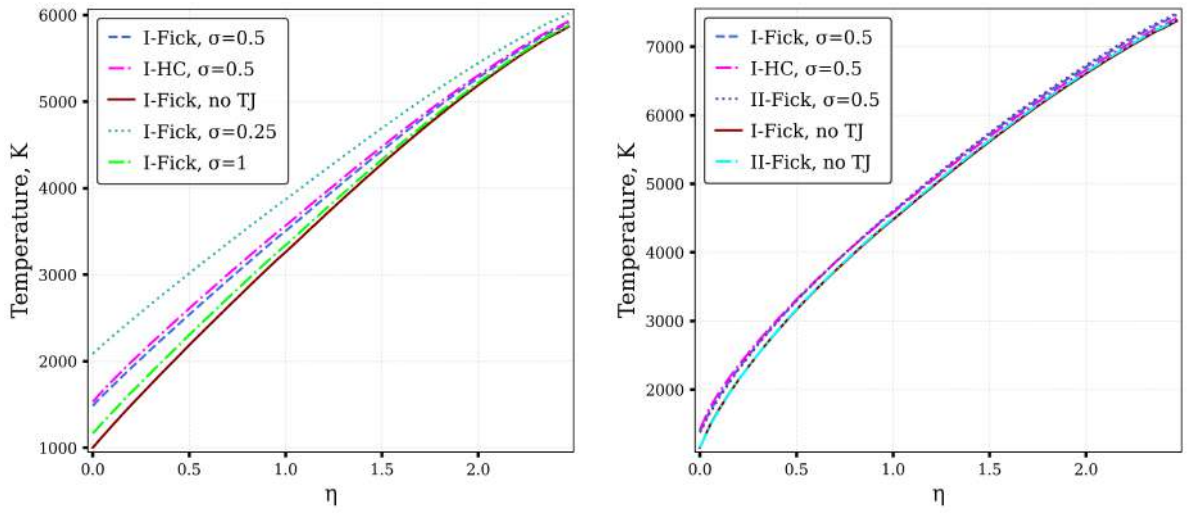

Figure 3.8 — Temperature profiles. Left – EP1 (85km) case, right – EP2 (60km) case.

Temperature profiles across the boundary layer are presented in Fig. 3.8, and, as can be seen, are barely affected by the chosen type of slip conditions and diffusion velocity model. The most significant difference is observed with the HC model, resulting in an approximate 2% increase in the wall temperature value.

Mass fraction variation in the boundary layer is plotted in Fig. 3.9 for N, N_2 particles. The impact of diffusion model is evaluated for nitrogen atoms and molecules as this effect is primarily observed for the chosen types of mixture species. First of all, it can be concluded that using original and modified kinetic boundary conditions yields similar results; maximum variation of up to 7% is observed in N mass fraction at the wall when the temperature jump is taken into account; for other fluid-dynamic variables, the effect is weaker. The impact of the diffusion model is much more significant, with N_2 showing changes up to 30% in the more rarefied gas case, EP1. Moreover, the diffusion effect is even more important than that of the temperature jump. Based on this analysis, it can be stated that using the Fick law may lead to noticeable inaccuracy in the mixture composition evaluation. Implementation of the kinetic theory diffusion model (Eq. (1.36)) or the relation with correction [142] requires further work and should be studied more thoroughly.

As for the total heat flux in the boundary layer (Fig. 3.10), the two types (I and II) of slip conditions have relatively minor effects, while the influence of the diffusion model is more significant. The difference is approximately 5% when considering or neglecting the temperature jump for the case of less rarefied gas scenario.

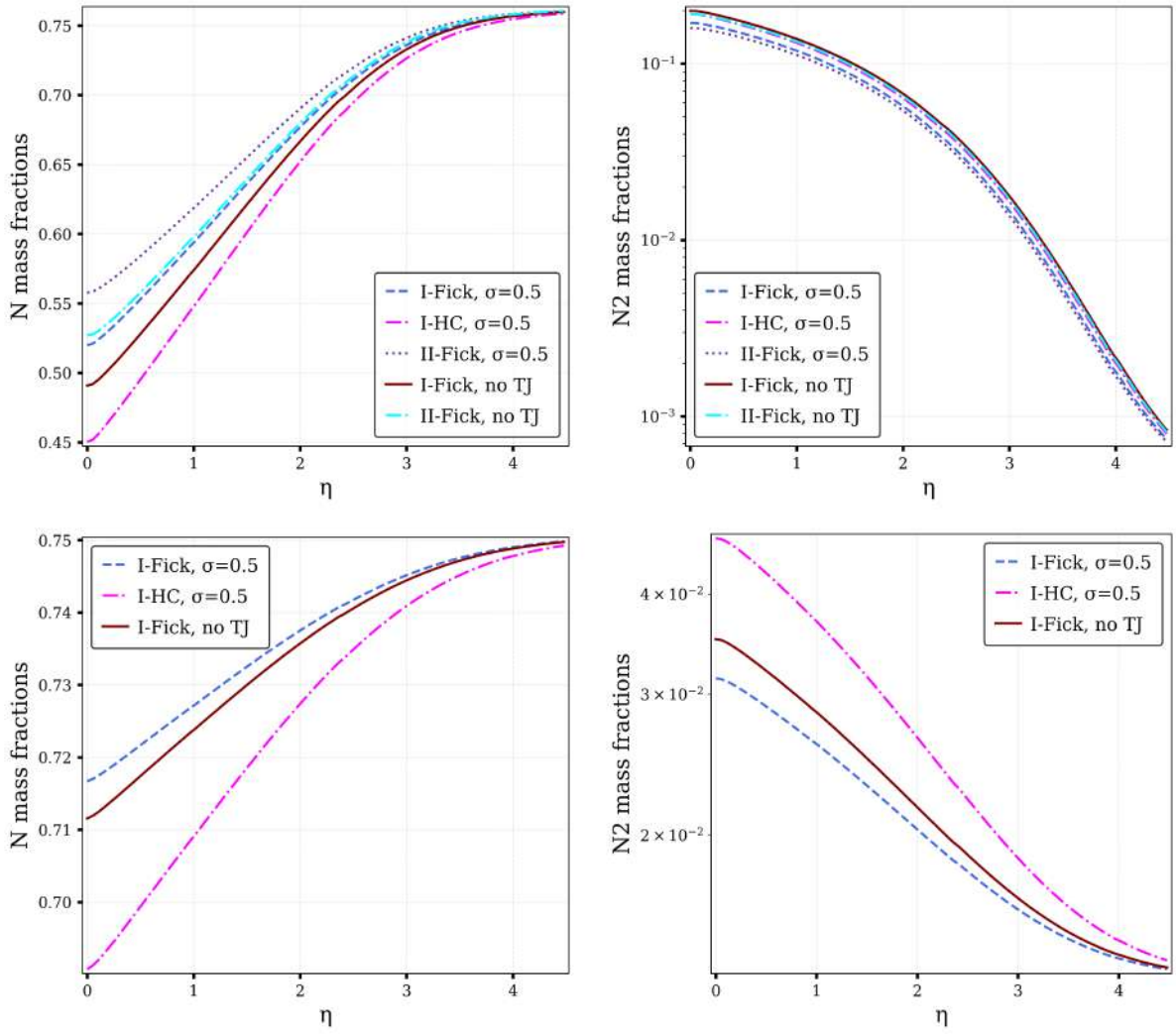

Figure 3.9 — N and N_2 mass fractions. Top – EP2 (60km) case, bottom – EP1 (85km) case.

3.2.7 Impact of accommodation coefficient

In this section, the accommodation coefficient, σ, appearing in the specular–diffusive model of particles scattering by solid wall is varied. Its influence on the air flow parameters in the boundary layer is examined for this set of values — $\{0, 0.1, 0.25, 0.5, 0.75, 1\}$. The notation for the test cases considered is the same, as in the previous section.

To begin with, as usual, the models impact on temperature should be evaluated. From Figs. 3.8 (1st one) and 3.11, one can notice that the influence of the accommodation coefficient is rather high. As the accommodation coefficient decreases, the temperature jump increases; this effect is stronger for $\sigma < 0.5$. This

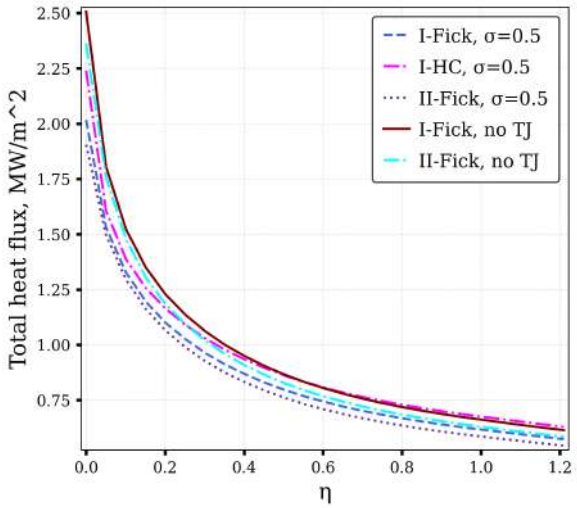

Figure 3.10 — Total heat flux, EP2 (60km) case.

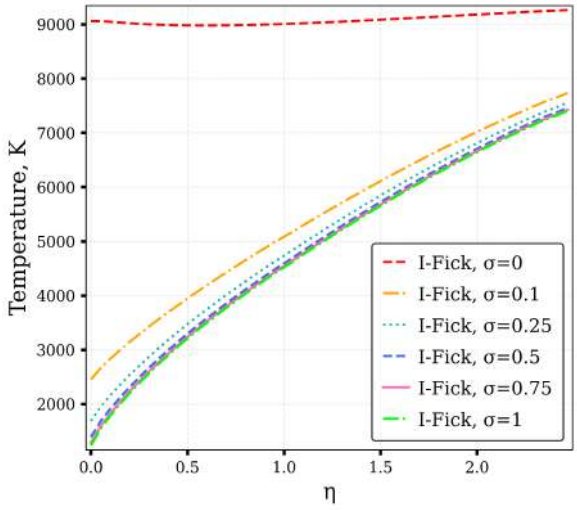

Figure 3.11 — Temperature profile for the EP2 (60km) case.

situation corresponds to the conditions when specular scattering dominates over diffuse scattering; $\sigma = 0$ corresponds to purely specular scattering by a solid wall. In the latter case, there is no energy exchange with the wall, which consequently is thermally insulated, therefore, the temperature remains constant along the boundary layer. The effects of temperature jump are stronger near the wall in the more rarefied case (EP1), as expected.

Distributions of oxygen atoms and molecules mass fractions through the boundary layer are presented in Fig. 3.12. The effects of the gas-surface interaction model on the fraction profiles are not as significant as observed for the temperature. The mass fractions show a monotonic behaviour for all species, except for oxygen molecules. In the case of oxygen, the fractions on the wall decrease with a decrease

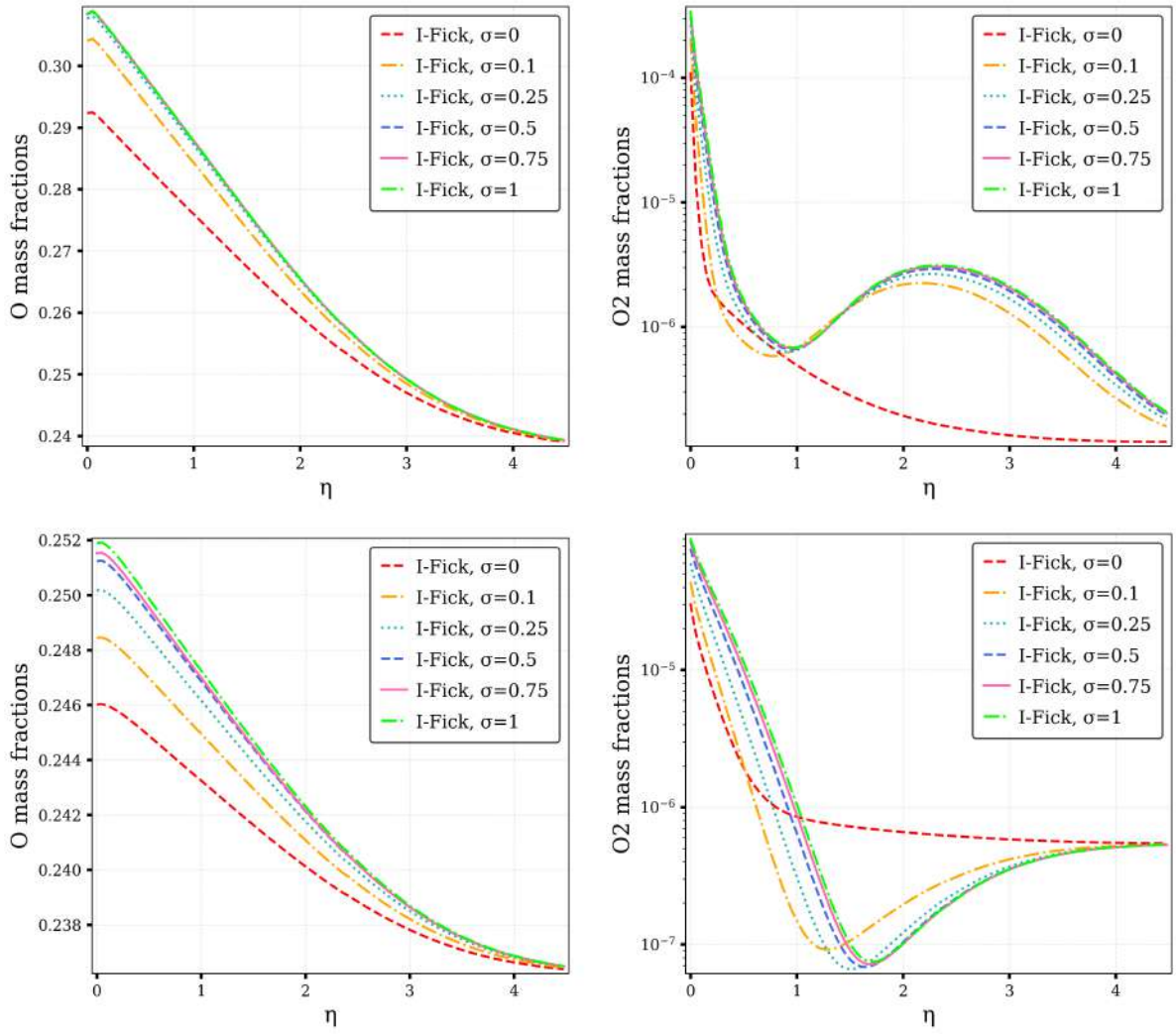

Figure 3.12 — O and O_2 mass fractions. Top – EP2 (60km) case, bottom – EP1 (85km) case.

in the accommodation coefficient. An interesting effect obtained for $\sigma = 0$ (purely specular scattering) may be observed for oxygen molecules. In this case, the distributions exhibit a consistent decrease near the wall. A similar effect is also observed for NO distributions (see Fig. 3.13). This behaviour is connected to the fact that the temperature is constant across the boundary layer, so the main influence is provided by the heterogeneous recombination, resulting in the observed profiles. Here as well, the temperature jump model provides stronger effects with increasing gas rarefaction.

The effect of different σ values on the total fluxes (Fig. 3.14) is opposite to their influence on temperature profiles: the total flux decreases with an increase in σ values. As expected, when $\sigma = 0$, the total heat flux becomes zero since the wall is thermally insulated and the temperature is constant across the layer.

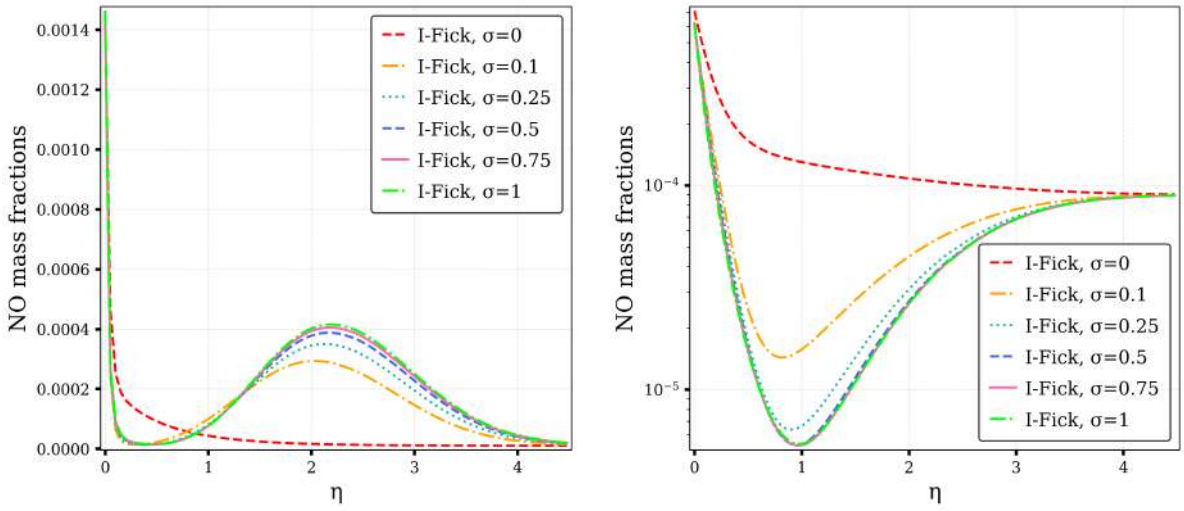

Figure 3.13 — NO mass fractions. Left – EP2 (60km) case, right – EP1 (85km) case.

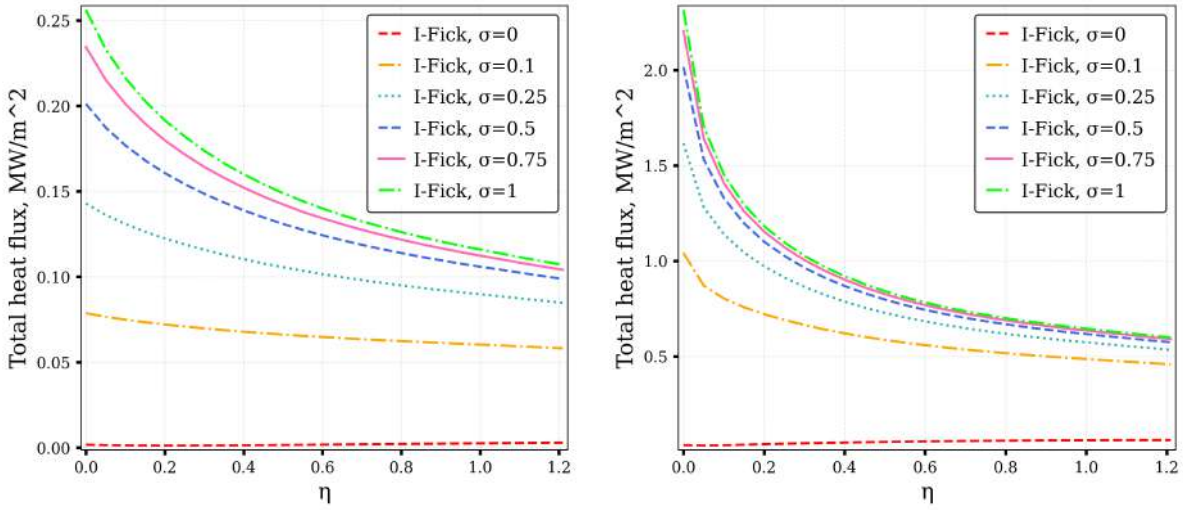

Figure 3.14 — Total heat fluxes. Left – EP1 (85km) case, right – EP2 (60km) case.

From the results provided in this section, it is clear that the variations in the accommodation coefficient values significantly impact the parameters of the hypersonic boundary layer airflow. This observation requires an additional justification of the coefficient value of 0.5 used in the previous sections. This justification runs out from the other studies on the boundary layer near a re-entry vehicle with a silica surface, conducted using DSMC and VSL methods [1; 146]. In these studies, a coefficient value of approximately 0.5 yielded the best agreement with experimental data from the Space Shuttle.

3.3 Conclusions of Chapter 3

In this Chapter, several theoretical approaches to derive state-specific slip boundary conditions are assessed, and the advantages of the self-consistent model developed in Chapter 2 are highlighted on the basis of numerical simulations of air flow in the boundary layer near stagnation point. The developed model has been chosen as a benchmark since it provided the best agreement with recombination rate coefficients obtained recently by molecular dynamic simulations.

Two cases corresponding to various gas rarefaction have been considered. The effect of gas-surface interaction models was evaluated by comparing the fluid-dynamic variables: temperature and mass fractions; vibrational energy distributions and heat fluxes. It is shown that the temperature jump is barely affected by heterogeneous recombination (its contribution is below 3%), except for the Barbato model. The values of the temperature jump itself, provided by the developed models, are similar to the DSMC results. The distributions of mass fractions and vibrational level populations noticeably depend on the model; the Barbato model yields qualitatively different distributions compared to other models.

As to the heat fluxes, whereas heterogeneous processes tend to increase the heating, the temperature jump causes a significant decrease in the surface heat flux. Moreover, the effect of temperature jump is dominating compared to the influence of heterogeneous reactions. This observation is confirmed by flight experiments and some other simulations by means of DSMC and VSL. For different degree of gas rarefaction, all the models retain key characteristics: with a lower degree of rarefaction the influence of wall catalyticity increases; on the opposite, the effects of temperature jump decrease.

Additionally, two diffusion models are assessed: the approximate Fick law and a more accurate Hirschfelder–Curtiss model. It is shown that using simplified diffusion models may considerably alter mixture composition near the surface. As for different types of extensions of the Chapter 2 model, it was shown that the discrepancy is small, less than the effect of diffusion model. The choice of accommodation coefficients strongly affects gas properties near the wall: fluid-dynamic variables vary considerably for $\sigma < 0.5$ (when specular scattering dominates), but with further increase in σ they remain almost unchanged. The effect of temperature jump becomes stronger for more rarefied flows.

Conclusions

This thesis focused on achieving a specific goal: development of a theoretical approach for deriving a closed set of slip boundary conditions for state-specific macroscopic parameters of reacting gas mixture flows. While being obtained, the slip conditions were designed to capture the effects of both physical and chemical interaction of non-equilibrium gas with the surface of a solid body. Coupling of physical-chemical processes in the gas phase and on the surface with non-equilibrium rarefied gas dynamics posed significant difficulties. Despite the initially derived boundary conditions being equivalent to other known and widely applied models in the limit case of local thermal equilibrium and chemical non-equilibrium and under some other simplifications, they appeared insufficient in describing heterogeneous reactions. The theoretical analysis of this situation unexpectedly revealed issues with the initial formulation of the approach, which obviously needed to be extended to fulfill the established expectations. The present Conclusions Chapter of the thesis will provide a brief description of the path followed to achieve the posed goal and the results obtained along the way.

The initial step was to develop an approach that would allow derivation of boundary conditions for the state-to-state set of macroscopic variables. For this objective, the state-specific kinetic boundary condition along with the normalization condition for the scattering kernel were developed. The approach was subsequently formulated. It introduces procedure for obtaining the boundary conditions in the same way, as the transport equations are derived from the Boltzmann equation, differing only in the integration procedure. Heterogeneous processes were incorporated into the approach through a modified normalization condition for the kernel. This modification accounts for the fact that not all particles are scattered; some are gained or lost due to surface processes.

Additionally, the Grad's technique was extended to the STS approximation as well. Both approaches were then applied to derive the slip boundary conditions under the assumption of the Maxwell gas-surface interaction model. It was shown that the resulting conditions are equivalent, as well as the approaches. The obtained boundary conditions consist of species mass fluxes, including fluxes of molecular vibrational level populations and chemical number densities, velocity slip, and temperature jump. The latter were also derived for the Cercignani-Lampis scattering

kernel by means of the new approach. The slip conditions for both considered kernels differ only in the temperature jump. In all the expressions, the impact of normal mean stress components, such as bulk viscosity and relaxation pressure, is introduced for the first time. Implementing these conditions in non-equilibrium flow simulations can be done with no additional difficulties, as they depend on the same expansion coefficients as transport coefficients, minimizing code complexity.

Although the proposed approach provided an ability, with minimal changes, to obtain state-specific expressions for macroscopic parameters on the boundary of a solid body for an arbitrary type of scattering kernel, the theoretical analysis of wall mass fluxes revealed an issue related to the impact of heterogeneous reactions. More precisely, the wall mass fluxes expressions, though equivalent to those obtained by means of other commonly applied approaches, did not correctly account for the increase in the number of particles due to surface processes. So reconsideration of the approach was required.

The proposed extension of the approach was based on the modification of the kinetic boundary condition. Furthermore, the proposed scheme retains all the advantages of the former one: 1) the slip conditions depend only on macroparameters, accommodation coefficients, and surface process probabilities without requiring further simplification; 2) there are no additional computational costs when all the transport coefficients and processes probabilities are known; 3) the procedure can be easily adapted to the one-temperature thermal equilibrium approximation.

Surface processes directly impact boundary conditions for species concentrations. The general form of the latter, when heterogeneous recombination is only considered, is similar to other known phenomenological and theoretical models designed to account for this process, although effective recombination coefficients are calculated theoretically. Non-equilibrium surface processes are not explicitly accounted for in the expressions for velocity and temperature on the wall, except for desorption, which affects velocity slip. Neglecting desorption, conditions for temperature and velocity, identical to those derived in the initial approach, are obtained.

The theoretical analysis of the BCs for species concentrations, along with the similarity of their general form to some known successfully applied phenomenological models, provided confidence that the approach is constructed correctly, thus confirming the reliability of the approach. However, to validate the assumptions

made, rigorous numerical calculations needed to be conducted. For this purpose, the problem of an air flow in the boundary layer near stagnation point was chosen. On the basis of this problem, the developed theoretical approaches to derive state-specific slip boundary conditions were assessed for two cases of gas rarefaction. Various test cases of slip conditions were implemented, considering three models for heterogeneous processes: the initial one, the extended model, and the Barbato model; in certain cases the temperature jump was taken into account whereas in other cases it was neglected.

First, the heterogeneous recombination models were compared with the results of recent molecular dynamic simulations by means of the effective recombination rate coefficients. The extended approach demonstrated the best agreement and was, therefore, selected as the benchmark.

The influence of the model on the wall temperature is following: the temperature jump is barely affected by heterogeneous recombination (its contribution is below 3%), except for the Barbato model; the values of the jump itself, provided by the developed models, are similar to the DSMC results, where the same Maxwell model was applied and the tangential momentum accommodation coefficient was selected to fit the experimental data.

The distributions of mass fractions are noticeably affected by the chosen type of model. The initial approach, whether with or without temperature jump, yields values that are nearly identical to those obtained when including no-slip conditions, supporting the critique of the approach and other associated theoretical models. All other cases of slip conditions provide different behavior of the species mass fractions near the surface, with qualitatively different distributions from the Barbato model.

Regarding the heat fluxes, the results obtained using the benchmark model and the Barbato model are in disagreement. The presence of heterogeneous processes increases the heat flux values near the silica surface, with the extended model showing a difference of about 25%, while the Barbato model shows an increase of over 200%. When the temperature jump is considered, it plays a major role in the heat flux values near the wall in the developed models, contrasting with the influence of heterogeneous reactions. This observation is supported by flight experiments and other simulations. The overall decrease in the wall heat flux in such cases may reach about 25%. The Barbato surface catalytic model, however, still provides an extreme increase in heat flux value, reaching up to 50%. Such a high catalytic effect cannot be confirmed.

If to compare results obtained for different gas rarefaction cases, then all the models retain key characteristics observed: with a lower degree of rarefaction the influence of wall catalyticity increases; on the opposite, the effects of temperature jump decrease.

Moreover, for the same flow, two diffusion models were evaluated in slip conditions: the simplified Fick law and the more accurate Hirschfelder–Curtiss model. The study revealed that the use of simplified diffusion models can significantly affect the mixture composition near the surface. Furthermore, it is crucial to consider that the choice of accommodation coefficients has a substantial impact on gas properties near the wall, emphasizing the recommendation to apply reliable data on this coefficient.

Overall, the conducted research provided an ability to obtain state-specific slip boundary conditions, accounting for rarefaction effects in the gas mixture, the way of particles scattering by the solid wall, and the influence of chemical processes on the surface. Further, in addition to theoretical analysis, the impact of these boundary conditions is studied in detail on the basis of an air flow in the boundary layer of a re-entering vehicle with a silica-based thermal protection system. The main conclusion of this research is that, when modeling non-equilibrium rarefied gas flows near solids, it is recommended to use detailed, self-consistent models coupled with the developed closed set of slip boundary conditions. Aforementioned conclusion is supported by the obtained results.

This study can be extended in various ways. The slip conditions can be derived for more advanced models of particles scattering by the solid wall, such as the Epstein model, and for the kernels that allows rotational state change of molecules during scattering. Additionally, the approach can be applied to obtain conditions in the case of multi-temperature models, accounting for all the surface processes considered in this study. Vibrational relaxation during particles interaction with the solid surface will be considered on the basis of «vibrational temperatures jumps». Such an approach, while providing some loss in accuracy, will significantly reduce computational costs. Besides that, there is a necessity for studying more carefully the influence of particles scattering model and the accommodation coefficients, and including adsorption and desorption in simulations. The implementation of detailed models of diffusion velocity for calculations is also crucial. Furthermore, the incorporation of a more advanced heterogeneous recombination Langmuir–Hinshelwood mechanism is essential, especially for the

range of wall temperatures considered in this study. Also, it is important to account for the pressure dependence of the recombination probabilities. Neglecting this results in a small increase in probability values from the actual ones. The last but not least extension goes far beyond this study. Specifically, it involves constructing models that can capture ablation processes. In the current form, the presented kinetic boundary condition is not capable of accounting for this process. Its modification and consideration of time-dependence are required to address the mentioned problem.

References

1. *Moss, J. N.* Direct simulation of transitional flow for hypersonic reentry conditions / J. N. Moss, G. A. Bird // Journal of Spacecraft and Rockets. — 2003. — Vol. 40, no. 5. — P. 830—843.
2. Direct simulation of non-equilibrium kinetics under shock conditions in nitrogen / D. Bruno [et al.] // Chemical Physics Letters. — 2002. — Vol. 360, no. 1. — P. 31—37.
3. Comparison of direct simulation Monte Carlo chemistry and vibrational models applied to oxygen shock measurements / I. Wysong [et al.] // Physics of Fluids. — 2014. — Vol. 26, no. 4. — P. 043101.
4. *Gimelshein, S.* DSMC modeling of flows with recombination reactions / S. Gimelshein, I. Wysong // Physics of Fluids. — 2017. — Vol. 29, no. 6. — P. 067106.
5. Classical impulsive model for dissociation of diatomic molecules in direct simulation Monte Carlo / H. Luo [et al.] // Phys. Rev. Fluids. — 2018. — Vol. 3, issue 11. — P. 113401.
6. *Chen, H.* Role of chemical reactions in the stagnation point heat flux of rarefied hypersonic cylinder flows / H. Chen, B. Zhang, H. Liu // Physics of Fluids. — 2020. — Vol. 32, no. 9. — P. 096105.
7. *Kustova, E.* Transport properties of a reacting gas mixture with strong vibrational and chemical nonequilibrium / E. Kustova, E. Nagnibeda // Chem. Phys. — 1998. — Vol. 233. — P. 57—75.
8. *Kustova, E.* On the simplified state-to-state transport coefficients / E. Kustova // Chem. Phys. — 2001. — Vol. 270, no. 1. — P. 177—195.
9. *Nagnibeda, E.* Nonequilibrium Reacting Gas Flows. Kinetic Theory of Transport and Relaxation Processes / E. Nagnibeda, E. Kustova. — Berlin, Heidelberg : Springer Verlag, 2009.
10. Kinetic and Continuum modeling of high-temperature oxygen and nitrogen binary mixtures / S. F. Gimelshein [et al.] // Journal of Thermophysics and Heat Transfer. — 2022. — Vol. 36, no. 2. — P. 399—418.

11. Kinetic and continuum modeling of high-temperature air relaxation / S. F. Gimelshein [et al.] // Journal of Thermophysics and Heat Transfer. — 2022. — Vol. 36, no. 4. — P. 870—893.

12. *Andrienko, D. A.* High fidelity modeling of thermal relaxation and dissociation of oxygen / D. A. Andrienko, I. D. Boyd // Phys. Fluids. — 2015. — Vol. 27, no. 11. — P. 116101.

13. Vibrational relaxation of carbon dioxide in various approaches / O. Kunova [et al.] // Physical Review Fluids. — 2020. — Vol. 5. — P. 123401.

14. Four-temperature kinetic model for CO_2 vibrational relaxation / A. Kosareva [et al.] // Physics of Fluids. — 2021. — Vol. 33, no. 1. — P. 016103.

15. Vibrational energy transfer rates using a forced harmonic oscillator model / I. Adamovich [et al.] // J. Thermophys. Heat Transfer. — 1998. — Vol. 12, no. 1. — P. 57—65.

16. Nonequilibrium shock-heated nitrogen flows using a rovibrational state-to-state method / M. Panesi [et al.] // Phys. Rev. E. — 2014. — Vol. 90. — P. 013009.

17. Non-equilibrium kinetics, diffusion and heat transfer in shock heated flows of N_2/N and O_2/O mixtures / O. Kunova [et al.] // Chem. Phys. — 2015. — Vol. 463. — P. 70—81.

18. *Kadochnikov, I.* Kinetics of nonequilibrium processes in air plasma formed behind shock waves: state-to-state consideration / I. Kadochnikov, I. Arsentiev // Journal of Physics D: Applied Physics. — 2018. — Vol. 51, no. 37. — P. 374001.

19. *Kunova, O.* State-to-state description of reacting air flows behind shock waves / O. Kunova, E. Nagnibeda // Chem. Phys. — 2014. — Vol. 441. — P. 66—76.

20. *Su, W.* State-specific modeling of vibrational relaxation and nitric oxide formation in shock-heated air / W. Su, D. Bruno, Y. Babou // Journal of Thermophysics and Heat Transfer. — 2018. — Vol. 32, no. 2. — P. 337—352.

21. Models validation and code profiling in state-to-state simulations of shock heated air flows / L. Campoli [et al.] // Acta Astronautica. — 2020. — Vol. 175. — P. 493—509.

22. *Alekseev, I.* Extended continuum models for shock waves in CO_2 / I. Alekseev, E. Kustova // Physics of Fluids. — 2021. — Vol. 33, no. 9. — P. 096101.

23. *Melnik, M. Y.* Impact of electronic excitation on the state-to-state vibrational-chemical CO kinetics / M. Y. Melnik, E. Kustova // Journal of Physics: Conference Series. Vol. 2308. — IOP Publishing. 2022. — P. 012014.

24. Non-Arrhenius NO formation rate in one-dimensional nozzle airflow / G. Colonna [et al.] // J. Thermophys. Heat Transfer. — 1999. — Vol. 13, no. 3. — P. 372—375.

25. On the non-equilibrium kinetics and heat transfer in nozzle flows / E. Kustova [et al.] // Chem. Phys. — 2002. — Vol. 276, no. 2. — P. 139—154.

26. The influence of nonequilibrium kinetics on the heat transfer and diffusion near re-entering body / I. Armenise [et al.] // J. Thermophys. Heat Transfer. — 1999. — Vol. 13, no. 2. — P. 210—218.

27. Non-equilibrium kinetics and heat transfer in O_2/O mixtures near catalytic surfaces / E. Kustova [et al.] // J. Thermophys. Heat Transfer. — 2002. — Vol. 16, no. 2. — P. 238—244.

28. State-to-State Catalytic Models, Kinetics and Transport in Hypersonic Boundary Layers / I. Armenise [et al.] // J. Thermophys. Heat Transfer. — 2006. — Vol. 20, no. 3. — P. 465—476.

29. State-to-state simulation of non-equilibrium nitrogen stagnation line flows: fluid dynamics and vibrational kinetics / A. Orsini [et al.] // J. Thermophys. Heat Transfer. — 2008. — Vol. 22, no. 3. — P. 390—398.

30. *Kustova, E.* State-resolved dissociation and exchange reactions in CO_2 flows / E. Kustova, A. Savelev, I. Armenise // J. Phys. Chem. A. — 2019. — Vol. 123, no. 49. — P. 10529—10542.

31. *Candler, G.* Detailed simulation of nitrogen dissociation in stagnation regions / G. Candler, J. Olejniczak, B. Harrold // Phys. Fluids. — 1997. — Vol. 9, no. 7. — P. 2108—2117.

32. *Armenise, I.* On different contributions to the heat flux and diffusion in non-equilibrium flows / I. Armenise, E. Kustova // Chem. Phys. — 2014. — Vol. 428. — P. 90—104.

33. Vibrationally relaxing flow of N past an infinite cylinder / D. Giordano [et al.] // J. Thermophys. Heat Transfer. — 1997. — Vol. 11, no. 1. — P. 27—35.

34. *Josyula, E.* Computational study of vibrationally relaxing gas past blunt body in hypersonic flows / E. Josyula // J. Thermophys. Heat Transfer. — 2000. — Vol. 14, no. 1. — P. 18—26.

35. State-to-state kinetic model for a viscous radiating hypersonic flow / E. Josyula [et al.] // 53rd AIAA Aerospace Sciences Meeting. — 53rd AIAA Aerospace Sciences Meeting, 2015. — P. 0475.

36. Unsteady behavior and thermochemical non equilibrium effects in hypersonic double-wedge flows / D. Ninni [et al.] // Acta Astronautica. — 2022. — Vol. 191. — P. 178—192.

37. On the influence of non equilibrium in the free stream conditions of high enthalpy oxygen flows around a double-cone / D. Ninni [et al.] // Acta Astronautica. — 2022. — Vol. 201. — P. 247—258.

38. *Panesi, M.* Collisional radiative coarse-grain model for ionization in air / M. Panesi, A. Lani // Physics of Fluids. — 2013. — Vol. 25, no. 5.

39. *Armenise, I.* State-to-state models for CO_2 molecules: from the theory to an application to hypersonic boundary layers / I. Armenise, E. Kustova // Chem. Phys. — 2013. — Vol. 415. — P. 269—281.

40. *Armenise, I.* Advanced models for vibrational and chemical kinetics applied to Mars entry aerothermodynamics / I. Armenise, P. Reynier, E. Kustova // J. Thermophys. Heat Transfer. — 2016. — Vol. 30, no. 4. — P. 705—720.

41. *Kustova, E.* On the applicability of simplified state-to-state models of transport coefficients / E. Kustova, M. Mekhonoshina, G. Oblapenko // Chem. Phys. Lett. — 2017. — Vol. 686. — P. 161—166.

42. The influence of vibrational state-resolved transport coefficients on the wave propagation in diatomic gases / G. M. Kremer [et al.] // Physica A. — 2018. — Vol. 490. — P. 92—113.

43. *Gupta, R.* Slip-boundary equations for multicomponent nonequilibrium airflow / R. Gupta, C. Scott, J. Moss // NASA Technical Paper 85820. — 1985.

44. *Maxwell, J. C.* On stresses in rarefied gases arising from inequalities of temperature / J. C. Maxwell // Proceedings of the Royal Society of London. — 1878. — Vol. 27, no. 185—189. — P. 304—308.

45. *Nocilla, S.* Basic concepts in the surface interaction of free-molecular flows or molecular beams / S. Nocilla // Meccanica. — 1967. — Vol. 2. — P. 34—40.

46. *Epstein, M.* A model of the wall boundary condition in kinetic theory / M. Epstein // AIAA J. — 1967. — Vol. 5, no. 10. — P. 1797—1800.

47. *Cercignani, C.* Kinetic models for gas-surface interactions / C. Cercignani, M. Lampis // Transport Theor. Stat. Ph. — 1971. — Vol. 1, no. 2. — P. 101—114.

48. *Klinc, T.* Slip coefficients for general gas-surface interaction / T. Klinc, I. Kuščer // Phys. Fluids. — 1972. — Vol. 15, no. 6. — P. 1018—1022.

49. *Lord, R. G.* Some extensions to the Cercignani–Lampis gas–surface scattering kernel / R. G. Lord // Phys. Fluid. A. — 1991. — Vol. 3, no. 4. — P. 706—710.

50. *Struchtrup, H.* Maxwell boundary condition and velocity dependent accommodation coefficient / H. Struchtrup // Phys. Fluids. — 2013. — Vol. 25, no. 11. — P. 112001.

51. *Liang, T.* Performance evaluation of Maxwell and Cercignani-Lampis gas-wall interaction models in the modeling of thermally driven rarefied gas transport / T. Liang, Q. Li, W. Ye // Phys. Rev. E. — 2013. — Vol. 88, issue 1. — P. 013009.

52. *Brull, S.* Gas-surface interaction and boundary conditions for the Boltzmann equation / S. Brull, P. Charrier, L. Mieussens // Kin. Rel. Models. — 2014. — Vol. 7. — P. 219—251.

53. *Wu, L.* Assessment and development of the gas kinetic boundary condition for the Boltzmann equation / L. Wu, H. Struchtrup // J. Fluid. Mech. — 2017. — Vol. 823. — P. 511—537.

54. *Lord, R. G.* Some further extensions of the Cercignani–Lampis gas–surface interaction model / R. G. Lord // Phys. Fluid. — 1995. — Vol. 7, no. 5. — P. 1159—1161.

55. Non-equilibrium physical-chemical processes in hypersonic aerodynamics / V. Berkut [et al.]. — Moscow : Energoatomizdat, 1994.

56. *Agrawal, A.* Survey on measurement of tangential momentum accommodation coefficient / A. Agrawal, S. V. Prabhu // Journal of Vacuum Science & Technology A. — 2008. — Vol. 26, no. 4. — P. 634—645.

57. Measurements of tangential momentum accommodation coefficient for various gases in plane microchannel / I. A. Graur [et al.] // Physics of Fluids. — 2009. — Vol. 21, no. 10. — P. 102004.

58. Computation of accommodation coefficients and the use of velocity correlation profiles in molecular dynamics simulations / P. Spijker [et al.] // Phys. Rev. E. — 2010. — Vol. 81, issue 1. — P. 011203.

59. *Yamaguchi, H.* Molecular-dynamics study on characteristics of energy and tangential momentum accommodation coefficients / H. Yamaguchi, Y. Matsuda, T. Niimi // Phys. Rev. E. — 2017. — Vol. 96, issue 1. — P. 013116.

60. Gas-surface scattering models for particle fluid dynamics: a comparison between analytical approximate models and molecular dynamics calculations / D. Bruno [et al.] // Chemical Physics Letters. — 2000. — Vol. 320, no. 3. — P. 245—254.

61. *Yamamoto, K.* Scattering properties and scattering kernel based on the molecular dynamics analysis of gas-wall interaction / K. Yamamoto, H. Takeuchi, T. Hyakutake // Physics of Fluids. — 2007. — Vol. 19, no. 8. — P. 087102.

62. *Hossein Gorji, M.* A gas-surface interaction kernel for diatomic rarefied gas flows based on the Cercignani-Lampis-Lord model / M. Hossein Gorji, P. Jenny // Physics of fluids. — 2014. — Vol. 26, no. 12. — P. 122004.

63. A modified Cercignani–Lampis model with independent momentum and thermal accommodation coefficients for gas molecules scattering on surfaces / J. Deng [et al.] // Physics of Fluids. — 2022. — Vol. 34, no. 10. — P. 107108.

64. *Choquet, I.* A new approach to model and simulate numerically surface chemistry in rarefied flows / I. Choquet // Physics of Fluids. — 1999. — Vol. 11, no. 6. — P. 1650—1661.

65. *Kovalev, V. L.* Dynamic Monte Carlo simulation of surface recombination / V. L. Kovalev, V. Y. Sazonenko, A. N. Yakunchikov // Moscow University Mechanics Bulletin. — 2007. — Vol. 62. — P. 53—58.

66. *Molchanova, A. N.* Surface recombination in the direct simulation Monte Carlo method / A. N. Molchanova, A. V. Kashkovsky, Y. A. Bondar // Physics of Fluids. — 2018. — Oct. — Vol. 30, no. 10. — P. 107105.

67. *Pitaevskii, L. P.* Course of theoretical physics: Physical kinetics. Vol. 10 / L. P. Pitaevskii, E. Lifshitz. — Butterworth-Heinemann, 2012.

68. *Dadzie, S. K.* Temperature jump and slip velocity calculations from an anisotropic scattering kernel / S. K. Dadzie, J. G. Méolans // Physica A: Statistical Mechanics and its Applications. — 2005. — Vol. 358, no. 2—4. — P. 328—346.

69. *Armenise, I.* Fourier and diffusive heat transfer in hypersonic nitrogen flows: the state-to-state approach / I. Armenise, M. Capitelli, S. Longo // Journal of Thermophysics and Heat Transfer. — 2009. — Vol. 23, no. 4. — P. 674—683.

70. *Deutschmann, O.* Modeling of nitrogen and oxygen recombination on partial catalytic surfaces / O. Deutschmann, U. Riedel, J. Warnatz // ASME. J. Heat Transfer. — 1995. — Vol. 117. — P. 495—501.

71. *Kiryutin, B. A.* Slip boundary conditions on a catalytic surface in a multicomponent gas flow / B. A. Kiryutin, G. A. Tirskii // Fluid Dyn. — 1996. — Vol. 31. — P. 134—143.

72. Nonequilibrium Vibrational Kinetics of an O_2/O Mixture Hitting a Catalytic Surface / I. Armenise [et al.] // J. Spacecraft Rockets. — 2000. — Vol. 37, no. 3. — P. 318—323.

73. *Siewert, C.* Viscous-slip, thermal-slip, and temperature-jump coefficients as defined by the linearized Boltzmann equation and the Cercignani–Lampis boundary condition / C. Siewert // Physics of Fluids. — 2003. — Vol. 15, no. 6. — P. 1696—1701.

74. *Stepanenko, A.* Boundary slip phenomena in multicomponent gas mixtures / A. Stepanenko, V. Zaznoba, V. Zhdanov // Physics of Fluids. — 2019. — Vol. 31, no. 6. — P. 062105.

75. Variational derivation of thermal slip coefficients on the basis of the Boltzmann equation for hard-sphere molecules and Cercignani–Lampis boundary conditions: Comparison with experimental results / N. N. Nguyen [et al.] // Physics of Fluids. — 2020. — Vol. 32, no. 10. — P. 102011.

76. *Li, R.* Slip and jump coefficients for general gas–surface interactions according to the moment method / R. Li, Y. Yang // Physics of Fluids. — 2023. — Vol. 35, no. 3.

77. *Sharipov, F.* Velocity slip and temperature jump coefficients for gaseous mixtures. I. Viscous slip coefficient / F. Sharipov, D. Kalempa // Physics of Fluids. — 2003. — Vol. 15, no. 6. — P. 1800—1806.

78. *Sharipov, F.* Velocity slip and temperature jump coefficients for gaseous mixtures. II. Thermal slip coefficient / F. Sharipov, D. Kalempa // Physics of Fluids. — 2004. — Vol. 16, no. 3. — P. 759—764.

79. *Sharipov, F.* Velocity slip and temperature jump coefficients for gaseous mixtures. III. Diffusion slip coefficient / F. Sharipov, D. Kalempa // Physics of Fluids. — 2004. — Vol. 16, no. 10. — P. 3779—3785.

80. *Grad, H.* On the kinetic theory of rarefied gases / H. Grad // Comm. Pure Appl. Math. — 1949. — Vol. 2, no. 4. — P. 331—407.

81. *Patterson, G. N.* Molecular Flow of Gases / G. N. Patterson. — Wiley, New York, 1956.

82. *Zade, A.* Slip/jump boundary conditions for rarefied reacting/non-reacting multi-component gaseous flows / A. Zade, M. Renksizbulut, J. Friedman // Int. J. Heat Mass Transf. — 2008. — Vol. 51, no. 21. — P. 5063—5071.

83. *Aoki, K.* Kinetic model of adsorption on crystal surfaces / K. Aoki, V. Giovangigli // Phys. Rev. E. — 2019. — Vol. 99, issue 5. — P. 052137.

84. *Aoki, K.* Kinetic theory of chemical reactions on crystal surfaces / K. Aoki, V. Giovangigli // Phys. A: Stat. Mech. Appl. — 2021. — Vol. 565. — P. 125573.

85. Numerical analysis of thermal-slip and diffusion-slip flows of a binary mixture of hard-sphere molecular gases / S. Takata [et al.] // Physics of Fluids. — 2003. — Vol. 15, no. 12. — P. 3745—3766.

86. *Loyalka, S. K.* Temperature jump and thermal creep slip: Rigid sphere gas / S. K. Loyalka // Phys. Fluids A. — 1989. — Vol. 1, no. 2. — P. 403—408.

87. *Shidlovskiy, V. P.* Introduction to dynamics of rarefied gases / V. P. Shidlovskiy. — Elsevier, New York, 1967.

88. *Shakurova, L.* State-specific boundary conditions for nonequilibrium gas flows in slip regime / L. Shakurova, E. Kustova // Phys. Rev. E. — 2022. — Vol. 105, issue 3. — P. 034126.

89. *Shakurova, L. A.* Boundary conditions for fluid-dynamic parameters of a single-component gas flow with vibrational deactivation on a solid wall / L. A. Shakurova, E. V. Kustova // Vestnik of Saint Petersburg University. Mathematics. Mechanics. Astronomy. — 2022. — Vol. 9, no. 2. — P. 366—377 ; — in Russian.

90. *Shakurova, L.* Slip boundary conditions for gas mixture flows with state-to-state vibrational-chemical kinetics / L. Shakurova, E. Kustova // AIP Conference Proceedings. — 2023. — Vol. accepted.

91. *Sone, Y.* Kinetic Theory and Fluid Dynamics / Y. Sone. — Birkhäuser, Boston, 2002.

92. *Sone, Y.* Molecular Gas Dynamics: Theory, Techniques, and Applications / Y. Sone. — Birkhäuser, Boston, 2007.

93. *Scott, C.* Wall boundary equations with slip and catalysis for multicomponent, nonequilibrium gas flows / C. Scott // NASA TM X-58111. — 1973.

94. *Xu, B.* Theoretical and numerical studies of non-equilibrium slip effects on a catalytic surface / B. Xu, Y. Ju // Combustion Theory and Modelling. — 2006. — Vol. 10, no. 6. — P. 961—979.

95. Theoretical derivation of slip boundary conditions for single-species gas and binary gas mixture / J. Zhang [et al.] // Phys. Rev. E. — 2021. — Vol. 104, issue 5. — P. 055103.

96. *Utyuzhnikov, S. V.* Hypersonic Aerodynamics and Heat Transfer / S. V. Utyuzhnikov, G. A. Tirskiy. — Begell House Inc. Publishers, NY, 2014.

97. *Hattori, M.* Slip boundary conditions for the compressible Navier-Stokes equations for a polyatomic gas / M. Hattori, S. Kosuge, K. Aoki // Phys. Rev. Fluids. — 2018. — Vol. 3, issue 6. — P. 063401.

98. Boundary conditions for two-temperature Navier-Stokes equations for a polyatomic gas / S. Kosuge [et al.] // Phys. Rev. Fluids. — 2021. — Vol. 6, issue 8. — P. 083401.

99. *Scott, C.* Catalytic recombination of nitrogen and oxygen on high-temperature reusable surface insulation / C. Scott // 15th Thermophysics Conference. — 1980. — P. 1477.

100. Methods and results of an experimental determination of the catalytic activity of materials at high temperatures / A. Vlasov [et al.] // Fluid Dynamics. — 2003. — Vol. 38, no. 5. — P. 815—825.

101. CFD evaluation of pressure effects on surface catalysis of SiO_2-based TPS / T. Kurotaki [et al.] // 43rd AIAA Aerospace Sciences Meeting and Exhibit. — 2005. — P. 388.

102. *Cacciatore, M.* Dynamical relaxation of H_2(v,j) on a copper surface / M. Cacciatore, G. Billing // Surface Science. — 1990. — Vol. 232, no. 1/2. — P. 35—50.

103. *Cacciatore, M.* Eley-Rideal and Langmuir-Hinshelwood recombination coefficients for oxygen on silica surfaces / M. Cacciatore, M. Rutigliano, G. Billing // J. Thermophys. Heat Transfer. — 1999. — Vol. 13, no. 2. — P. 195—203.

104. Analysis of heterogeneous recombination of oxygen atoms on aluminum oxide by methods of quantum mechanics and classical dynamics / V. L. Kovalev [et al.] // Acta Astronautica. — 2011. — Vol. 68. — P. 686—690.

105. *Borman, V.* The theory of nonequilibrium phenomena at the gas-solid interface / V. Borman, S. Krylov, A. Prosianov // Zh. Eksp. Teor. Fiz. — 1988. — Vol. 94. — P. 271—289.

106. New mechanism of mass transfer in a gas-adsorbate-solid system / A. Prosyanov [et al.] // Phys. Lett. A. — 1989. — Vol. 140, no. 1. — P. 55—58.

107. *Seward, W.* Model for oxygen recombination on silicon-dioxide surfaces / W. Seward, E. Jumper // Journal of thermophysics and heat transfer. — 1991. — Vol. 5, no. 3. — P. 284—291.

108. *Kovalev, V.* Experimental and theoretical simulation of heterogeneous catalysis in aerothermochemistry (a review) / V. Kovalev, A. Kolesnikov // Fluid Dynamics. — 2005. — Sept. — Vol. 40. — P. 669—693.

109. *Nasuti, F.* Material-dependent recombination modeling for hypersonic flows / F. Nasuti, M. Barbato, C. Bruno // J. Thermophys. Heat Transfer. — 1996. — Vol. 10, no. 1. — P. 131—136.

110. Model for heterogeneous catalysis on metal surfaces with applications to hypersonic flows / M. Barbato [et al.] // Journal of Thermophysics and Heat Transfer. — 2000. — Vol. 14, no. 3. — P. 412—420.

111. *Armenise, I.* N + O_2(v) collisions: reactive, inelastic and dissociation rates for state-to-state vibrational kinetic models / I. Armenise, F. Esposito // Chemical Physics. — 2021. — Vol. 551. — P. 111325.

112. *Shakurova, L.* State-specific slip boundary conditions in non-equilibrium gas flows: Theoretical models and their assessment / L. Shakurova, I. Armenise, E. Kustova // Physics of Fluids. — 2023. — Vol. 35, no. 8.

113. *Shakurova, L.* Effect of slip boundary conditions on nonequilibrium reacting air flows / L. Shakurova, I. Armenise, E. Kustova // Journal of Theoretical and Applied Mechanics, Sofia. — 2023. — Vol. 53. — P. 253—269.

114. *Kustova, E.* Cross-coupling effects in chemically non-equilibrium viscous compressible flows / E. Kustova, D. Giordano // Chem. Phys. — 2011. — Vol. 379, no. 1—3. — P. 83—91.

115. *Kustova, E.* Mutual effect of vibrational relaxation and chemical reactions in viscous multitemperature flows / E. Kustova, G. Oblapenko // Phys. Rev. E. — 2016. — Vol. 93. — P. 033127.

116. *Ferziger, J.* Mathematical Theory of Transport Processes in Gases / J. Ferziger, H. Kaper. — North-Holland Publishing Co., Amsterdam, London, 1972.

117. *Ern, A.* Multicomponent transport algorithms. Vol. 24 / A. Ern, V. Giovangigli. — Springer Science & Business Media, 1994.

118. *Campoli, L.* KAPPA: Kinetic approach to physical processes in atmospheres library in C++ / L. Campoli, G. Oblapenko, E. Kustova // Comp. Phys. Comm. — 2019. — Vol. 236. — P. 244—267.

119. *Goniak, R.* Corrective term in wall slip equations for Knudsen layer / R. Goniak, G. Duffa // J. Thermophys. Heat Transfer. — 1995. — Vol. 9, no. 2. — P. 383—384.

120. *Cercignani, C.* Scattering kernels for gas-surface interactions / C. Cercignani // Transport Theor. Stat. Ph. — 1972. — Vol. 2, no. 1. — P. 27—53.

121. *Cercignani, C.* The Boltzmann Equation and Its Applications / C. Cercignani. — Springer, New York, NY, 1988.

122. *Kogan, M.* Rarefied Gas Dynamics / M. Kogan. — Boston, MA: Springer, 1969.

123. *Li, Z.* Gas-Nanoparticle Scattering: A Molecular View of Momentum Accommodation Function / Z. Li, H. Wang // Phys. Rev. Lett. — 2005. — Vol. 95, issue 1. — P. 014502.

124. *Kovalev, V.* Heterogeneous Catalytic Processes in Aerothermodynamics / V. Kovalev. — M.: FIZMATLIT, 2002.

125. *Anderson, J.* Hypersonic and High-temperature Gas Dynamics / J. Anderson. — American Institute of Aeronautics, Astronautics, 2006.

126. Dependence of heat transfer on the formation of vibrationally excited nitrogen molecules during the recombination of atoms in a boundary layer / V. M. Doroshenko [et al.] // High Temperature. — 1990. — Vol. 28. — P. 70—76.

127. *Billing, G. D.* VV and VT rate coefficients in N_2 by a quantum-classical model / G. D. Billing, E. Fisher // Chemical Physics. — 1979. — Vol. 43, no. 3. — P. 395—401.

128. *Capitelli, M.* V-V pumping up in non-equilibrium nitrogen: Effects on the dissociation rate / M. Capitelli, C. Gorse, G. Billing // Chemical Physics. — 1980. — Vol. 52, no. 3. — P. 299—304.

129. *Billing, G. D.* Vibration-vibration and vibration-translation energy transfer, including multiquantum transitions in atom-diatom and diatom-diatom collisions / G. D. Billing // Nonequilibrium Vibrational Kinetics. — Berlin, Heidelberg : Springer Berlin Heidelberg, 1986. — P. 85—112.

130. *Billing, G.* Vibrational relaxation of oxygen. State to state rate constants / G. Billing, R. Kolesnick // Chemical Physics Letters. — 1992. — Vol. 200, no. 4. — P. 382—386.

131. *Armenise, I.* State to state vibrational kinetics in the boundary layer of an entering body in earth atmosphere: particle distributions and chemical kinetics / I. Armenise, M. Capitelli // Plasma Sources Sci. Technol. — 2005. — Vol. 14, no. 2. — S9.

132. *Armenise, I.* N_2, O_2, NO state-to-state vibrational kinetics in hypersonic boundary layers: The problem of rescaling rate coefficients to uniform vibrational ladders / I. Armenise, F. Esposito // Chemical Physics. — 2015. — Vol. 446. — P. 30—46.

133. *Esposito, F.* N–N_2 state to state vibrational-relaxation and dissociation rates based on quasiclassical calculations / F. Esposito, I. Armenise, M. Capitelli // Chemical Physics. — 2006. — Vol. 331, no. 1. — P. 1—8.

134. O–O_2 state-to-state vibrational relaxation and dissociation rates based on quasiclassical calculations / F. Esposito [et al.] // Chemical Physics. — 2008. — Vol. 351, no. 1. — P. 91—98.

135. Reaction cross sections for two direct simulation Monte Carlo models: Accuracy and sensitivity analysis / I. Wysong [et al.] // Physics of Fluids. — 2012. — Apr. — Vol. 24, no. 4. — P. 042002.

136. *Esposito, F.* Reactive, Inelastic, and Dissociation Processes in Collisions of Atomic Oxygen with Molecular Nitrogen / F. Esposito, I. Armenise // The Journal of Physical Chemistry A. — 2017. — Vol. 121, no. 33. — P. 6211—6219.

137. Hypersonic Boundary Layers: Oxygen Recombination on SiO_2 Starting from Ab Initio Coefficients / I. Armenise [et al.] // Journal of Thermophysics and Heat Transfer. — 2011. — Vol. 25, no. 4. — P. 627—632.

138. *Rutigliano, M.* Vibrationally excited hydrogen molecules formation on a cesiated surface / M. Rutigliano, A. Palma, N. Sanna // Plasma Sources Science and Technology. — 2018. — Vol. 27, no. 7. — P. 075014.

139. *Rutigliano, M.* Hydrogen atom recombination on graphite at 10 K via the Eley–Rideal mechanism / M. Rutigliano, M. Cacciatore, G. Billing // Chemical Physics Letters. — 2001. — Vol. 340, no. 1. — P. 13—20.

140. *Rutigliano, M.* Recombination of Oxygen Atoms on Silica Surface: New and More Accurate Results / M. Rutigliano, M. Cacciatore // Journal of Thermophysics and Heat Transfer. — 2016. — Vol. 30, no. 1. — P. 247—250.

141. *O., H. J.* Molecular theory of gases and liquids / H. J. O., C. F. Curtiss, R. B. Bird. — New York: Wiley, 1964.

142. *Giovangigli, V.* Convergent iterative methods for multicomponent diffusion / V. Giovangigli // IMPACT of Computing in Science and Engineering. — 1991. — Vol. 3, no. 3. — P. 244—276.

143. *Giacomazzi, E.* A review of chemical diffusion: Criticism and limits of simplified methods for diffusion coefficient calculation / E. Giacomazzi, F. Picchia, N. Arcidiacono // Combustion Theory and Modelling. — 2008. — Vol. 12, no. 1. — P. 135—158.

144. Surface recombination coefficients and boundary-layer hypersonic-flow calculations on different surfaces / I. Armenise [et al.] // Journal of spacecraft and rockets. — 2004. — Vol. 41, no. 2. — P. 310—313.

145. *Kroupnov, A.* Interaction of dissociated air with the surface of β-cristobalite material / A. Kroupnov, M. J. Pogosbekian // Acta Astronautica. — 2023. — Vol. 203. — P. 454—468.

146. *Shinn, J.* Comparison of viscous-shock-layer heating analysis with Shuttle flight data in slip flow regime / J. Shinn, A. Simmonds // 22nd Aerospace Sciences Meeting. — 1984. — P. 226.

147. *Fay, J. A.* Theory of stagnation point heat transfer in dissociated air / J. A. Fay, F. R. Riddell // Journal of the Aerospace Sciences. — 1958. — Vol. 25, no. 2. — P. 73—85.

148. *Goulard, R.* On catalytic recombination rates in hypersonic stagnation heat transfer / R. Goulard // Journal of Jet Propulsion. — 1958. — Vol. 28, no. 11. — P. 737—745.

149. *Fenster, S. J.* Stagnation-point heat transfer for a new binary air model including dissociation and ionization / S. J. Fenster // AIAA Journal. — 1965. — Vol. 3, no. 12. — P. 2189—2196.

150. *Sutton, K.* A general stagnation-point convective heating equation for arbitrary gas mixtures : tech. rep. / K. Sutton, R. A. Graves Jr ; NASA. — 1971.

151. *Lee, S.* Evaluation of Fay and Riddell formula under hypersonic flight conditions / S. Lee, Y. Yang, J. G. Kim // International Journal of Numerical Methods for Heat & Fluid Flow. — 2023. — Vol. 33, no. 1. — P. 14—41.

152. *Brykina, I.* Asymptotic investigation of heat transfer and skin friction in three--dimensional hypersonic rarefied gas flows / I. Brykina // Journal of Applied Mathematics and Mechanics. — 2016. — Vol. 80, no. 3. — P. 244—256.

153. *Brykina, I.* Approximate analytical solutions for heat fluxes in three-dimensional hypersonic flow over blunt bodies / I. Brykina // Fluid Dynamics. — 2017. — Vol. 52. — P. 572—586.

Appendix A

Publications on the topic of the dissertation

1*. *Shakurova L., Kustova E.* State-specific boundary conditions for nonequilibrium gas flows in slip regime // Physical Review E, 2022. Vol. 105, no. 3. P. 034126.

2*. *Shakurova L.A., Kustova E.V.* Boundary conditions for fluid-dynamic parameters of a single-component gas flow with vibrational deactivation on a solid wall // Vestnik St. Petersburg University, Mathematics, 2022. Vol. 55, no. 2. P. 249–256.

3*. *Shakurova L., Armenise I., Kustova E.* State-specific slip boundary conditions in non-equilibrium gas flows: Theoretical models and their assessment // Physics of Fluids, 2023. Vol. 35, no. 8. P. 086109

4*. *Shakurova L., Armenise I., Kustova E.* Effect of slip boundary conditions on nonequilibrium reacting air flows // Journal of Theoretical and Applied Mechanics, 2023. Vol. 53. P. 253-269.

5*. *Shakurova L., Kustova E.* Slip boundary conditions for gas mixture flows with state-to-state vibrational-chemical kinetics // 32nd International Symposium on Rarefied Gas Dynamics, Vol. 2996 no. 1 of AIP Conference Proceedings. — AIP Publishing, 2024. P. 130002.

6*. *Kustova E.V., Shakurova L.A.* Boundary conditions on a body surface for macroparameters of non-equilibrium flows with different scattering kernels // Proceedings of the XIII International Conference on Applied Mathematics and Mechanics in the Aerospace Industry (AMMAI'2020), 2020. P. 238. (in Russian)

7*. *Shakurova L.A., Kustova E.V.* Boundary conditions on a partially catalytic surface in the case of state-to-state modeling of non-equilibrium flows // Proceedings of the XXII International Conference on Computational Mechanics and Modern Applied Software Systems (CMMASS'2021), 2021. P. 401–402. (in Russian)

8*. *Alekseev I.V., Kustova E.V., Shakurova L.A.* Effect of slip boundary conditions on non-equilibrium kinetics in the case of planar Couette flow

// Proceedings of the 21st International Conference on the Methods of Aerophysical Research (ICMAR 2022), Part II, 2022. P. 10.

9*. *Shakurova L.A., Kustova E.V.* Influence of slip boundary conditions on transport processes in O/O_2 mixture // Proceedings of the XIV International Conference on Applied Mathematics and Mechanics in the Aerospace Industry (AMMAI'2022), 2022. P. 141–142. (in Russian)

10*. *Shakurova L.A., Kustova E.V.* Modeling of slip boundary conditions and their influence on the parameters of non-equilibrium flows // Proceedings of the XIII All-Russian Congress on Theoretical and Applied Mechanics, Vol. 2, 2023. P. 855–856. (in Russian)

11*. *Norkin M.M., Kustova E.V., Shakurova L.A.* Investigation of non-equilibrium processes influence on rarefied gas flows via the planar Couette problem case // Proceedings of the XXIII International Conference on Computational Mechanics and Modern Applied Software Systems (CMMASS'2023), 2023. P. 398–399. (in Russian)

12*. *Shakurova L.A., Kustova E.V.* Validation of slip boundary condition models in highly non-equilibrium gas flows // Proceedings of the XXIII International Conference on Computational Mechanics and Modern Applied Software Systems (CMMASS'2023), 2023. P. 448–449. (in Russian)

Personal contribution of the author to publications

In all the joint publications, the main idea of the study, the formulation of the problem, and the discussion of the results belong to the scientific supervisor E.V. Kustova. In papers [3*, 4*], Dr. I. Armenise conducted numerical modeling of various test cases for air flows in the boundary layer, implemented the slip boundary conditions into the code and contributed to the analysis of the obtained results. In [8*], I.V. Alekseev proposed the numerical scheme for the Couette flow problem. M.M. Norkin is responsible for the numerical implementation of the Couette flow problem and the calculations of different test cases in work [11*].

In all the papers listed above, the author of the dissertation was responsible for formulating the approaches to obtain the slip boundary conditions and deriving the conditions themselves. Additionally, further calculations for some fluid dynamic

quantities were conducted within the framework of the boundary layer problem. The development of test cases and their comparison were also provided. Moreover, a comparison of the flow characteristics obtained during modeling with other calculations was made, and the text of the articles was prepared.